

Review

Cellulose Structures as a Support or Template for Inorganic Nanostructures and Their Assemblies

Alojz Anžlovar *  and Ema Žagar 

National Institute of Chemistry, Hajdrihova 19, SI-1000 Ljubljana, Slovenia; ema.zagar@ki.si

* Correspondence: alojz.anzlovar@ki.si; Tel.: +386-1-4760-204; Fax: +386-4760-300

Abstract: Cellulose is the most abundant natural polymer and deserves the special attention of the scientific community because it represents a sustainable source of carbon and plays an important role as a sustainable energent for replacing crude oil, coal, and natural gas in the future. Intense research and studies over the past few decades on cellulose structures have mainly focused on cellulose as a biomass for exploitation as an alternative energent or as a reinforcing material in polymer matrices. However, studies on cellulose structures have revealed more diverse potential applications by exploiting the functionalities of cellulose such as biomedical materials, biomimetic optical materials, bio-inspired mechanically adaptive materials, selective nanostructured membranes, and as a growth template for inorganic nanostructures. This article comprehensively reviews the potential of cellulose structures as a support, biotemplate, and growing vector in the formation of various complex hybrid hierarchical inorganic nanostructures with a wide scope of applications. We focus on the preparation of inorganic nanostructures by exploiting the unique properties and performances of cellulose structures. The advantages, physicochemical properties, and chemical modifications of the cellulose structures are comparatively discussed from the aspect of materials development and processing. Finally, the perspective and potential applications of cellulose-based bioinspired hierarchical functional nanomaterials in the future are outlined.

Keywords: cellulose; metallic and metal oxide nanostructures; metal sulfide nanostructures; mesoporous nanostructures; hierarchical nanostructures; heterogeneous catalysis



Citation: Anžlovar, A.; Žagar, E. Cellulose Structures as a Support or Template for Inorganic Nanostructures and Their Assemblies. *Nanomaterials* **2022**, *12*, 1837. <https://doi.org/10.3390/nano12111837>

Academic Editors: Carlos Miguel Costa and Senentxu Lanceros-Mendez

Received: 3 April 2022

Accepted: 25 May 2022

Published: 27 May 2022

Publisher's Note: MDPI stays neutral with regard to jurisdictional claims in published maps and institutional affiliations.



Copyright: © 2022 by the authors. Licensee MDPI, Basel, Switzerland. This article is an open access article distributed under the terms and conditions of the Creative Commons Attribution (CC BY) license (<https://creativecommons.org/licenses/by/4.0/>).

1. Introduction and Scope

With the aim to meet the global challenges that humanity is facing nowadays such as a lack of energy and fossil resources as well as increasing environmental issues, green and progressive strategies are expected to sustain the research impulse. In this context, cellulose, with its derivatives, will certainly play a significant role in this demanding task since it has an annual average output of 10^{11} – 10^{12} tons in nature and only 2×10^6 tons are used by people [1,2]. Bio-based materials are attractive as the basis for sustainable development and innovative solutions to a wide range of technological challenges as well as environmental problems. Cellulose and cellulose-based materials are not only earth abundant and biocompatible, but also contain intrinsic structures for transformative device performance [3]. While many innovative structures and devices as well as applications have been published and demonstrated, substantial challenges still exist in the fundamental science, and the commercialization of cellulose-based materials is a necessity in solving the emerging problems and demands [3–6]. The great advantage of cellulose or cellulose-based products and materials is that they can be produced from various byproducts or waste products emerging during food production such as various straws, peelings, husks, bagasse, corn stalks, or cobs, etc., or during wood processing [7–10].

Cellulose is the most abundant natural polymer globally, and is present in a large number of living species, mostly plants and bacteria, but also in animals [11,12]. It is a biodegradable and biocompatible as well as renewable polymer and it is a green alternative

to fossil-fuel carbon sources [13,14]. Cellulose has also attracted the special attention of the scientific community as a versatile and abundant “green” template [15]. The formation of functional nanomaterials via biomineralization or biotemplating is a topic that is attracting an enormous amount of interest from academia and the industry because it is promising for a more precise control over the positioning and connecting of different functional nanostructures into complex nano- and macro-devices [16,17].

The natural cellulose molecule is actually a long polysaccharide chain. It consists of a variable number of β -1,4 linked glucopyranose rings as repeating units [18]. Cellulosic polymer chains are, due to a vast number of hydroxyl groups, associated via hydrogen bonds forming bundles of fibrils (microfibrillar aggregates), where highly ordered regions (crystalline domains) alternate with disordered regions (amorphous domains) inside the cellulose fibrils, which constitute the walls of plant cells [19,20]. This highly ordered structure gives cellulose a very high elastic modulus and specific strength, making it an ideal reinforcing material for polymer matrices [21–23] in a variety of forms such as macroscopic fibers (hemp, jute, and kenaf), microfibrillated cellulose (MFC), cellulose nanofibrils (CNFs), or cellulose nanocrystals (CNCs) [13,24].

On the other hand, the scientific and research communities have experienced an immense rise in interest in the areas of nanoscience and nanotechnology during the last few decades. These are nowadays at the center of our technological progress due to their outstanding capability to manipulate matter on a nanometer scale. The capability to directly design, synthesize, and control systems at the same scale as nature is a huge scientific and technological challenge [25]. Over billions of years, nature has evolved nanoscale biological systems for the efficient production of energy and materials. By mimicking such systems, scientists aim to reach the goal of a sustainable society in the future [25]. Therefore, nanomaterials and nanotechnology have been regarded as a huge leap toward miniaturization and nanoscaling, generating various subfields with the aim to study these materials in detail. Nanotechnology as a scientific field is highly multidisciplinary; contributions from biologists, chemists, physicists, and engineers are indispensable to the advancement in the understanding the formation, application, and impact of new nanostructures and innovative nanotechnologies, which can potentially provide a very efficient approach to the production of chemicals, fuels, energy, and energy efficient materials [25–28].

1.1. Types and Forms of Cellulose

1.1.1. Cellulose Fibers and Fibrils (CF)

Native cellulose, defined as the cellulose I polymorph, does not exist as an isolated individual molecule, but is found as highly organized assemblies of individual cellulose chains, forming extended structures—fibers. The ultrastructure of cellulose fibers exhibits a hierarchical arrangement, starting from cellulose molecules to elementary fibrils and further to micro- as well as macrofibers. When cellulose molecules are synthesized as individual molecules, they immediately undergo spinning in a hierarchical order at the site of biosynthesis. Typically, up to 36 individual cellulose molecules are self-organized into larger units known as elementary fibrils (protofibrils) that are further packed into so-called microfibrils, and these are finally assembled into cellulose fibers with diameters of a few micrometers and lengths of up to a few thousands millimeters. Depending on the biosynthesis conditions, celluloses from different sources may occur in different packing that results in the different morphologies and properties of cellulose fibers [11,20]. For various purposes, cellulose needs to be isolated from its source, followed by purification and possible modification. Methods of extraction, purification, and modification affect the physical and chemical properties of cellulose such as the chain lengths and their distribution, the degree of crystallinity, the mechanical properties, thermal stability, solubility, the distribution of functional groups in the monomer units of the cellulose polymer chain, and the ratio of inter- and intra-molecular hydrogen bonds in the cellulose molecules. These physico-chemical properties play a key role in the determination of industrial and commercial applications of cellulose fibers [29–31].

1.1.2. Regenerated Cellulose (RC)

Regenerated cellulose, defined as a cellulose II polymorph, is obtained by the chemical regeneration process comprising the dissolution or swelling of native cellulose I fibers, followed by its reprecipitation in water. Suitable solvents for cellulose include cupric hydroxide in aqueous ammonia (cuoxam) or cupriethylenediamine (cuen), ammonia or amine/thiocyanate, hydrazine/thiocyanate, lithium chloride/N,N-dimethylacetamide (LiCl/DMAc), and N-methylmorpholine-N-oxide (NMMO)/water systems, and lately, ionic liquids (IL). Most of these solvents are limited on a pilot-scale except for NMMO, which is commercially used for the production of regenerated cellulose fibers called Lyocell [32]. Although viscose technology is still the most widely used process to manufacture regenerated cellulose fibers, this technology has many disadvantages related to environmental issues. A special case is mercerization (i.e., the swelling of the native cellulose in concentrated sodium hydroxide solution followed by the removal of the swelling agent). All of these processes finally produce fibers of the cellulose II polymorph. During the conversion (I to II), the conformation of hydroxyl groups is changed, causing a rearrangement in the entire hydrogen-bonded network while the dimensions of regenerated fibers remain mostly unchanged. Compared to cellulose I with a parallel up arrangement, the chains in cellulose II are in an antiparallel arrangement, producing a more stable fibrillary structure that is preferable for various practical applications [11,20]. One of the easiest ways to prepare regenerated cellulose is by dissolving raw cellulose in a NaOH/urea or thiourea aqueous solution [33]. An innovative approach toward regenerated cellulose is the dissolution of raw cellulose in various ionic liquids, representing a more sustainable strategy. Here, the choice of cation and anion is critical not only to the degree of the dissolution, but also to the ultimate sustainability of such processes. Studies have revealed that the interactions between the anion and cellulose play a key role in cellulose solvation, however, opinions on the cation role are still conflicting [34]. Oxidized regenerated cellulose (ORC), obtained by transforming its primary alcohol groups into carboxyl groups, is of special interest because of the various attractive medical applications and is among one of the most widespread hemostatics being used in almost any kind of surgery [2].

1.1.3. Microcrystalline Cellulose (MCC)

Microcrystalline cellulose is a pure, partially degraded native cellulose I, derived from high-quality wood pulps. It is prepared either by enzyme-mediated reactive extrusion, steam explosion, or acid hydrolysis with strong mineral acids (H_2SO_4 , HCl, or HBr). During this treatment, a partial degradation of cellulose fibers (preferentially in amorphous regions) takes place, producing a stable, chemically inactive, and physiologically inert cellulose material with attractive binding properties. The average dimension of MCC particles is above 5 μm . MCC offers the opportunity for a variety of applications (e.g., in the pharmaceutical industry as a tablet binder, in food applications as a texturizing agent, fat replacer, emulsifier, and bulking agent as well as an additive in paper and composite applications) [11]. MCC is one of the most useful and attractive fillers because of its high dilution potential, excellent compactibility at low pressures, and superior disintegration properties. Its chemical inertness and compatibility with a large number of drugs make MCC a highly attractive pharmaceutical agent [29]. Recently, various alternative sources of MCC have been studied. Although all microcrystalline cellulose is made of the same biopolymer, different raw materials can be used to obtain MCC tailored to specific needs [35].

1.1.4. Microfibrillated Cellulose (MFC)

Microfibrillated (MFC) and/or nanofibrillated cellulose (NFC) consist of long, entangled, and flexible cellulose (nano)fibers composed of alternating crystalline and amorphous phases. The difference between MFC and NFC is in the average width, which is much smaller in NFC (10–50 nm) than in MFC (10–500 nm). An aqueous MFC or NFC suspension consists of interconnected hydrophilic cellulose I (nano)fibers, inducing a gelation of the suspension at low mass contents of only a few percent. These can be isolated us-

ing different mechanical treatments, which usually involve a refining step followed by a high-pressure homogenization step, although cryocrushing and grinding methods have also been applied. Mechanical treatments produce a network of interconnected cellulose microfibrils with diameters from 10 to 500 nm and aspect ratios from 50 to 100. MFC and NFC are generally produced from wood pulp, though other cellulose sources originating from agricultural byproducts are also important such as wheat straw, sugar beet pulp, oil palm kernel, potato pulp, or sugar cane bagasse, etc. [13,36]. NFC production can be commercially competitive through the choice of less energy intensive processes and by using low-cost raw materials [37,38]. Additionally, to enhance NFC production and reduce energy consumption, various physical, chemical, and biological pretreatments have been applied. NFC is frequently produced through alkali and enzymatic pretreatment followed by grinding or by using TEMPO-mediated oxidation, followed by homogenization. These pretreatments substantially improve the production yield and properties of NFC. Therefore, NFC production is a combination of several operations, and by changing their sequence, different types of NFC can be isolated [39].

1.1.5. Bacterial Nanocellulose (BNC)

Cellulose fibers are secreted extracellularly by several bacterial species including Gram-negative bacteria such as *Acetobacter*, *Alcaligenes*, *Azotobacter*, *Rhizobium*, *Salmonella*, *Pseudomonas*, and Gram-positive bacteria such as *Sarcina ventriculi*. Bacterial cellulose (BNC) is produced most efficiently by the bacteria of the *Acetobacter* genus such as *Acetobacter G. xylinus*, *Acetobacter hansenii*, or *Acetobacter pasteurianus* species during cultivation in an aqueous culture media containing carbon and nitrogen sources in a time of a few days. The resulting cellulosic structure is in the form of a pellicle of randomly assembled ribbon shaped fibrils with a width of less than 100 nm, which are further composed of bundles of much finer nanofibrils (2 to 4 nm in diameter). These bundles are relatively straight and dimensionally uniform, and they further form a continuous three-dimensional network. Compared to plant cellulose, BNC is chemically a cellulose of high purity without the presence of hemicellulose and lignin. It shows higher hydrophilicity and water holding capacity, and in general, a higher tensile strength, resulting from a higher degree of polymerization and ultrafine network architecture [20,40]. The microbial process is an environmentally-friendly and effective method to produce high-yield BNC from various sources. However, the physiochemical characteristics (crystallinity and morphology) as well as yield of BNC are significantly influenced by the culture medium used [39].

1.1.6. Cellulose Nanocrystals (CNCs)

CNCs, also called cellulose whiskers or nanocrystalline cellulose (NCC), are predominantly isolated from cellulosic fibers by a simple process involving the acid hydrolysis of the biomass using mostly concentrated H_2SO_4 or other strong acids. CNCs, isolated by using (60–64%) H_2SO_4 , possess a higher colloidal stability than CNCs produced by other acids. Severe environmental pollution concerns due to strong acid hydrolysis has encouraged the use of recyclable acids (maleic acid, formic acid, citric acid), thus ensuring a more environmentally-friendly process design. Additionally, multiple acid blends (strong and weak acid) have also been employed, resulting in highly crystalline CNCs with a better surface chemistry due to the strong and weak acid contribution. The production of CNCs can also be achieved by using oxidizing agents, ionic liquids, and subcritical water. CNCs produced by oxidation comparatively possess higher colloidal stability, crystallinity, and uniform nanoscale dimension [39]. During CNC processing, disordered (amorphous) regions of cellulose are selectively degraded, while leaving the more acid resistant crystalline regions mostly intact to produce rod-shaped cellulose nanocrystalline particles [41–43]. Their dimensions depend on the cellulose source and type of the isolation process used. Consequently, their widths and lengths can vary from 5 to 20 nm and from 100 nm to 1–2 μm , respectively [44]. In polar solvents, CNCs do not flocculate due to electrostatic repulsion forces originating from their negative charges on the surface, which results in

stable suspensions for several months. One of the most interesting features originates from the ability of these suspensions to self-organize into stable, chiral nematic phases (characteristic for liquid crystals) that give the CNC suspension unique optical properties when a critical CNC concentration is reached [13]. The CNCs isolated by phosphoric acid (PCNCs) showed excellent flame-retardant properties due to the ability of the phosphate groups to enhance char formation, thus making PCNCs a self-extinguishing material. The incorporation of PCNCs in the nanocomposite foam also substantially improved the mechanical properties. Furthermore, PCNCs are also promising biomedical materials that can be used as a bone-scaffolding material [13,45,46]. Aside from weak acids, ionic liquids (ILs) are also used to isolate CNCs as well as other types of nanocellulose. ILs can be used alone or in combination with mineral acids, enzymatic treatment, or with physical treatment. The most suitable ILs are [BMIm]HSO₄ and [BMIm]Cl [13,47,48]. The production of nanocellulose using ionic liquids has many benefits including the usage of atmospheric pressure, small amounts of solvents, the regeneration of ionic liquids, and working with an odorless and relatively safe solvent. On the other hand, this method also has disadvantages that include the relatively high costs of ionic liquids and the unsatisfactory efficiency of the extraction process [49].

1.2. Cellulose Gels as Supports or Templates for Nanostructured Materials

1.2.1. Cellulose Hydrogels

Cellulose hydrogels are physically or chemically cross-linked three dimensional hydrophilic cellulose networks capable of absorbing large amounts of water (or biological fluids) and swelling. The hydrogel stability is ensured either by physical interactions (chain entanglements, van der Waals forces, hydrogen bonds, crystallite association, and/or ionic interactions) or chemical cross-links (covalent bonding) [50]. Aqueous CNC or MFC suspensions are generally characterized by their gel like properties due to the presence of long interconnected hydrophilic cellulose microfibrils and to intense interaction between the cellulose fibers or nanocrystals. The properties of bacterial cellulose (BC) hydrogels are unique and quite different from those based on plant cellulose because of its ultrafine network structure, high hydrophilicity, and high purity as well as culturing without using any cross linker. Cellulose-based hydrogels can be prepared from wastepaper or various cellulose-containing agricultural wastes. Hydrogels have been extensively studied for a wide variety of applications because their properties and chemical compositions can be easily manipulated. Frequently studied applications of hydrogels are biomedical applications such as drug delivery, wound dressings, and tissue engineering. Additionally, studies have reported evaluating cellulose-based hydrogels as water reservoirs and controlled release fertilizer carriers in horticulture and agriculture [51]. Lately, more technical applications of hydrogels have also been investigated. Cellulose-based hydrogels can be applied as various sensors [52–54], heat harvesting [55], fire prevention, and firefighting [56], or in cancer detection or therapy [57,58]. Moreover, cellulose-based composite hydrogels have been studied for the massive uranium extraction from seawater to cope with the severe shortage of onshore uranium reserves [59].

1.2.2. Cellulose Aerogels

Aerogels, on the other hand, are ultra-light weight and highly porous materials that are formed by the replacement of a liquid solvent in a gel by air. In this process, the volume of the gel body or the network structure is maintained, or in other words, the shrinkage phenomena are significantly reduced or eliminated. The interest in these materials originates from their strongly attractive characteristics including low density (typically between 0.004 and 0.500 g cm⁻³), high porosity (typically greater than 80%) as well as high specific surface area, low thermal conductivity, excellent shock absorption, and low dielectric permittivity [50,60].

Cellulose aerogels are prepared from aqueous cellulose suspensions—hydrogels. Subsequent replacement of water with air using freeze-drying (FD) or CO₂ supercritical drying

produces a porous material with the structure displaying entangled cellulose I nanofibers or nanocrystals. In general, the properties of the resulting material depend on several parameters including the initial cellulose nanofiber concentration, drying technique, speed of freezing the suspension before drying, and the chemical or enzymatic pre-treatment of the starting cellulose material. One of the main advantages of using cellulose nanofibers to form the porous material originates from the high reactivity of free hydroxyl groups on their surface. Consequently, the chemical functionalization of cellulosic aerogels represents an attractive approach to tailor the properties of these structures and further broaden their scope of applications. Thus far, two routes have been reported to obtain functionalized porous structures: (1) Preparing the aerogel and modifying it afterward, or (2) derivatizing the nanofibers prior to the formation of the aerogel [13]. Both approaches have been used for the formation of inorganic nanoparticles as well as their organized or assembled structures by applying cellulose as a template. The sources to produce cellulose aerogels are diverse, but cellulose-originated wastes, especially biomass and textile waste, are of primary interest since they are appropriate for the development of eco-friendly production technologies with the use of renewable feedstocks. Aerogels prepared from cellulose-rich waste are biodegradable, easy to functionalize for different uses, and are inexpensive due to the abundance of raw materials [61]. Cellulose aerogels have a wide area of potential applications such as particle filters, particle trappers, catalyst supports, and heat insulators [62,63] and have been evaluated for their capability to remove various pollutants from an aqueous medium [61,64,65]. Additionally, the application of cellulose aerogels for oil absorption applications has also been investigated [66]. Furthermore, cellulose composite aerogels with inorganic nanostructures have also studied been as antibacterial materials for their application in medicine [67,68]. Moreover, a polydopamine-filled cellulose aerogel was developed and studied as a device for seawater and wastewater purification [69]. Another type includes composite aerogels (i.e., cellulose aerogels combined with other materials such as Ag nanowires), which are used to produce materials with a unique combination of mechanical, electrical, magnetic, and thermal properties for application in EMI shielding, electrical switches, and solar–thermal energy conversion [70,71].

The successful design and formation of inorganic nanostructures require effective and convenient methods for their fabrication. In this context, the synthesis of nanomaterials from biopolymers as the templates is a promising approach, which enables the design of complex hierarchical material systems or nanodevices. Celluloses and nanocelluloses are particularly attractive as bio-templating materials because of their highly interactive surface due to a large number of reactive hydroxyl groups that can efficiently nucleate inorganic phases around the rod-like cellulose structures. Cellulose fibers and cellulose nanostructures are supposed to direct the formation, growth, and patterning of inorganic materials to produce various types of nanostructures (nanoparticles, nanowires, or nanotubes) with unique combinations of optical, electrical, and catalytic properties [13]. High open porosity, large surface area, and high mechanical strength make any form of cellulose almost an ideal candidate for the supporting medium in the synthesis of nanostructures.

Recent progress reported in the scientific literature suggests that a synergetic use of the cellulose (nano)fibers together with suitable functionalization pathways will constitute a breakthrough in the formation of templated metallic- and metal oxide hierarchical nanostructures in the near future. Therefore, this review focuses on the utilization of cellulose and nanocellulose materials as templates or building blocks for the formation of nanomaterials and hierarchical functional materials. It provides a review of the applications of any form of cellulose as a template, supporting medium, or growing vector for the formation of inorganic nanostructures. With respect to the presence of cellulose in the final product, these applications can be divided into two groups: cellulose-supported structures and pure inorganic cellulose-templated structures. The first group comprises the publications reporting on the nanostructures where cellulose remains a constitutive component of the final nanocomposite structure, whereas the second group constitutes the publications dealing with the formation of metallic- or metal oxide nanostructures followed by subsequent

elimination of the cellulose by calcination, resulting in pure inorganic structures. A special subgroup represents the inorganic nanostructures supported by carbon fibers formed from cellulose fibers by calcination in an inert atmosphere. These two main groups can be further divided based on a type of inorganic material into: metallic nanostructures, metal oxide nanoparticles, metal sulfide and other inorganic compound nanostructures as well as complex hybrid structures containing various metallic and/or metal oxide nanoparticles. For this reason, the review section is divided into five chapters: (2) Cellulose supported metallic nanoparticles; (3) cellulose supported metal oxide nanostructures; (4) cellulose templated pure metal oxide nanostructures; (5) cellulose supported/templated nanostructures of metal sulfides, hydroxyapatites, and other inorganic compounds; and (6) cellulose supported/templated hybrid nanostructures. Each chapter is further organized with respect to the size of the cellulose structures used as a support/template: macrostructured cellulose (cellulose fiber and fibril—CF, regenerated cellulose—RC); microstructured cellulose (microcrystalline cellulose—MCC, microfibrillated or nanofibrillated cellulose—MFC); and nanostructured cellulose (bacterial nanocellulose—BNC, cellulose nanofibril—CNF, cellulose nanocrystal—CNC). The number of publications reporting on cellulose supported or templated inorganic nanostructures in the last 20 years numbers in the hundreds or even thousands. Many research groups have reported on the outstanding capability of any form of cellulose to stabilize and support the growing inorganic nanostructures, thus forming hierarchical nanostructures with exceptional combinations of properties that are practically impossible to prepare in any other way. A large number of publications have suggested that a review is necessary to identify and monitor the trends of where this research area is heading and to list the achievements produced. There have been about ten different review articles published in the last ten years dealing with cellulose and inorganic materials, however, they are limited either by the type of cellulose or by the type of inorganic nanostructures or by the application area of these hybrid nanomaterials. Therefore, this publication offers a review over a wide range of cellulose structures (from cellulose fibers to cellulose nanocrystals) and a wide range of cellulose supported or templated inorganic nanostructures (metals, metal oxides, metal sulfides, hybrid inorganic nanostructures) as well as a wide range of the various application areas of these hierarchical nanomaterials.

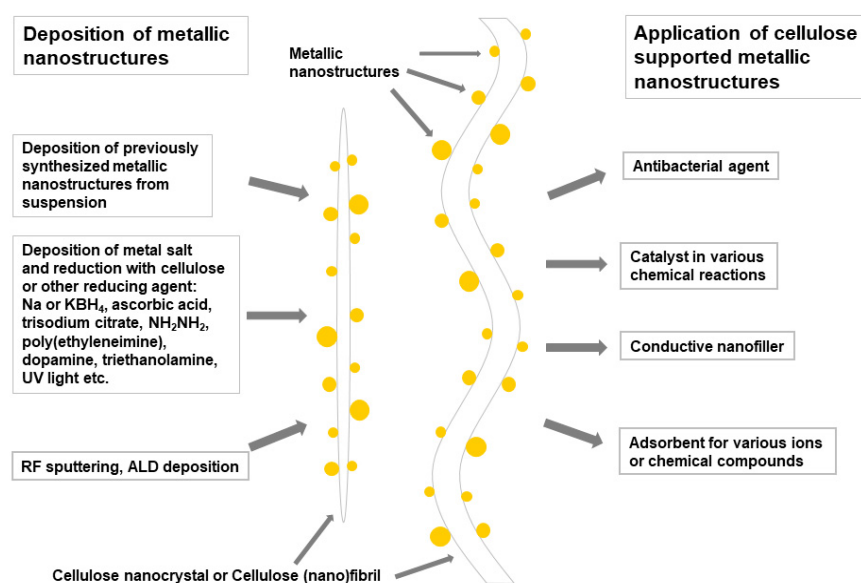
2. Cellulose Supported Metallic Nanostructures

Various procedures of the formation of metallic nanostructures on the surface of cellulose have been reported. Authors have frequently used nanocellulose as a metallic nanoparticle support, but other forms of cellulose, even native cellulose fibers, are also useful for this purpose. With respect to the type of metal, mostly noble and particles of some transition metals are deposited on the cellulose surface.

The most abundant metal studied is Ag since it has strong antibacterial activity and together with cellulose structures, it represents almost ideal material for wound dressings or other biomedical applications. There is a substantial number of publications on this topic [72]. Aside from cellulose–Ag, cellulose–Au hybrid materials have also been extensively studied [73]. Cellulose–Au hybrid materials are very attractive due to their chemical inertness and high resistance toward oxidation, making them interesting materials for biomedical applications. Additionally, Ag and Au have been studied as antiviral agents and their hybrid materials with cellulose can be applied in disinfectant wipes or as anti-viral layers in facemasks [74]. This potential application is highly important in the time of the COVID-19 pandemic. Cellulose structures decorated with Pt or Pd nanostructures are lightweight, flexible, environmentally-friendly membranes with strong catalytic activity. Many of the cellulose supported metallic nanostructures have shown strong catalytic activities for numerous chemical reactions [75]. Additionally, these lightweight hierarchical cellulose metallic nanostructures have potential applications in electronics, electro-optics, and chemical sensing. The ether oxygen and the hydroxyl functional groups of the cellulose anchor metal ions tightly on the cellulose fibers via ion–dipole interactions. They also stabilize metallic nanoparticles by the strong bonding interaction with the particle surface, thus

enabling the formation of hierarchical metallic nanostructures that are otherwise almost impossible to prepare. Due to the strong interaction between the forming nanoparticles and the cellulose surface, the agglomeration and Ostwald ripening of these nanoparticles are generally prevented. Many authors have reported that cellulose itself possesses reducing properties and the capability to reduce the salts of noble metals to the metallic state, but in most cases, the authors have used reducing agents to form metallic particles on the surface of cellulose.

The presentation of the versatility of cellulose substrates, the formation processes of the metallic particles, and the potential application of these hierarchical structures is shown in Scheme 1.



Scheme 1. Schematic representation of the cellulose/metallic particle nanocomposites, synthetic routes, and their most frequent applications.

2.1. Cellulose Supported Noble Metallic Nanostructures

Cellulose in any form has been applied as a support or template in the formation of various metallic nanostructures including noble (Ag, Au, Pt, Pd) as well as other transition (Co, Ni, Cu) metals [25]. Theoretically, by using strong reducing agents such as H_2 or $NaBH_4$, any metallic particles, even metallic Fe, can be formed on the cellulose support. On the other hand, noble metals can be reduced to the metallic state by cellulose itself or by using mild biobased reducing agents such as leaf extracts [76].

Various methodologies to synthesize gold and silver nanoparticles on the surface of the cellulose fibers have been explored and compared. Treatment of the cellulose fibers with an alkaline solution of $H AuCl_4$ or $AgNO_3$ led to the growth and deposition of Au and Ag nanoparticles on their surface. When the cellulose fibers were treated with lecithin or surface modified with thiol, a high temperature was not essential for the growth of nanostructures on the cellulose. With such treatment and modification, uniform metallic nanoparticles were obtained in relatively high yields (~43 wt.% of Au on the cellulose fibers modified with thiol) at room temperature. Reduction with borohydride resulted in substantially lower loading (~22 wt.%) and a wide size distribution of Au and Ag nanostructures on the cellulose fibers. These hierarchical structures were studied as catalysts in the reduction of 4-nitrophenol into 4-aminophenol. Thiol modified cellulose–gold nanoparticle composites quantitatively reduced 4-nitrophenol into 4-aminophenol in 90 min in the presence of $NaBH_4$ [77].

Silver nanoparticles (AgNPs) synthesized with four different processes were studied as a disinfectant for cellulose-based wipes. These four techniques are: (1) cotton yarn as a reducing agent with trisodium citrate; (2) cotton fabric as a reducing agent with trisodium

citrate; (3) an aqueous solution of PVA in the presence of glucose as a reducing agent; and (4) the photochemical reaction of polyacrylic acid in a AgNO_3 solution. The prepared AgNPs with particle sizes between 10 and 70 nm were deposited on cellulose fabrics to be used as wipes for the disinfection of surfaces. The assessment of active solutions of silver nanoparticles for the antiviral and antimicrobial activities was evaluated. The results showed a significant effect of the AgNP preparation process on their disinfectant performance. The evaluation of antimicrobial and antiviral activities proved their effectiveness against fungi (*A. niger* and *C. albicans*), coronavirus (MERS-CoV) as well as bacteria (*E. coli* and *P. mirabilis* as Gram-negative bacteria, *S. aureus* and *B. subtilis* as Gram-positive bacteria). The AgNPs prepared by using cotton fabric as a reducing agent (2) showed the highest antiviral activity with 51.7% viral inhibition at 0.0625 μL with moderate cytotoxicity activity. Disinfectant cellulose-based wipes treated with antimicrobial and antiviral silver nanoparticles were successfully prepared to be applied for the prevention of the contamination and transmission of several pathogenic viruses (coronavirus) and microbes to humans in critical areas such as hospitals and health care centers [78].

Flexible and highly-porous cellulose sponges (CS)-based on the microfibrillated cellulose were prepared by cross-linking with γ -glycidoxypropyltrimethoxysilane (GPTMS) and polydopamine (PDA) and were applied as a support for the synthesis of Pd nanostructures (Pd NPs) (Figure 1). Catechol moieties of polydopamine formed chelates with Pd ions, enabling the nucleation and thus governing the growth of Pd nanostructures on the PDA modified cellulose fibers. The resulting spherical Pd NPs with a narrow particle size distribution between 2 and 6 nm were homogeneously dispersed on the surface of the cellulose fibers. The formed Pd NPs supported by CS exhibited a high catalytic activity in the Suzuki and Heck cross-coupling reactions with almost no leaching of Pd as well as good recyclability. The reported nanostructures represent an innovative approach toward the formation of highly effective, non-leaching, and recyclable metallic heterogeneous catalytic systems [79].

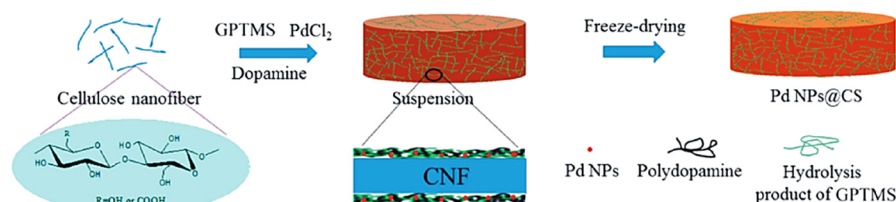


Figure 1. The schematic of the formation of Pd NPs supported by cellulose sponges. Reprinted with permission from [79]. Copyright 2017 American Chemical Society.

Microcrystalline cellulose was applied as a cellulose support in the microwave-assisted synthesis of Ag nanostructures from the AgNO_3 precursor using ascorbic acid (AAc) as a reducing agent to prepare cellulose–Ag nanocomposites. The properties of the nanocomposites were studied as a function of the microwave heating time and AAc concentration, and the average particle size of the Ag nanostructures varied between 50 and 250 nm. The results confirmed that the AAc concentration played an important role in the nanostructure formation, and a homogeneously decorated cellulose surface by Ag nanostructures was obtained. Since such a microwave-assisted method can be carried out without any seed or surfactant, it represents a fast and convenient approach to a cost-effective and large-scale production of cellulose–Ag nanocomposites [80].

A novel method was developed to synthesize and deposit silver nano particles (Ag-NPs) on the surface of bacterial cellulose (BNC) by applying polyvinyl alcohol (PVA) to form a nano porous matrix and to reduce the cytotoxicity of the deposited silver nanoparticles in comparison with those synthesized by the chemical reduction. Polyvinyl alcohol was used to reduce the absorbed silver ions (Ag^+) on the surface of the BNC to the metallic silver nanoparticles (Ag^0). The size and size distribution were controlled by adjusting the molar ratio of PVA: AgNO_3 . At the optimized reaction conditions, well dispersed and regular

spherical AgNPs were formed with particle sizes ranging from 15 to 35 nm. The AgNPs displayed an optical absorption band around 420 nm. The cytotoxicity of these AgNPs were determined by using the MTT assay and the IC_{50} values to demonstrate the effect of the AgNP preparation method on the cytotoxicity of the formed AgNPs on the A549 viable cells. The results showed that PVA and BNC significantly reduced the concentration of Ag^+ ions on the contact surface with A549 cells, thus significantly reducing the cytotoxicity of the so-prepared hybrid AgNPs–PVA–BNC materials [81].

An innovative cellulose–palladium nanocatalytic system (cell-OOCPhPPH₂-Pd) has been developed using a convenient synthesis approach and simple precursors. Microcrystalline cellulose (MCC) was first tosylated and further reacted with 2-(diphenylphosphino) benzoic acid to produce microcrystalline cellulose–phosphinite. This modified MCC was then reacted with Pd(OCH₃)₂ to produce Pd doped MCC–phosphinite. Pd nanostructures have sizes from 1 to 5 nm and showed high activity in C–H activation as well as in three other types of cross-coupling reactions (Suzuki–Miyaura, Heck, and Sonogashira). All types of transformations were carried out with a single type of nanocatalyst and the yields were higher than 60%. The reaction products contained low Pd residues and the studied catalyst was readily recycled by simple filtration without significant loss in the catalytic activity, even after several runs. The above features suggest that this catalyst is highly promising for applications in the pharmaceutical industry [82].

Innovative composites of bacterial cellulose and Au nanoparticles were formed by a single-step biotemplated process in an aqueous suspension by applying polyethyleneimine (PEI) as a reducing agent. The thickness of the Au shell in the Au–BC nanocomposites was controlled by adding various halides, while the PEI, adsorbed to the surface of the BC nanofibers via hydrogen bonding, functioned both as a reducing agent and as a linker for the Au nanostructures. The average particle size of the grown Au nanoparticles was between 5 and 20 nm. Subsequently, horseradish peroxidase (HRP) was embedded into the fibrous structure of the Au–BC nanocomposites without any reduction in its bioactivity. Thus, the prepared HRP biosensor demonstrated a highly-sensitive detection of H₂O₂ with a detection limit close to 1 μ M. The obtained Au–BC nanocomposites offer a promising support for the immobilization of other enzymes and enable biosensor fabrication for a wide range of applications in bioelectrocatalysis and bioelectroanalysis [83].

On many occasions, the authors used surfactants as stabilizers or agents for positioning particles on the cellulose surface. For example, tunicate CNCs were modified on their surface with metallic nanoparticles using the cationic surfactant cetyltrimethylammonium chloride (CTAB), which served as a stabilizer of the metallic nanoparticles and as a distributing agent for the nanoparticles on the surface of the CNCs (Figure 2). This synthetic path enabled the effective formation of Pt, Au, Cu, and Ag nanoparticles on the surface of the CNCs. With respect to the particle size distribution, the nanoparticles were polydisperse, which was ascribed to the competition of two processes, nucleation and particle growth, which governed their formation. The nanoparticles' average size (5–20 nm) and the thickness of the metallic layer on the CNCs were both controlled by the pH of the salt solution, the reduction time, and the concentration of CTAB. The applied CTAB stabilized the metallic nanoparticles and increased their interaction with the cellulosic substrate, resulting in the enhanced coverage of the surface of the CNCs with metallic nanostructures [16].

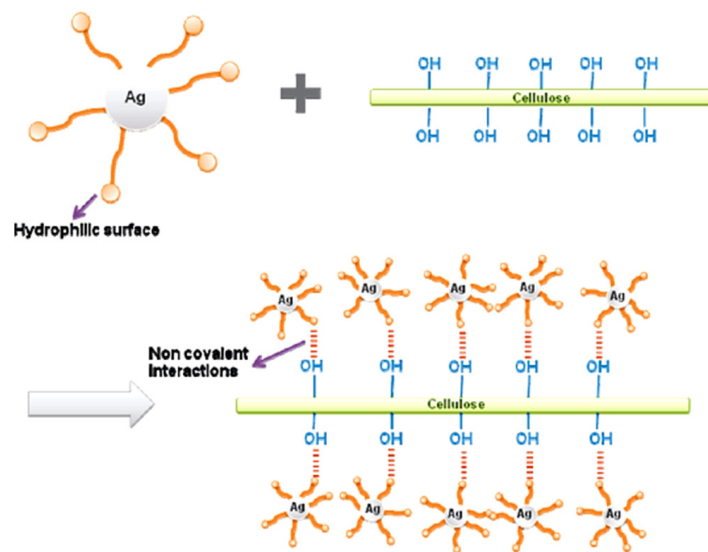


Figure 2. The synthesis mechanism for the formation of Ag nanoparticles on the surface of the CNCs. Reprinted with permission from [16]. Copyright 2010 American Chemical Society.

CNCs were used as a support to synthesize gold nanoparticles (Au NPs) by heating the aqueous mixture of polyethylene glycol, CNCs, and HAuCl_4 at $80\text{ }^\circ\text{C}$ for 1 h. In this way, extreme conditions and toxic chemicals as well as a complicated procedure were avoided (Figure 3). The prepared CNC-supported Au NPs demonstrated high catalytic activity for the reduction of 4-nitrophenol using sodium borohydride. The maximum turnover frequency and the apparent rate constant reached 641 h^{-1} and $1.47 \times 10^{-2}\text{ s}^{-1}$, respectively. Due to the large concentration of highly dispersed Au NPs (average size 2–15 nm) that was deposited onto the CNC surface, a high catalytic performance was observed. The reported procedure proved to be environmentally-friendly, low-cost, and simple and has a large potential in medical and industrial applications [84].

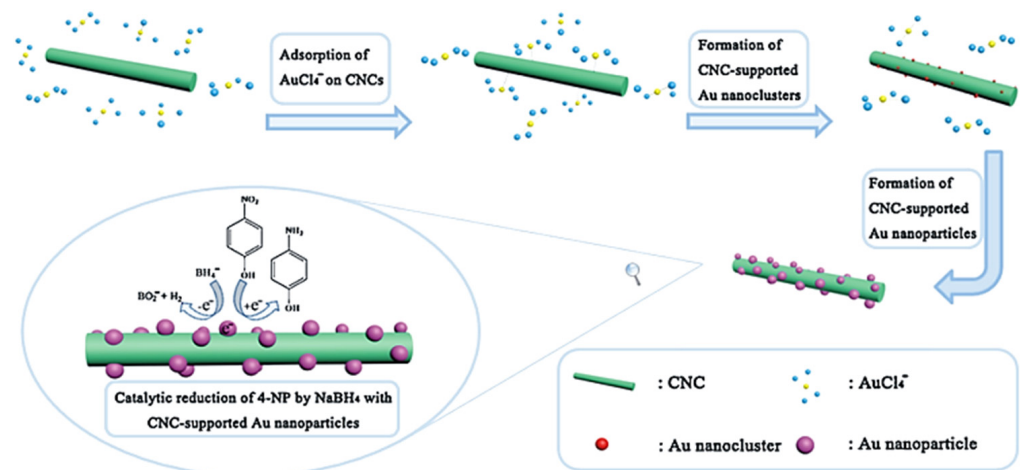


Figure 3. The schematic illustration of the formation process of CNC-supported Au NPs and their catalytic activity in the reduction of nitrophenol. Reprinted from [84]. Copyright 2015, with permission from Elsevier Ltd.

2.2. Cellulose Supported Non-Precious Metallic Nanostructures

Aside from noble metal nanoparticles, semi- and non-precious metallic nanoparticles have also been successfully formed on the surface of various cellulose structures. A green synthetic approach to prepare cobalt/cellulose nanocomposites with antibacterial and magnetic properties has been developed by the in situ reduction of cobalt nitrate

on the substrate surface using hydrogen gas or NaBH_4 as reducing agents. Spherical, cellulose-stabilized cobalt metallic nanoclusters with an average diameter of 7 nm were formed with cubic cobalt (α -cobalt) as the main component when hydrogen gas was used as a reducing agent. The cellulose-stabilized, metallic cobalt nanoclusters were homogeneously distributed on the surface of the cellulose fibers. The cobalt/cellulose nanocomposites were contaminated with almost insignificant traces of boron. In contrast, the in situ reduction of cobalt ions on the cellulose surface with sodium borohydride leads to amorphous cobalt/cellulose composites with a significant contamination of boron. All of the cobalt/cellulose nanocomposites showed significant antibacterial action against the tested bacterial isolates [85].

CNCs were used as a support in the growth of copper nanoparticles (Cu NPs) by the reduction of $\text{CuSO}_4 \cdot 5\text{H}_2\text{O}$, representing an environmentally-friendly, low-cost, and simple preparation method. Aqueous NaOH, ascorbic acid, and hydrazine were used as the pH controller, antioxidant, and reducing agent, respectively. The product was high purity spherical Cu NPs with the average size of ~ 3 nm. Compared to the unsupported Cu NPs, the reported Cu NPs–NCC demonstrated superior catalytic activity and high sustainability for the reduction of methylene blue in an aqueous solution of NaBH_4 at RT. The prepared Cu NPs–NCC quantitatively reduced the methylene blue in the reaction time of 12 min with the rate constant of 0.7421 min^{-1} and the correlation coefficient (R^2) of 0.9922 [86].

CNCs were applied as a support in the formation of metallic iron nanoparticles (Fe NPs, 3–10 nm or 15–40 nm, depending on the quantity of CNCs) by an environmentally-friendly single-step procedure. Hydroxyl groups on the surface of the CNCs served as anchor points for the stabilization of Fe NPs and as a reducing agent in the growth of Fe NPs. Additionally, CNCs acted as corrosion inhibitors for metallic Fe NPs and increased their catalytic activity since they retained the metallic state even after 5 days of air exposure. The CNC-stabilized Fe NPs exhibited a catalytic activity toward the methylene blue degradation. It was demonstrated to be a promising and nontoxic nanocatalyst for the hydrogenation reaction of 4-nitrophenol into 4-aminophenol. Additionally, the autonomous motion of the CNC-supported Fe NPs was observed in the presence of H_2O_2 and their trajectories were controlled externally by the pH gradient and magnetic field. It was demonstrated that their speed and controlled trajectory could be remotely tuned, making these nanomotors potential innovative nanomachines in drug delivery, imaging applications, and as sensors [87].

The number of publications on metallic nanostructures supported and templated by cellulose structures is vast and not all of them can be included within this review. Therefore, the additional information on publications dealing with the cellulose-metallic nanostructures is summarized in Table 1. Most commonly, the cellulose is decorated or coated with noble metal (Au and Ag) nanostructures and the most widely used reducing agent is NaBH_4 , or simply cellulose itself, while frequent applications of these hierarchical structures are in catalysis, medicine (as antibacterial agents), and electronics (as conductors) (Table 1). The most common method of deposition is the adsorption of metallic ions to the cellulose surface and their subsequent reduction to metallic particles. Alternative approaches include the separate formation of metallic nanoparticles and their subsequent deposition to cellulose fibers, or physical methods such as atomic layer deposition or plasma sputtering.

Table 1. The list of publications on cellulose supported metallic nanostructures. The list is organized from large cellulose structures (CF and RC) via microstructured celluloses (MCC and MFC) to nanostructured celluloses (BNC and CNCs).

Inorg. Particle (Size—nm)	Cellulose Used	Precursor (Synthetic Path)	Application	Reference
Precious Metallic Cellulose Supported Nanostructures				
Au NPs (~2 nm)	CF	Bis(ethylenediamine) Au(III)Cl ₃ , (CH ₃) ₂ Au(III) acetylacet.,(red.by NaBH ₄)	Catalyst (glucose oxidation)	[88]
Ag NPs (8–20 nm)	RC	AgNO ₃ (hydrothermal reduction)	Catalyst (reduction of 4-nitrophenol)	[89]
Au NPs (<5 nm)	MFC	HAuCl ₄ (reduction by NaBH ₄)	Catalyst (reduction of 4-nitrophenol)	[90]
Au–Ag NPs	MFC		Conductive nanofiller	[91]
Au–Pd NPs (4–9 nm)	MFC	HAuCl ₄ , [Pd(NH ₃) ₄].Cl ₂ (reduction by NaBH ₄)	Catalyst (reduction of 4-nitrophenol)	[92]
Au/Ag NPs	BNC	HAuCl ₄ , AgNO ₃ (reduc. by poly(ethyleneimine))	-	[93]
Au NPs	BNC	HAuCl ₄ (reduction by cellulose)	Conductive nanofiller	[94]
AuNR@AgNCs	BNC	HAuCl ₄ , NaBH ₄ , AgNO ₃ , CTAC	SERS–detection of TNT	[95]
Au NPs (2–10 nm)	CNCs	HAuCl ₄ , trisodium citrate, oleylamine, mercaptocation	Chiral photonic materials	[96]
Au NPs (20–30 nm)	CNCs	HAuCl ₄ , NaOH (reduction by CNCs)	Photothermal nanocomposite materials	[97]
Au NPs (30.5 nm)	CNCs	HAuCl ₄ (reduction by cellulose)	Catalyst (reduction of 4-nitrophenol)	[98]
Au NPs (4.5–7.1 nm)	CNCs	HAuCl ₄ (reduction by NaBH ₄)	Biosensor (for 2-mercaptoethanol)	[99]
Au NPs (2–3 nm)	CNCs	HAuCl ₄ (reduction by—HS groups on the CNC surface)	Catalyst (alkyne–aldehyde–amine-coupling)	[100]
Au NPs (2–4 nm)	CNCs	HAuCl ₄ (reduced with no and by NaBH ₄)	Catalyst (reduction of 4-nitrophenol)	[101]
Au NPs (~3 nm)	CNCs	HAuCl ₄ (reduction by NaBH ₄)	Catalyst (reduction of 4-nitrophenol)	[102]
Au, Ag NPs	CNCs	HAuCl ₄ , AgNO ₃ , ascorbic acid	Catalyst (reduction of 4-nitrophenol, 4-aminophenol)	[103]
Au NPs(30–80 nm)	CNF	HAuCl ₄ , Na ₃ Cit·2H ₂ O	Substrate–SERS spectroscopy	[104]
Au NPs (30–80 nm)	CNCs	HAuCl ₄ , K ₂ CO ₃ , NaOH	Seeds for Au coating of CNCs with tunable optical properties	[105]
Au NPs (35 nm)	CNCs	HAuCl ₄ (reduction by trisodium citrate)	Sorption and detection of Au nanoparticles in H ₂ O	[106]
Pt NPs (1–5 nm)	CF	H ₂ PtCl ₆ , Na rhodizonate	Catalyst (reduction of 4-nitrophenol, methyl orange)	[107]
Pt NPs	CNF	H ₂ PtCl ₆ , (reduction by NaBH ₄)	Catalyst (reduction of 4-nitrophenol)	[108]
Pt NPs (5–30 nm)	CNCs	H ₂ PtCl ₆ (reduction by CNCs)	—	[109]
Pt NPs (11–101 nm)	CNCs	H ₂ PtCl ₆ (reduction by wood nanomaterial)	Catalyst (reduction of 4-nitrophenol)	[110]
Pt NPs (~2 nm); Pd NPs (~20 nm)	CNCs	H ₂ PtCl ₆ (reduction by CNCs)	Electrocatalyst (oxygen reduction)	[111]
Pd NPs (~20 nm)	BNC	PdCl ₂ (reduction by KBH ₄)	Catalyst (Heck reaction)	[112]
Pd NPs (~20 nm)	BNC	K ₂ PdCl ₄ (reduction by NaBH ₄)	Catalyst (Suzuki–Miyaura reaction)	[113]
Pd NPs (3.6 nm)	CNCs	PdCl ₂ (reduction by H ₂)	Catalyst (hydrogenation of phenol; Heck Coupling)	[114]
Pd NPs (1–7 nm)	CNCs	PdCl ₂ (reduction by CNCs)	Catalyst (red. of methylene blue and 4-nitrophenol)	[115]

Table 1. Cont.

Inorg. Particle (Size—nm)	Cellulose Used	Precursor (Synthetic Path)	Application	Reference
Precious Metallic Cellulose Supported Nanostructures				
Pd-Cu NPs	BNC	PdCl ₂ and CuCl ₂ (reduction by KBH ₄)	Catalyst (water denitrification)	[116]
Ru NPs (~8 nm)	MFC	RuCl ₃ (reduction by NaBH ₄)	Catalyst (aerobic oxidation of benzyl alcohol)	[117]
Ag-Au NPs (8–10 nm)	CF	AgNO ₃ , HAuCl ₄ , NaOH, urea	Antibacterial agent	[118]
Ag NPs	CF	RF sputtering	Antibacterial agent	[119]
Ag NPs (3–15 nm)	MCC	AgNO ₃ , UV light reduction	Catalyst (reduction of p-nitrophen. to p-aminophen.)	[120]
Ag NPs (~6 nm)	MFC	AgNO ₃ (reduction by NaBH ₄)	Catalyst (reduction of rhodamine B)	[121]
Ag nanowires	MFC	Previously formed Ag nanowires	Conductor in transparent nanopaper	[122]
Ag NPs (3–4 nm)	MFC	AgNO ₃ , UV light triggered reduction by MFC	Aerogels	[123]
Ag nanowires	MFC	Previously formed Ag nanowires	Conductive nanofiller	[124]
Ag NPs (~4 nm)	MFC	AgNO ₃ (reduction by NaBH ₄)	Catalyst (aza-Michael reaction)	[117]
Ag NPs (~6 nm)	MFC	AgNO ₃ (reduction by NaBH ₄)	Antibacterial agent	[125]
Ag nanowires	MFC	-	Conductive nanofiller	[126]
Ag NPs	BNC	AgNO ₃ (reduction by sodium citrate)	SERS substrate-pesticides detection	[127]
Ag NPs (var. sizes)	CF, MCC, CNCs	AgNO ₃ , (reduction by cellulose)	-	[128]
Ag NPs (<10 nm)	BNC	AgNO ₃ (reduction by NaBH ₄)	Antibacterial agent	[129]
Ag NPs (17 nm)	BNC	AgNO ₃ (reduction by cellulose)	Antibacterial agent	[130]
Ag NPs (~30 nm)	BNC	AgNO ₃ (red. by NH ₂ NH ₂ , NH ₂ OH, ascorbic acid)	Antibacterial agent	[131]
Ag NPs (8–15 nm)	BNC	AgNO ₃ (reduced by triethanolamine)	Antibacterial agent	[132]
Ag NPs (~16 nm)	BNC	AgNO ₃ , (reduction by BNC)	Antibacterial agent	[133]
Ag NPs (5–50 nm)	CNFs	AgNO ₃ (reduction by Na citrate)	Flusilazole adsorption and analysis	[134]
Ag NPs	CNFs	AgNO ₃ (reduction by Na citrate)	SERS probe for carbendiazim	[135]
Ag NPs (10–50 nm)	CNCs	AgNO ₃ (reduction by CNC)	Electrocatalyst (reduction of oxygen)	[136]
Ag NPs (<10 nm)	CNCs	AgNO ₃ (reduction by NaBH ₄)	DNA biosensor	[137]
Ag NPs (10–15 nm)	CNCs	AgNO ₃ (reduction by NaBH ₄)	Antibacterial agent	[138]
Ag NPs (1 nm–10 μm)	CNCs	AgNO ₃ (reduction by CNCs)	Antibacterial agent	[139]
Ag NPs (20–45 nm)	CNCs	AgNO ₃ (reduction by CNCs)	Antibacterial agent	[140]
Ag NPs (2–3 nm)	CNCs	AgNO ₃ (reduction by NaBH ₄)	—	[141]
Ag NPs (~10 nm)	CNCs	AgNO ₃ (reduction by dopamine)	Catalyst (reduction of 4-nitrophenol)	[142]
Ag NPs (~7 nm)	CNCs	AgNO ₃ (reduction with dopamine hydrochloride)	Antibacterial agent	[143]
Ag NPs (10–80 nm)	CNCs	AgNO ₃ (reduction by NaBH ₄)	—	[144]
Ag NPs (1–2 nm)	CNCs	Ag wire and AgNO ₃ (reduction by CNCs)	Catalyst (hydrogenation of aldehydes, nitrophenol, alkenes and alkynes)	[145]
Ag NPs (10–50 nm)	CNCs	AgNO ₃ (reduction by NaBH ₄)	Plasmonic activators for shape memory polymers	[146]

Table 1. Cont.

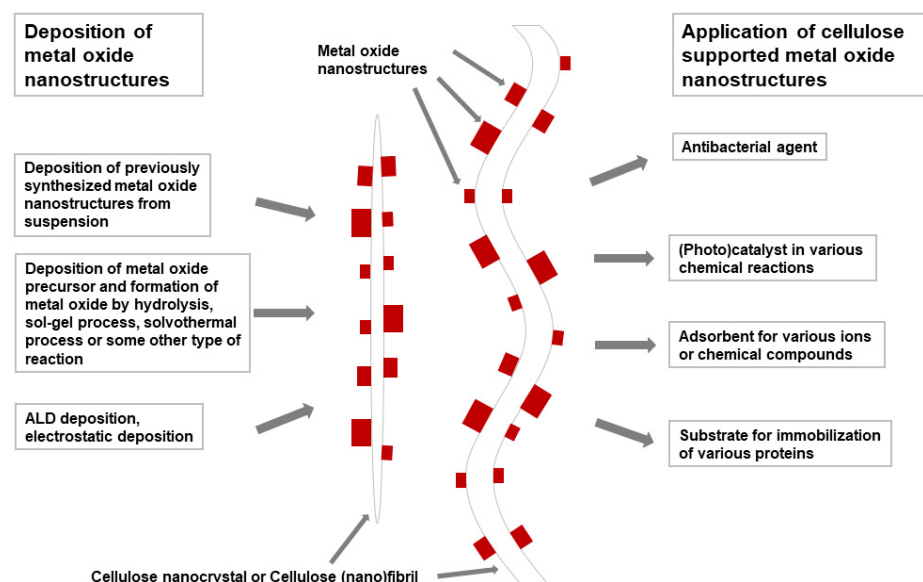
Inorg. Particle (Size—nm)	Cellulose Used	Precursor (Synthetic Path)	Application	Reference
Semi- and non-precious cellulose supported metallic nanostructures				
Cu NPs	CF	CuSO ₄ , poly(ethylenimine)	-	[147]
Cu NPs (~5 nm)	MFC	CuCl ₂ (reduction by ascorbic acid)	Catalyst for the reduction of 4-nitrophenol	[148]
Cu NPs	CNCs	Cu(OCOCH ₃) ₂ , NaOH (reduction by ascorb. acid)	Conductive nanofiller	[149]
Cu NPs (50 nm)	CNCs	CuSO ₄ , (reduction by ascorbic acid and NaBH ₄)	Catalyst for C–N coupling reactions	[150]
Cu NPs (10–20 nm)	CNCs	CuSO ₄ (reduction by hydrazine)	Catalyst for oxidation of sulfides and alcohols	[151]
Fe NPs (200–300 nm)	CF	FeSO ₄ (reduction by NaBH ₄)	Adsorbent for Cd(II) ions	[152]

3. Cellulose Supported Metal Oxide Nanostructures

Cellulose structures were used as supports and templates for the formation of various metal oxide nanostructures. In contrast to metallic nanostructures that are mainly limited to noble or semi-noble metals, practically any type of metal oxide can be deposited on the cellulose surface with TiO₂, Fe₃O₄, and ZnO being the most abundant. For this purpose, various cellulose types have been applied, spanning from natural cellulose fibers to cellulose nanocrystals in the original or chemically modified form.

Various metal oxide nanostructures were deposited or formed on the cellulose surface that serves as the support and template in the formation of nanostructures. By using cellulose templates, various hierarchically organized nanostructured metal oxide particles were synthesized. The most widely used metallic oxides have been TiO₂, ZnO, Fe₃O₄, and Fe₂O₃. Using cellulose as a support enables the formation of lightweight, highly flexible, porous, mechanically resistant, and environmentally-friendly structures accompanied with interesting catalytic, electronic, optical, magnetic, and antibacterial properties. The principal application of such structures have been found in heterogeneous catalysis and in the removal of toxic heavy metal ions (Pb²⁺, As⁵⁺, Mn²⁺, and Cr³⁺) from water. In particular, for the latter application, cellulose structures are particularly suitable since a comparison of the heavy metal ion absorption capacities of various inorganic sorbents and organically-modified cellulose structures is significantly in favor of the latter ones [153]. Cellulose gels with their specific structure, high specific surface, and porosity as well as a high concentration of functional groups are very suitable for the removal of various pollutants from water [153]. The incorporation of various inorganic compounds into cellulose gels enhances the pollutant removal capability and efficiency, and introduces a specific affinity toward certain pollutants. Aquatic pollutants that can be removed in this way comprise various metal ions, organic dyes, and some anions. Additionally, the ZnO/cellulose hierarchical nanostructures show a high applicative potential in medicine as wound protective materials due to the antibacterial properties of nano ZnO. Moreover, CuO, Cu₂O, ZnO, and TiO₂ were studied as antiviral agents and their hybrid materials with cellulose are potentially applicable in disinfectant wipes or as anti-viral layers in facemasks [74]. For example, CuO showed an intense antiviral activity and such hybrid nanomaterials were applied as an antiviral protection layer in respiratory facemasks. The practical tests demonstrated that CuO impregnated masks safely reduced the risk of influenza virus environmental contamination without altering the filtration capacities of the masks and that the manufacture of the mask with CuO layers would not add any significant costs to the price of such masks [154]. These applications are highly important nowadays, leading to the development of masks with improved protection against COVID-19. On the other hand, Fe₃O₄/cellulose structures are lightweight, flexible, magnetic materials that offer a wide range of potential applications. Cellulose can stabilize not only the metallic nanoparticles, but also the metal oxide nanoparticles by the strong bonding interaction of

metal oxide nanoparticles with the cellulose surface, enabling the formation of hierarchical metallic oxide nanostructures that are otherwise practically impossible to prepare. The presentation of the versatility of cellulose substrates, the formation processes of metal oxide nanostructures, and the potential applications of these hierarchical structures is given in Scheme 2.



Scheme 2. The schematic representation of the cellulose/metal oxide particle nanocomposites, the synthetic routes, and the most frequent applications of such materials.

3.1. Cellulose Supported TiO_2

The most frequently used metallic oxide for the decoration of the cellulose surface is TiO_2 , since it offers various functionalities (photocatalytic activity, energy conversion, heavy metal absorption, etc.) and a broad range of potential applications including self-cleaning and dynamically responsive materials. Rutile TiO_2 nanoparticles (average particle size 100–250 nm) have been prepared via in situ synthesis using cellulose fibers as a support to form cellulose fiber/nano- TiO_2 composites. Additionally, CF/ TiO_2 was also prepared by the electrostatic deposition of commercial TiO_2 . Subsequently, composite membrane beds were prepared using a wet-laid procedure. After this, the dynamic Pb^{2+} adsorption was studied by passing the feed solution through the prepared beds using a single-pass flow mode. The impacts of parameters such as the bed stacking pattern, flow rate, and bed height on the bed breakthrough performance were studied. The results demonstrated that the CF/in situ- TiO_2 bed had more favorable characteristics than the others, since its Pb^{2+} loading capacity was 9-times higher than that of the CF/self-assembled TiO_2 bed and 13-times higher than that of the pure CF bed before 10% breakthrough occurred. Moreover, this bed showed high selectivity for Pb^{2+} toward Ca^{2+} , and was easily regenerated for repeated use by rinsing with 0.1 M HCl solution. The excellent performance of the in situ- TiO_2 /CF bed was ascribed to its faster adsorption kinetics and larger fiber adsorption capacity compared to other types of beds with equal bed structures [155].

TiO_2 nanocrystals (TiO_2 NCs) were formed in situ on the surface of the cellulose fibers (CFs) by a simple hydrolysis of TiOSO_4 to prepare the cellulose/ TiO_2 nanocomposites. Initially, cellulose was applied as a scaffold for the TiO_2 NC immobilization. However, the results showed that CF also functioned as a chemical template, directing the crystal growth of TiO_2 (Figure 4). Consequently, uniformly dispersed spindle rutile TiO_2 crystals (length ~180 nm and width ~50 nm) were formed on the CF surface, which exhibited a tendency to the adsorption of heavy metal ions such as Pb^{2+} . The CF/ TiO_2 composites demonstrated an improved high selectivity for lead (Pb^{2+}) removal, high adsorption capacity, and good regenerability. Nonwoven filter beds were easily prepared using the prepared composite

fibers that were further used in the dynamic filtration experiment. The CF/TiO₂ beds showed a 12-fold increase in the filtered bed volume before the breakthrough occurred when compared to that of the pure CF beds. This study represents a green route toward the preparation of highly efficient and low-cost nanosorbents for water decontamination using CF as the support and template [156].

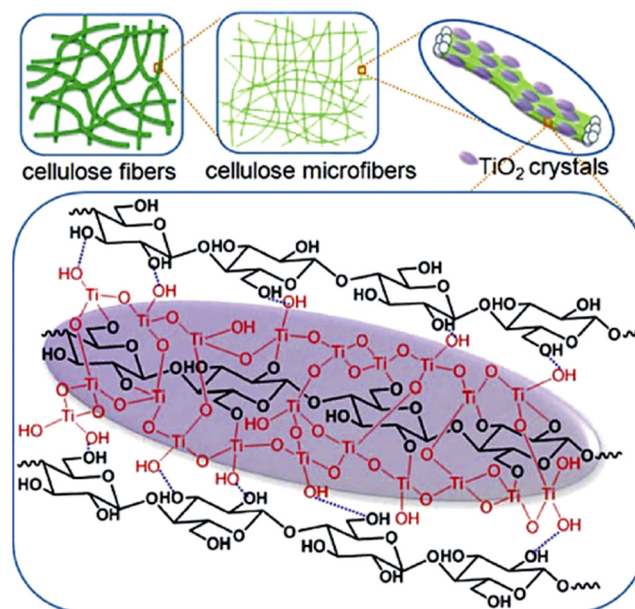


Figure 4. The schematic illustration of the in situ directional growth of spindle TiO₂ along the cellulose microfibrils. Reprinted from [156]. Copyright 2015, with permission from Elsevier Ltd.

The TiO₂ nanostructures (particle size 2–10 nm) were formed by in situ precipitation in the micronanoporous structure of the regenerated cellulose matrix using a sol–gel method to prepare the titania/cellulose composite films. The titania nanoparticles were formed inside the cellulose matrix, which provided reaction nanocavities for the formation of TiO₂ nanostructures and hydroxyl groups for their interactive adsorption. The composite films showed high photocatalytic activity in the degradation reaction of phenol using low intensity UV light. The nano TiO₂/regenerated cellulose films with interesting mechanical properties proved to be an efficient and reusable catalyst in the photodegradation of organic pollutants such as phenol [157].

A thin TiO₂ film was formed on lightweight native nanocellulose aerogels using a chemical vapor deposition method (CVD), producing a new type of photo switching functional material between water-repelling and water-absorbing states. Uniform titania coatings with an average thickness of ~7 nm were prepared on cellulose fibers of the aerogel. As shown by weighing, the TiO₂-coated aerogel samples practically did not absorb water during exposure, which was also proven by a high surface contact angle for water of 140°. After UV exposure, they intensively absorbed water (16-times their own weight) and showed a very low surface contact angle that is characteristic of superabsorbents. The recovery of the original properties was observed after storage in the dark for 2 weeks. Additionally, the TiO₂-coated nanocellulose aerogels demonstrated a photocatalytic activity in the photooxidative decomposition of methylene blue, which, combined with the highly porous structure, provides a high potential in water purification applications [158].

Cellulosic aerogels have been modified with TiO₂ nanoparticles using a chemical vapor deposition process, introducing oleophobic functionality in such systems. It was demonstrated that functionalization of the native cellulose nanofibrils of the aerogel with an oleophilic and hydrophobic titania coating produced a water floating and selectively oil-absorbing material. These surface modified aerogels enabled the removal of organic contaminants from the water surface due to the low density combined with the capability

to absorb large amounts of nonpolar liquids and oils (Figure 5), and moreover, they were recyclable and reusable after washing or alternatively, they could be incinerated together with the absorbed liquid [159].

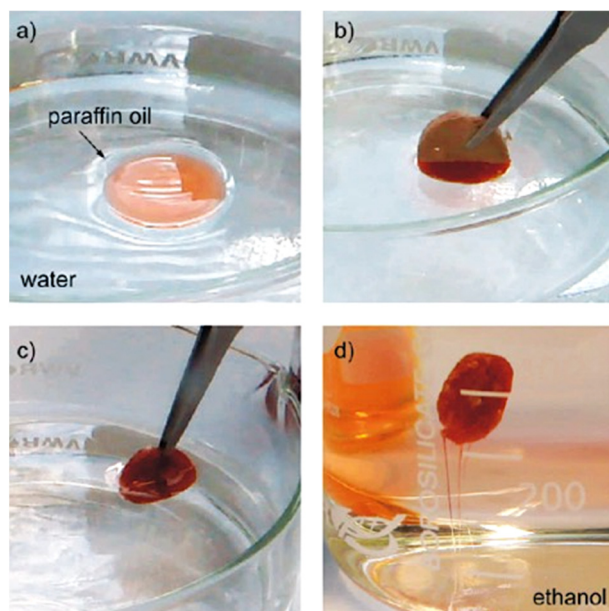


Figure 5. Oil spill removal from water. Paraffin oil (colored for clarity) floating on water (a); oil being absorbed into the aerogel (b); all of the floating oil has been absorbed (c); oil-filled aerogel can be washed simply by immersing it in a solvent such as ethanol. The oil is removed as shown by the red streaks (d). Reprinted with permission from [159]. Copyright 2010 American Chemical Society.

3.2. Cellulose Supported Fe_3O_4 and Other Iron Oxides

Cellulose structures are often decorated with Fe_3O_4 to introduce magnetic properties on the cellulose surface for various applications including magnetic resonance imaging for enzyme immobilization, clinical diagnosis, hyperthermia anticancer treatment, and magnetic drug targeting. Iron oxides such as magnetite (Fe_3O_4) and maghemite ($\gamma-Fe_2O_3$) have been proposed for these technological applications because of their high magnetic transition temperatures, high saturation magnetization, and their biocompatibility. In particular, water-dispersible polymer-based magnetic micrometer-sized spheres have attracted high attention for immobilizing various biopolymers such as enzymes and other drugs for diagnostic applications, controlled drug delivery, cell labeling, and separation purposes.

Fe_3O_4 nanoparticles (particle size 5–12 nm) were precipitated on the surface of the regenerated cellulose fibers to prepare nano-magnetic cellulose (MCGT) with excellent magnetic properties during the process of cellulose regeneration. Subsequently, a highly efficient adsorbent was formed by grafting MCGT with glycidyl methacrylate and tetraethylenepentamine and the final product was evaluated for the removal of Ag(I), Cu(II), and Hg(II). The measured adsorption capacities were 1.2, 1.5, and 2 mmol g^{-1} for the Ag(I), Cu(II), and Hg(II), respectively. The kinetic studies revealed that adsorption followed the pseudo-second-order kinetic model, whereby the adsorption equilibrium was reached within 3–5 min. The thermodynamic parameters revealed the spontaneous and exothermic adsorption of ions. Grafted MCGT was easily separated and regenerated from the adsorption medium by using an external magnetic field while thiourea was applied for the removal of adsorbents. It was tested for a real industrial wastewater treatment, demonstrating a high removal efficiency of pollutants, making the prepared MCGT a promising substrate for these purposes [160].

Fe_3O_4 spherical nanoparticles were formed on the bacterial cellulose (BC) and new BC/ Fe_3O_4 nanocomposites (BC/ Fe_3O_4) were prepared during BC biosynthesis from the *G. xylinum* fermentation by using an innovative pH controlling method. The fermentation

produced Fe_3O_4 nanoparticles with the average diameter of 15 nm being uniformly distributed in BC. The BC/ Fe_3O_4 nanocomposites with a 33 wt.% of Fe content showed the saturated magnetization (σ_s) of 41 emu g^{-1} and the coercivity of 27 Oe. The adsorption and elution characteristics of the BC/ Fe_3O_4 nanocomposites for the Cr^{3+} , Pb^{2+} , and Mn^{2+} ions were studied. Their adsorption capacities were found to differ significantly at the same concentration of an ion and they were ranked in the order $\text{Cr}^{3+} < \text{Mn}^{2+} < \text{Pb}^{2+}$, whereas the sequence of the elution capacity followed the order $\text{Cr}^{3+} < \text{Pb}^{2+} < \text{Mn}^{2+}$. The BC/ Fe_3O_4 nanocomposites were recyclable by applying magnetic field separation after the elution of the adsorbed heavy metal ions [161].

Never dried bacterial cellulose (BC) nanofibrils were surface functionalized with aminated magnetite nanoparticles (AMH). Particles were formed by the solvothermal reaction of FeCl_3 , 1,6-hexanediamine, and BC pellicles in ethylene glycol medium at 200°C with a 6 h reaction time. Cellulose accelerated the growth of Fe_3O_4 nanostructures and facilitated their deposition on the cellulose nanofibers. The AMH attached on the cellulose nanofibril surface significantly improved the mechanical and thermal properties as well as increased the amine concentration of the BC pellicles. The BC-AMH pellicles exhibited a high adsorption capacity toward the As^{5+} ions due to their high AMH contents. Almost 90 mg of As^{5+} per gram of the BC-AMH composite was achieved. The high mechanical and chemical stability, large surface area as well as the high content of surface amine groups in the BC-AMH pellicles show that these structures have potential in applications such as enzyme immobilization, drug delivery, and catalysis [162].

The Fe_3O_4 nanostructures were deposited on the surface of the carboxyl cellulosic nanospheres by using a simple co-precipitation process to form magnetic cellulose nanocrystal particles (MNPs) (Figure 6). The morphology and structure of the Fe_3O_4 nanoparticles (size $\sim 50 \text{ nm}$) were controlled by cellulosic nanospheres that functioned as a template for their stabilization. The MNPs were efficiently recycled and reused by using an external magnetic field. The spherical MNPs showed a superparamagnetic behavior accompanied by a sensitive magnetic response under an external magnetic field, and functioned as highly efficient nanocatalysts in the Fenton-like system for the rapid removal of Navy blue textile dye from an aqueous solution. By using MNPs that were prepared with H_2O_2 at the feed ratio of 1:2, 90.6% of Navy blue was removed in the first min and 98.0% in 5 min time, while 75.0% of the removal efficiency was preserved in the fifth cycle by optimizing the reaction conditions. Because of the low-cost, large surface area, good dispersibility, strong catalytic activity, and facile preparation as well as the ability of magnetic recycling and reuse, the reported MNPs showed potential application as highly effective heterogeneous nanocatalysts [163].

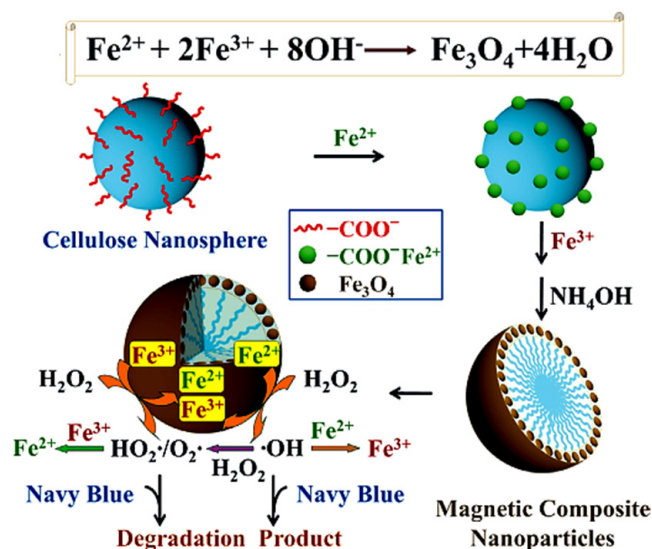


Figure 6. The formation and catalytic mechanism of MNPs. Magnetic iron oxides were anchored on the cellulose nanospheres by using a co-precipitation process; the rapid removal of textile dye Navy blue was achieved in the Fenton-like system. Reprinted from [163]. Copyright 2015, with permission from Elsevier Ltd.

3.3. Cellulose Supported ZnO

A frequently used metal oxide for cellulose decoration is definitely ZnO due to its wide range of outstanding physical and chemical properties. Optical and electrical properties make it attractive in various optical, electrical, and electro-optical applications, whereas chemical properties make it highly promising in a large number of catalytical and accelerating applications. Finally, the antibacterial properties of ZnO show that it has high potential in various medical and other protective applications.

The ZnO nanostructures were formed on regenerated cotton cellulose by a simple one-pot wet chemical method using the Zn–amine complex to prepare nano ZnO–cellulose hybrid materials. The Zn–amine complex was prepared from ZnNO_3 as a precursor and triethanolamine without thermal treatment. The hybrid material contained around 40 wt.% of ZnO nanoparticles (size ~250 nm) with a uniform distribution of nano ZnO through the cross section of the material. The ZnO–cellulose hybrid film was formed by the initial adsorption of Zn^{2+} ions to the surface of the hydrophilic cellulose fibrils, followed by the alkaline hydrolysis of the Zn–amine complex and the growth of ZnO nanostructures. Possible applications of the reported nano ZnO–cellulose hybrids are in optoelectronics as flexible display devices and biomedical or strain sensors [164].

The ZnO nanoparticles were formed simultaneously with the ZnO/cellulose nanocrystal (ZnO/CNC) nanohybrids by the hydrolysis of commercial microcrystalline cellulose (MCC) with citric/hydrochloric acid, followed by precipitation using an aqueous solution of zinc nitrate. The prepared carboxylated CNCs functioned as the stabilizing and supporting agent for the growing ZnO nanoparticles, anchoring them to the surface. ZnO nanostructures with hexagonal wurtzite structure with an average diameter of 42.6 nm were deposited onto the surface of the CNCs. The prepared ZnO/CNC nanohybrids demonstrated a high antibacterial activity and improved the thermal stability and photocatalytic activity for methylene blue (MB) as 93% of MB was decomposed after the UV light exposure within 100 min [165]. Therefore, the reported ZnO/CNC hybrids are promising photocatalytic or biomedical materials.

Spherical nanocrystalline ZnO particles with an average size of 100 nm have been formed through a simple in situ polyol method by using an amidoxime modified bacterial cellulose (Am–BC) as a template. The hydroxyl and amidoxime groups of the Am–BC functioned as reactive sites for the growth of zinc oxide NPs. The Am–BC nanoreactor as a template produced ZnO NPs in a much higher yield compared to those based on the

unmodified BC. Moreover, Am-BC prevented the aggregation of ZnO NPs, resulting in well-dispersed and regular ZnO NPs assembled in situ into the Am-BC network, which showed excellent photocatalytic properties. The reported synthetic process represents a simple and effective approach for the formation of other metallic nanostructures [166].

The BC was applied as a bio-template in the precipitation of crystalline ZnO nanoparticles by a simple polyol method (Figure 7). Their particle size and morphology were to a large extent affected by the hydrolysis time and concentration of the $\text{Zn}(\text{OOCCH}_3)_2$ precursor. Under the optimal reaction conditions (hydrolysis time: 10 min, concentration of Zn^{2+} : 0.5 wt.%), nano ZnO with an average size of 100 nm was formed. The BET surface areas of the pure BC fibers and the ZnO/BC composites were found to be 55.36 and 101.34 $\text{m}^2 \text{g}^{-1}$, respectively, indicating these structures as promising photocatalytic materials. The obtained ZnO/BC composites showed a relatively high photocatalytic activity with a maximal decolorization efficiency of 70% at 0.5 wt.% of Zn^{2+} [167].

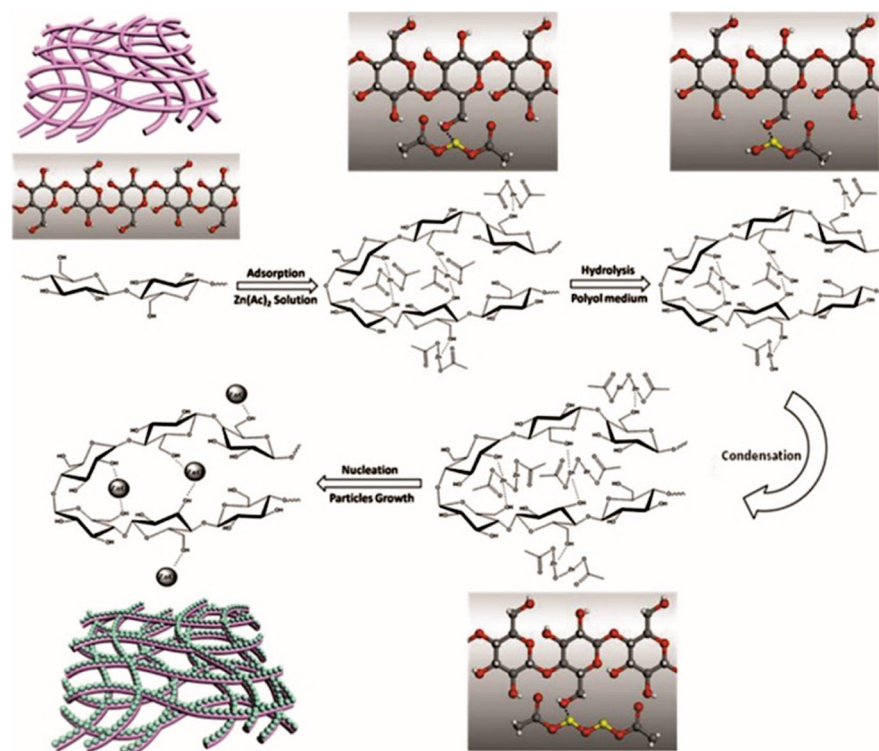


Figure 7. The schematic illustration of the formation of the ZnO nanoparticles impregnated into the BC [167]. Copyright 2013, with permission from Elsevier Ltd.

By using an ultrasonic-assisted in situ synthesis, nano ZnO particles were formed and incorporated simultaneously into bacterial cellulose (BC) pellicles. The BC pellicles were initially dispersed in a zinc acetate solution, followed by the addition of Zn^{2+} -adsorbed BC pellicles to the ammonium hydroxide solution accompanied by simultaneous ultrasonic treatment. The influences of the immersion time of the BC pellicles in the zinc acetate solution as well as the ultrasonic exposure time on the weight percent and particle size of the deposited nano ZnO were studied. The average particle size of the ZnO formed within the BC pellicles was in the range of 54–63 nm. The ZnO particles deposited inside the BC showed an unusual morphology, which was explained by the growth, with their direction being perpendicular to the alignment of the BC nanofibrils. The prepared BC-nano ZnO sheets showed a high antibacterial activity against Gram-negative and Gram-positive bacteria. The reported BC sheets decorated with nano ZnO are promising materials for effective antibacterial wound dressings [168].

Composites of regenerated bacterial cellulose (RBC) with nano ZnO (ZnO-RBC) were prepared for enhanced biomedical applications by using previously synthesized ZnO NPs.

Various concentrations of ZnO NPs were admixed to the solution of RBC dissolved in N-methylmorpholine-N-oxide, and RBC nanocomposite films containing 1 and 2 wt.% of ZnO were cast from the solutions by using an applicator. The prepared ZnO–RBC nanocomposites showed substantially improved mechanical, thermal, and biological properties. Moreover, the testing of the ZnO–RBC nanocomposites revealed significantly enhanced antibacterial properties and materials that were biocompatible with excellent cell adhesion capabilities. The potential applications of the studied ZnO–RBC nanocomposites are in bioelectroanalysis and other biomedical fields [169].

Flower-like zinc oxide (ZnO) nanorod clusters were grown on the surface of spherical cellulose nanocrystals (SCNs with cellulose II crystal structure) applied as a growth substrate by a simple chemical precipitation process. In strongly alkaline (pH = 11) conditions, flower-like ZnO nanorod cluster nanohybrids were grown at a temperature of 100 °C in 2 h of reaction time. On the other hand, rod-like ZnO particles were formed at a temperature of 90 °C in weakly alkaline (pH = 9.3 and 10.5) conditions. A possible growth mechanism for the flower-like ZnO on SCNs is that by increasing the NH₃ concentration (pH = 11), a larger number of hydroxyl groups favors the formation of Zn(OH)₄²⁻ rather than Zn(NH₃)₄²⁺. This restricts the continuous growth of ZnO nanorods, resulting in the formation of new ZnO nuclei on sites of the SCN surface, and finally, in the growth of flower-like ZnO nanorod clusters. The flower-like nanohybrids exhibited enhanced antibacterial activity against *E. coli* and *S. aureus*, and higher photocatalytic activity compared to the rod-like nanohybrids and commercial ZnO [170].

3.4. Cellulose Supported Miscellaneous Inorganic Oxides

Additionally, other metallic oxides have been successfully formed on the cellulose surface for various purposes. For example, Cu₂O was formed by an innovative synthetic approach that exploited the dual properties of the thiol-grafted cellulose paper and was developed for promoting copper-catalyzed [3+2]-cycloadditions of organic azides with alkynes (Click reaction) and for adsorbing/eliminating of the residual copper species from the reaction solution. The cellulose paper was functionalized with thiol (-SH) groups by grafting the cellulose with thioglycolic acid. The -SH grafted cellulose (Cel-SH) had a dual function, that is, promoting the Cu-catalyzed Huisgen synthesis of 1,4-disubstituted triazoles through the reduction of CuSO₄·5H₂O to Cu₂O as well as adsorbing and eliminating copper byproducts from the reaction medium. The thiol-modified cellulose paper reduced Cu^{II} to catalytically active Cu^I and acted as an effective adsorbent for copper, thereby simplifying the synthetic process and resulting in the reaction mixture being almost free of copper residues after a single filtration (Table 2). Highly complex organic molecules were synthesized to demonstrate the robustness of the reported cellulose-supported catalytic system as well as the related synthetic approach [171].

Table 2. The adsorption properties of Cel-SH for the copper-catalyzed (cellulose supported Cu₂O) Huisgen 1,3-dipolar cycloaddition of azide with the terminal alkyne forming 1-(benzyl-1H-1,2,3-triazol-4-yl)methanol [171]. Copyright 2016 John Wiley & Sons Inc. Reproduced with permission.

Entry ^[a]	SH Loading (mol%)	Yield ^[b] [%]	Cu Adsorbed [%]
1	0	<5	0
2	3.2	41	4
3	8	43	58
4	16	87	94
5	24	88	97
6	32	91	97.5

^[a] Reaction conditions: benzyl azide (1 mmol), propargyl alcohol (1.5 mmol), CuSO₄·5H₂O and Cell-SH were stirred in 5 mL of t-BuOH/H₂O (1:1) for 14 h at the specified temperature. ^[b] Yield of the isolated product.

Magnetic CoFe_2O_4 nanoparticles were deposited into the cellulose structure to prepare lightweight and flexible magnetic cellulose aerogels by a simple method. Their porosities varied from 52 to 78%, while their density and internal specific surface area were between $0.25\text{--}0.39\text{ g cm}^{-3}$ and $300\text{--}320\text{ m}^2\text{ g}^{-1}$, respectively. The concentration of the incorporated CoFe_2O_4 nanoparticles increased by increasing the precursor concentration, however, the particle size practically did not change. The deposited CoFe_2O_4 nanoparticles showed a superparamagnetic behavior as well as interesting mechanical properties and changed the microstructure of the cellulose aerogels. Because of the cellulose sustainability and availability in large quantities, the reported process with a simple concept is suitable for the industrial-scale up and is also applicable for many other types of nanoparticles [172].

The lightweight porous magnetic aerogels were prepared from the bacterial cellulose (BC) aerogels as templates, which were compacted into a stiff magnetic nanopaper. Non-agglomerated ferromagnetic CoFe_2O_4 nanostructures, with diameters ranging from 40 to 120 nm, were formed from FeSO_4 and CoCl_2 precursors in a mixture of NaOH and KNO_3 on BC nanofibrils functioning as templates. The reported dry magnetic aerogels were flexible, porous (98%), lightweight, and they were actuated by a small magnet to absorb water and release it during the compression. Due to their high porosity, large surface area, and flexibility, these aerogels are promising materials for electronic actuators and microfluidic device applications [173].

An alternative method for the treatment of brain aneurysms was developed by applying magnetized bacterial nanocellulose (BNC) as a platform for both magnetic and cell attraction as well as for cell proliferation (Figure 8). The preparation of magnetic bacterial nanocellulose (MBNC) was carried out via the reaction of Fe II and Fe III precursors, precipitating superparamagnetic iron oxide nanoparticles, which were afterward coated with polyethylene glycol to enhance their biocompatibility. The biocompatibility and cytotoxicity testing of MBNC showed suitable cell viability and minimal cytotoxicity. The study of cellular magnetic attraction and the cell migration tests revealed the viability of MBNC as a multifunctional coating of stents for the treatment of brain aneurism [174].

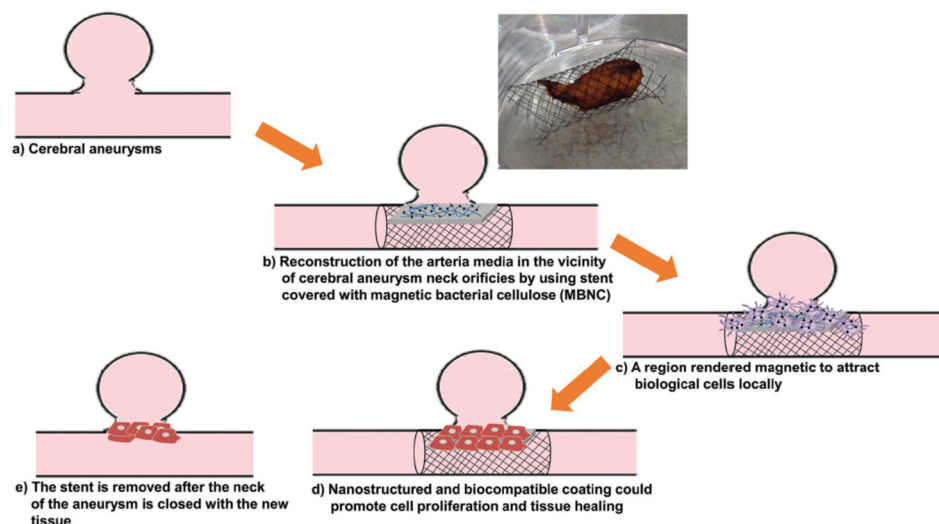


Figure 8. The schematic presentation of the concept of endovascular treatment at the neck orifice in cerebral aneurysms (a). The process consists of arterial media reconstruction by using a stent covered with the magnetic bacterial nanocellulose (MBNC) (b) designed to attract cells to the aneurysm region (c). With time, new tissue grows over the stent, closing the neck of the aneurysm (d) and ultimately, the removal of the stent (e). The photographic image of the Nitinol stent covered with MBNC revealed their good adhesion to the stent [174]. Copyright 2017 John Wiley & Sons Inc. Reproduced with permission.

Cellulose nanocrystal (CNC) films and electrospun composite CNC fibers with magnetic properties were prepared. Magnetism was introduced into the CNC by CoFe_2O_4 nanoparticles immobilized on the CNC nanofibrils. The CNCs (ca. 150 nm length) and the aqueous dispersion of the cobalt–iron oxide nanoparticles (10–80 nm diameter) were applied as precursors for the preparation of composite fibers as well as composite films. The CNC– CoFe_2O_4 composite fibers showed ferromagnetic properties, having a saturation magnetization of $\sim 20 \text{ emu g}^{-1}$. The potential application of precursor dispersions was demonstrated, and possible applications of the studied CNC-based magneto-responsive materials in the biomedical and magneto-optical components were highlighted such as magnetic shielding, packaging, separation applications, cell treatment, and drug delivery [175].

The number of publications on cellulose supported/templated inorganic oxide nanostructures is also extensive and therefore not all of them can be included in the text of the review. Consequently, the information on the inorganic oxides supported by the cellulose structures is collected in Table 3. The most commonly used method of metal oxide deposition on the cellulose is the adsorption of metallic ions via hydroxyl groups, followed by the formation of oxide particles by a hydrothermal or solvothermal reaction, or by a sol–gel process. Alternative methods of deposition involve a separate formation of nanoparticles, followed by their deposition onto the cellulose surface or commercial powders as well as various physical methods such as laser vaporization or ultrasonication, etc. The types of cellulose substrate range from natural cellulose fibers (CF) via microcrystalline cellulose (MCC) or microfibrillated cellulose (MFC) to bacterial nanocellulose (BNC) and cellulose nanocrystals (CNCs). The most common applications of these structures range from various (photo)catalytic systems to antibacterial agents in medicine and as adsorbents for drinking and wastewater purification.

Table 3. The list of publications on the cellulose supported metal oxide nanostructures. The list is organized from large cellulose structures (CF and RC) via microstructured celluloses (MCC and MFC) to nanostructured celluloses (BNC and CNCs).

Inorg. Particle (Size—nm)	Cellulose Used	Precursor (Synthetic Path)	Application	Reference
Cellulose Supported TiO_2 Nanostructures				
TiO_2 NPs (5–100 nm)	CF	$\text{Ti}(\text{OBU})_4$, HCl (hydrothermal reaction)	Photocatalyst for CO_2 reduction	[176]
TiO_2 NPs (40–250 nm)	CF	Commercial TiO_2 (hydrothermal treatment)	Photocatalyst, antibacterial agent	[177]
TiO_2 NPs (~4 nm)	CF	TiCl_4 (hydrothermal reaction—ultrasonication)	Photocatalyst in self-cleaning fabric	[178]
TiO_2 NPs (10–20 nm)	CF	Ti(IV) isopropoxide (hydrothermal reaction)	Photocatalyst and antibacterial agent	[179]
TiO_2 NPs	CF	TiOSO_4 , urea	Adsorbent for phosphate removal	[180]
TiO_2 NPs	MCC	TiCl_4 , EtOH (sol–gel process)	Adsorbent for Pb^{2+} , Cd^{2+} , Zn^{2+} ions	[181]
TiO_2 NPs (300–900 nm)	MCC	TiCl_3 , NH_3 (hydrothermal reaction)	Photocatalyst (H_2 production)	[182]
TiO_2 nanorods (l.: 26 nm; w.: 16 nm)	MFC	Commercial TiO_2 NPs	—	[183]
TiO_2 NPs	MFC	Commercial TiO_2 NPs	Antibacterial agent	[184]
TiO_2 NPs-anatase	BNC	TiO_2 powder, laser vaporization	Photocatalyst, purification of drinking water	[185]

Table 3. Cont.

Inorg. Particle (Size—nm)	Cellulose Used	Precursor (Synthetic Path)	Application	Reference
Cellulose Supported TiO₂ Nanostructures				
TiO ₂ NPs (5–15 nm)	BNC	Ti(IV) n-butoxide, sol–gel process	Detector for phosphopeptides	[186]
TiO ₂ NPs	BNC	Ti(IV) n-butoxide Solvothermal process	Photocatalyst (methyl orange degradation)	[187]
TiO ₂ NPs	CNF	Commercial TiO ₂	Photoanodes	[188]
TiO ₂ NPs	BNC	Ti(IV) isopropoxide, Sol-Gel process	Antibacterial agent	[189]
TiO ₂ NPs	BNC	Commercial TiO ₂	Adsorbent for water contaminants	[190]
Black TiO ₂ NPs	BNC	Ti[OCH(CH ₃) ₂] ₄ , microwave-assist. sonochem. process	Interfacial solar evaporator	[191]
TiO ₂ NPs	CNCs	TiOSO ₄ (hydrolysis with sulfuric acid)	UV absorber in skin care products	[192]
TiO ₂ NPs (50–100 nm)	CNCs	Commercial nano TiO ₂	Drug release system	[193]
Cellulose supported iron oxide nanostructures				
Fe ₃ O ₄ NPs	CF	FeSO ₄ , NH ₃ , H ₂ O ₂ , PEG, previously formed Fe ₃ O ₄	Magnetic fibers	[194]
Fe ₂ O ₃ NPs (50–200 nm)	CF	FeSO ₄ , NaOH (ultrasonication)	Magnetic paper	[195]
Fe ₃ O ₄ NPs	CF	FeCl ₃ , FeCl ₂ , NaOH	Cancer treatment with 5-Fluorouracil	[196]
Fe ₂ O ₃ NPs	CF	(NH ₄) ₂ Fe(SO ₄) ₂ , NaH ₂ PO ₂ ,	Encapsulation and delivery-biologically active compounds	[197]
Fe ₂ O ₃ nanoplatelet (48 nm)	RC	FeCl ₂ , FeCl ₃ (reaction with NaOH)	—	[198]
Fe ₃ O ₄ NPs	CF	FeCl ₂ , FeCl ₃ (reaction with NaOH)	Immobilization of prenyltransferase NovQ	[199]
Fe ₃ O ₄ NPs	MCC	FeSO ₄ , FeCl ₃ , NH ₃	Biotechnology, water purification	[200]
Fe ₃ O ₄ NPs (~3 nm)	MCC	FeCl ₃ , FeCl ₂ , NH ₃	Antibacterial and contrasting agent	[201]
Fe ₃ O ₄ NPs (~9 nm)	BNC	Fe(III) acetylacetonate, (microwave sol–gel process)	Magnetic paper	[202]
Fe ₃ O ₄ NPs	BNC	Fe ₂ (SO ₄) ₃ , FeSO ₄ , reaction with NaOH	Absorbing agent (removal of Cr(VI) ions)	[203]
Fe ₃ O ₄ NPs	CNFs	Fe(NO ₃) ₃ , FeSO ₄ , NaOH, citric acid, nano TiO ₂	Recoverable catalyst-H ₂ photogeneration	[204]
Fe ₃ O ₄ NPs (~10 nm)	CNCs	FeCl ₂ , FeCl ₃ , NH ₃ (precipitation)	Substrate for protein separation	[205]
Fe ₃ O ₄ NPs	CNCs	FeCl ₂ and FeCl ₃ reaction with ammonia	Targeted delivery of doxorubicin	[206]
Fe ₃ O ₄ NPs	CNCs	FeCl ₂ , FeCl ₃ (reaction with ammonia)	Semiconductor in antistatic paper	[207]
Cellulose supported ZnO nanostructures				
ZnO nanorods	CF	(Zn(CH ₃ COO) ₂ , hexamethylenetetramine	Antibacterial agent in packaging	[208]
ZnO nanowires	CF	Previously synthesized ZnO NWs, Zn(CH ₃ COO) ₂ (solvothermal hydrolysis)	Piezoelectric accelerometer	[209]
ZnO NPs (3–30 nm)	CF	Zn(CH ₃ COO) ₂ , reaction with NaOH	Antibacterial agent	[210]

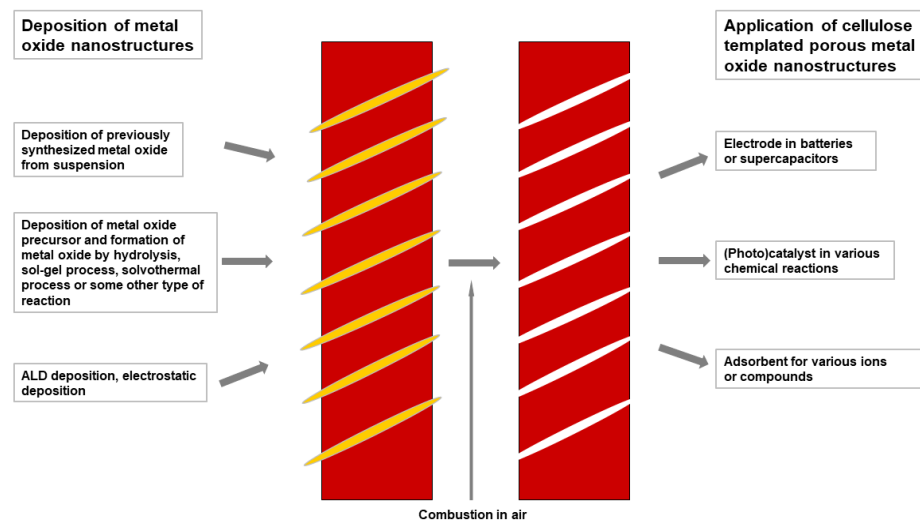
Table 3. Cont.

Inorg. Particle (Size—nm)	Cellulose Used	Precursor (Synthetic Path)	Application	Reference
Cellulose supported ZnO nanostructures				
ZnO nanorods	CF	Zn(NO ₃) ₂ (hydrothermal growth)	Semi-conductor	[211]
ZnO rods	CF	Zn(NO ₃) ₂ , (CH ₂) ₆ N ₄ , (hydrothermal synthesis)	Antibacterial rubber	[212]
ZnO NPs	CF	Zn(NO ₃) ₂ , urea (hydrothermal process)	Photocatalyst (methyl orange degradation)	[213]
ZnO nanorods	BNC	Zn(NO ₃) ₂ , (CH ₂) ₆ N ₄ , (hydrothermal synthesis)	—	[214]
ZnO NPs	BNC	Zn(NO ₃) ₂ , solution plasma process	Antibacterial agent	[215]
ZnO NPs (100–200 nm)	BNC	Zn(OOCCH ₃) ₂ , solvothermal process	Antibacterial agent	[216]
ZnO NPs	BNC	Zn(NO ₃) ₂ , NaOH	Antibacterial dressing for burn wounds	[217]
ZnO NPs	CNCs	Commercial nano ZnO	Semiconductor in flexible electronic applications	[218]
ZnO nanorod clusters	CNCs	Zn(CH ₃ COO) ₂ , reaction with NaOH	Antibacterial agent	[219]
ZnO NPs (10–50 nm)	CNCs	ZnCl ₂ , NaOH	Catalyst in degrad. of tetracycline	[220]
Cellulose supported miscellaneous oxide nanostructures				
BiVO ₄	CF	Bi(NO ₃) ₃ ·5H ₂ O, citric acid	Photocatalyst for methyl orange	[221]
Ti ₃ (PO ₄) ₄	CF	Waste Ti metal, H ₂ SO ₄ , Na ₃ PO ₄	Photocatalyst for crystal and methyl violet	[222]
MnO ₂ (150 nm)	MCC	MnSO ₄ , KMnO ₄	Adsorbent of Pb ²⁺ , H ₂ O purification	[223]
In ₂ O ₃ –10 wt.% SnO ₂	MFC	RF sputtering	Semiconductive nanofiller	[128]
Ag ₂ O NPs (2–20 nm)	MFC	AgNO ₃ , NH ₃ , NaOH	Adsorbent for I [−] ions	[224]
H ₃ PW ₁₂ O ₄₀	BNC	Commercial PTA	Photochromic agent	[225]
Mn ₃ O ₄ (300 nm)	BNC	KMnO ₄ , reduction by carboxymethyl cellulose	Electrode material	[226]
ZnO–CdS NPs	BNC	Zn(NO ₃) ₂ , CdSO ₄	Photocatalyst (degr. of methyl orange)	[227]
BaTiO ₃	BNC	Ti(OC ₄ H ₉ -n) ₄ , H ₄ Ba ₆ (O)(OCH ₂ CH ₂ OCH ₃) ₁₄ , hydrolysis	Piezoelectric paper	[228]
BaTiO ₃	CNCs	Commercial BaTiO ₃	Piezoelectric energy harvester	[229]
La ₂ CuO ₄	BNC	La(NO ₃) ₃ /Cu(NO ₃) ₂ hydrothermal process	Catalyst-methanol steam reforming	[230]
CoFe ₂ O ₄	BNC	FeCl ₃ and CoCl ₂ , reaction with NaOH	Magnetic paper	[231]
V ₂ O ₅	BNC	Vanadium(V) oxytriisopropoxide hydrolysis with HCl	Semiconductive nanofiller	[232]
CuO NPs	BNC	Previously prepared CuO NPs	Antimicrobial agent	[233]
CuO NPs	BNC	Cu(OOCCH ₃) ₂ , CH ₃ COOH, ethylene glycol	Antibacterial agent	[234]
CuO NPs (~7 nm)	CNCs	CuSO ₄ (reduction by NaBH ₄)	Catalyst (reduction of 4-nitrophenol)	[235]
FeMnO _x (50–100 nm)	CF	KMnO ₄ , FeSO ₄ , NaOH, cetyltrimethyl ammonium Br	Adsorbent for As(III) and As(V) removal	[236]
CeO ₂ NPs (10–40 nm)	RC	Ce(NO ₃) ₃ , NaOH	UV shielding	[237]

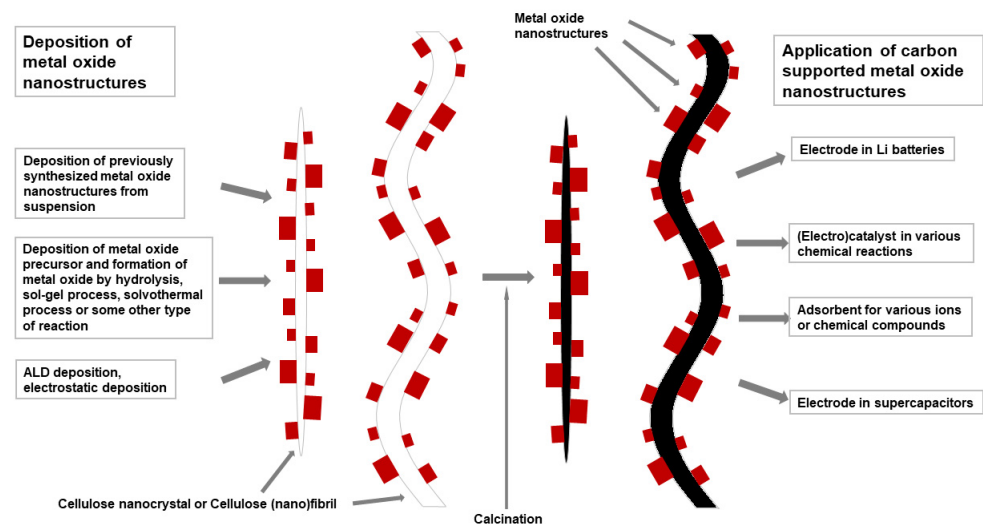
4. Cellulose Templated Pure Metal Oxide Nanostructures

The sol–gel mineralization of cellulose nanofibers is a flexible way to produce inorganic frameworks of a controlled size, structure, and porosity. For example, hollow nano-objects have raised interest in applications such as sensing, encapsulation, and drug-release [238]. A porous inorganic structure template by the cellulose structures can be prepared by the formation of metallic oxides on the surface of the cellulose and subsequent calcination. In some cases, the solvothermal removal of the cellulose template is also used [239]. Various porous structures of a wide range of pure metal oxides have been reported to be prepared by chemical or physical methods using different cellulose structures as templates. Porosity significantly increases the specific surface of these materials, giving these materials a high potential in catalysis, photovoltaics, sensorics, electrochemical energy storage, etc. [15]. The tunable porosity of inorganic oxide thin films is a key factor for their successful applications in photovoltaics, sensing, and photocatalysis. Direct cellulose templating of inorganic oxides has been carried out with nanocellulose aerogels, microfibrillated cellulose, bacterial cellulose, nanocrystalline cellulose, filter paper, and green leaves. It is expected that the pore size is a function of the shape and dimensions of the applied cellulose template. The resulting materials were sponge-like inorganic oxide monoliths, freestanding films, or powders. Additionally, titania powders biotemplated with cotton fibers were further processed to a paste that was afterward coated on conducting substrates and applied in a solar-cell assembly.

Cellulose in all of its structures and variations proved to be a highly suitable sacrificial biotemplate for the synthesis and formation of porous and mesoporous hierarchical structures or aerogels of the whole variety of inorganic oxides. All types of cellulose have been applied as biotemplates for the porous structures of inorganic oxides. The list includes TiO_2 , ZnO , Fe_2O_3 , CuO , Mn_3O_4 , Nb_2O_5 , Co_3O_4 , SnO_2 , and more complex mixed oxides such as indium tin oxide, $\text{Cu}_{0.5}\text{Co}_{0.5}\text{Fe}_2\text{O}_4$, or $\text{BaFe}_{12}\text{O}_{19}/\text{CoFe}_2\text{O}_4$. Unfortunately, there are very few reviews based solely on cellulose-templated porous pure inorganic materials [240]. The most frequently studied cellulose template porous material is TiO_2 , which is a very promising catalyst in the photoelectrochemical water splitting of cells [241]. Porous materials are also important in the sorption of gases such as CO_2 , which is highly important for the reduction in the CO_2 concentration in the environment [242]. Recently, the last area of application is gaining significant importance since the number of electrically driven vehicles is rapidly increasing [243]. Cellulose, as an environmentally-friendly shape persistent biotemplate, offers the possibility of the formation of new shapes and forms of inorganic oxides with tunable porosity through mostly simple and environmentally-friendly procedures followed by calcination. Cellulose is an ideal organic support and sacrificial template since it contains a lot of oxygen, and upon calcination in air, it completely degrades, leaving pure inorganic compounds with high porosity. If the calcination is performed in an inert atmosphere, carbon-supported or carbon-doped materials are formed [240]. Aside from a high specific surface, the density of the prepared material was significantly reduced, and in many cases, special structures were formed such as hollow 1-D fibers, microrods, nanowires, or nanotubes. The capability of the cellulose nanocrystals to organize into lyotropic liquid crystalline structures was exploited in the formation of nematic mesoporous silica films that were further applied as templates for inorganic oxides organized into photonic crystals with periodic order and tunable optical properties [244]. In addition to classical chemical synthesis, other innovative processes have also been applied such as the sonochemistry process, microwave-assisted ionic liquid process, evaporation-induced self-assembly, and atomic layer deposition method. In Scheme 3, the versatility of cellulose substrates, the formation processes of metal oxide porous nanostructures, and the potential applications of these structures are presented. The versatility of the cellulose substrates, the formation processes of carbon fibers supported metal oxide nanostructures, and the potential applications of these hierarchical structures is presented in Scheme 4.



Scheme 3. The schematic representation of the cellulose/metal oxide nanocomposites and porous metal oxide structures, synthetic routes, and the most frequent applications of these materials.



Scheme 4. The schematic representation of the carbon fiber supported metal oxide nanostructures, synthetic routes, and most frequent applications of such materials.

4.1. Cellulose Templated Porous TiO₂

This section addresses the formation of (nano)porous TiO₂ structures using any type of cellulose as a sacrificial template. The formation of nanotube aerogels with a framework composed of inorganic hollow nanotubes was reported. A preparation route of TiO₂, Al₂O₃, and ZnO nanotube aerogels by applying biological aerogel templates such as microfibrillated cellulose (MFC) or cellulose nanocrystals (CNC) (Figure 9) using the atomic layer deposition method (ALD) was demonstrated. Freeze-drying or supercritical-drying was used for the preparation of aerogel templates as freestanding objects or films on substrates from nanocellulose hydrogels. Supercritical-drying produced nanocellulose aerogels without major interfibrillar aggregation, even in thick films. Uniform oxide layers were readily formed by ALD onto the fibrils, producing organic–inorganic core-shell nanofibers. The cellulose core was removed by calcination at 450 °C, forming inorganic self-supporting aerogels containing hollow nanotubular networks. They were also dispersed in ethanol by grinding to prepare a hollow nanotube slurry, which was cast to form a porous inorganic film. The TiO₂ nanotube network was tested as a fast response humidity sensor [238].

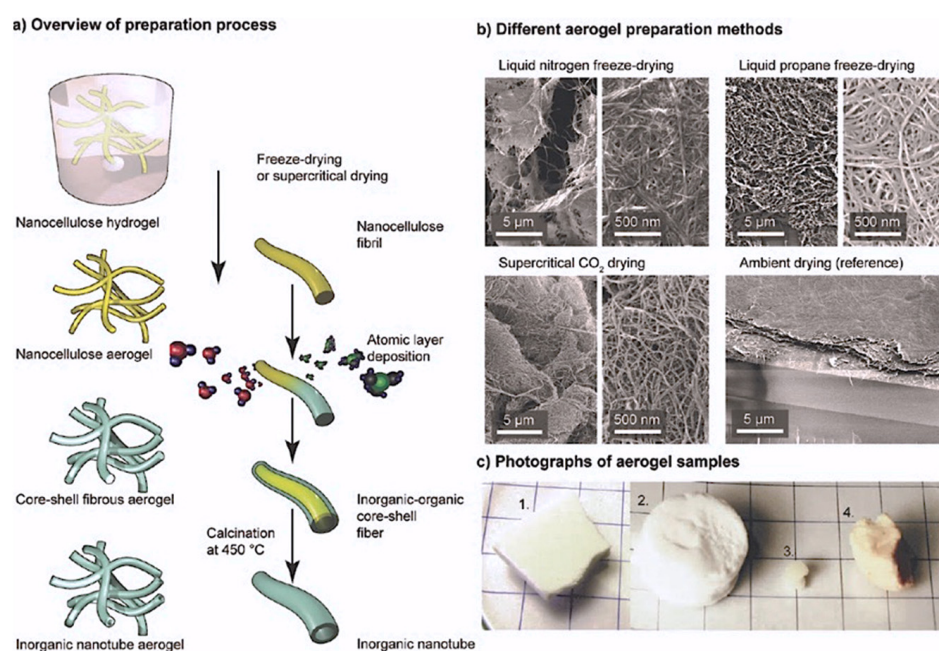


Figure 9. (a) The schematic presentation of the inorganic hollow nanotube preparation process. First the nanocellulose hydrogel is dried to obtain the aerogel, which is then coated with inorganic oxides using the ALD method to form composite organic/inorganic nanofibers. Finally, the composite was calcined to inorganic hollow nanotubes. (b) The SEM images demonstrating the effect of different drying methods: freeze-drying by freezing the nanocellulose hydrogel in liquid nitrogen, followed by the sublimation of ice in vacuum, leads to aerogels with sheet-like aggregates; freeze-drying in liquid propane leads to fibrillar aerogels with suppressed aggregation, given the sample is sufficiently thin; supercritical-drying leads to fibrillar aerogels without aggregates, even in thick samples; drying at ambient conditions leads to the collapse of the structure. (c) Photographs of the aerogel samples: (1) Liquid propane freeze-dried aerogel of 2 mm thickness; (2) supercritically-dried sample with ca. 12 mm in diameter and 10 mm in height; (3) atmospherically-dried sample that completely collapsed. Wet dimensions were the same as in the supercritically-dried sample; (4) Supercritically-dried aerogel after ALD showed a slight yellow color on the surface. Reprinted with permission from [238]. Copyright 2011 American Chemical Society.

Cellulose nanocrystals (CNCs) were applied as a shape-persistent template allowing for the straightforward formation of mesoporous TiO₂ films (Figure 10). The formed TiO₂ structures were high porosity anatase films with narrow pore size distributions and well-defined pores. By varying the template to the TiO₂ ratio, the pore size, pore anisotropy, surface area, and diameter of the titania nanoparticles in the films were controlled. Then, by applying a post-treatment at high humidity followed by slow template removal, the pore widening was achieved and this procedure was useful for the multilayer deposition to prepare thick films. Homogeneous and transparent films were prepared by the spin- or dip-coating on various substrates such as glass, silicon, and transparent conducting oxide (TCO). The formed mesoporous TiO₂ films exhibited high activity in the degradation of 4-chlorophenol as well as in the photocatalytic conversion of nitrogen oxide and they were successfully applied as anodes in dye-sensitized solar cells. The results revealed that CNC-templating offered the potential to supersede conventional processes toward porous TiO₂ and that this process showed a potential for application in the preparation of mesoporous films with other inorganic oxides [15].

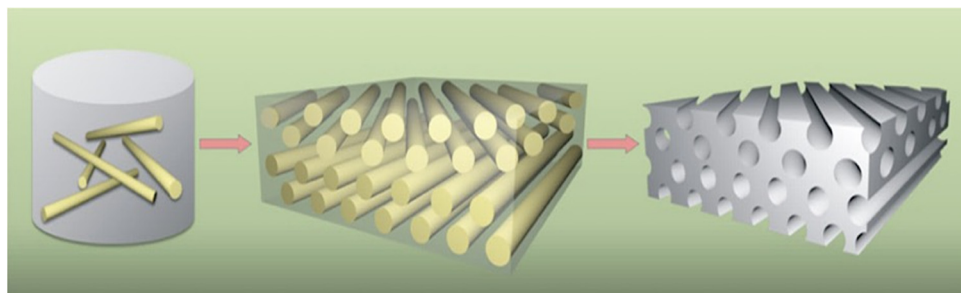


Figure 10. The synthesis approach to the NCC-templated mesoporous TiO₂ film. Reprinted with permission from [15]. Copyright 2014 American Chemical Society.

Mo-doped titania thin films with high transparency were formed on an ITO glass substrate by spin-coating the titania composite precursor, which was prepared by mixing titanium(IV) ethoxide and HCl, followed by the addition of CNCs and molybdenum(V) chloride. Subsequently, the prepared composite film was calcined at 400 °C for 1 h to obtain an ITO supported titania porous film. Due to the presence of CNCs as a sacrificial template, deposited titania films, composed of TiO₂ crystals with average particle sizes of 10 nm, contained slit-like pore channels with a pore width ranging from 5.7 to 7.8 nm and a surface area of 150 m² g⁻¹. The photocatalytic properties of the formed films were studied for the degradation of trichloro ethylene (TCE) relative to the non-templated solid titania film as well as to the undoped CNC-templated porous titania film. This evaluation showed that both the CNC-templating and the Mo-doping significantly increased the photocatalytic activity of the TiO₂ films for TCE degradation. Additionally, the Mo-doped TiO₂ films exhibited very strong visible-light absorption and are expected to have high potential as sustainable coatings for photocatalysis and solar cells. The reported synthesis method of TiO₂ with the application of CNCs as a sacrificial template was demonstrated to be a low-cost, simple, and energy saving process to fabricate highly transparent and mesoporous thin photocatalytic films, offering a significant enhancement in the photocatalytic performance with a two-fold faster degradation of TCE [245].

Recently, a new class of mesoporous materials with a chiral nematic pore structure templated by the lyotropic liquid-crystalline phase of cellulose nanocrystals (CNCs) was developed. The condensation of Si(OMe)₄ as a silica precursor in the presence of CNCs produced a composite material in which CNC particles with a nematic chiral organization were embedded in the SiO₂ matrix. The helical pitch in the mesoporous SiO₂ was tuned by varying the ratio of the CNC to Si(OMe)₄, thus changing the reflected light wavelength in the range from the near IR to the UV. After the removal of the CNC with 12 M HCl at 85 °C followed by a short oxidizing treatment with H₂SO₄/H₂O₂ (5:1), porous SiO₂ was obtained as a freestanding film with a long-range chiral nematic structure. The mesoporous anatase TiO₂ was synthesized from TiCl₄ by calcination at 600 °C by using a nematic chiral mesoporous SiO₂ film, acting as a hard template, which was subsequently removed by etching with 2 M NaOH to prepare a free-standing structure of the mesoporous TiO₂ with a specific surface area between 150 and 230 m² g⁻¹. The structure of the chiral nematic SiO₂, originating from the lyotropic liquid crystalline ordering of CNC, was preserved in the final product, producing a chiral nematic mesoporous TiO₂ film, reflecting the circularly polarized light. This study is the original approach toward organizing a crystalline metal oxide into a chiral nematic structure. The reported synthetic method is highly attractive for preparing new catalytic and photonic materials [246].

4.2. Cellulose Templated Porous Iron Oxides

Cotton cellulose was applied as a sacrificial template in the in situ formation of porous and hollow CoFe₂O₄/BaFe₁₂O₁₉ microrods. The cellulose template was removed by calcination at 250 °C for 2 h and additionally at 900 °C for 3 h. The resulting composites possessed the porous hollow microrod morphology with soft ferrite (CoFe₂O₄) and hard

ferrite ($\text{BaFe}_{12}\text{O}_{19}$) being uniformly deposited along the microrods. Due to the exchange-coupled interaction and their specific morphological effects, the microwave absorption characteristics of the microrods were substantially enhanced, as shown by electromagnetic studies. The microwave absorption bandwidth with the reflection loss less than -10 dB was expanded to 8.1 GHz, while at the same time, the weight content of the ferrite component in the composites was reduced to 60 wt.%. Therefore, the application of cellulose as a template proved to be an efficient approach to simultaneously reduce the mass of conventional ferrites and enhance the microwave absorption properties. The reported simple formation process of hollow porous $\text{CoFe}_2\text{O}_4/\text{BaFe}_{12}\text{O}_{19}$ microrods also increases the opportunities to develop a variety of soft/hard ferrite composite materials for other potential applications such as sensors, permanent magnets, and ultra-high-density data storage [247].

A simple method for the synthesis of crystalline and highly porous $\alpha\text{-Fe}_2\text{O}_3$ thin films with various nanomorphologies has been developed by using the CNCs as a biotemplate. FeCl_3 , FeCl_2 , and $\text{Fe}(\text{NO}_3)_3$ were used as precursors in the CNC-templated synthesis. It was demonstrated that after the post-synthetic humidity treatment at 100°C , the crystallization of Fe_2O_3 proceeded via the formation of $\beta\text{-FeOOH}$ of a highly anisotropic shape. The porosity and homogeneity of the Fe_2O_3 films were preserved despite the complex crystallization behavior of Fe_2O_3 due to the shape persistence of CNCs. The calcination procedure of the CNC/ Fe_2O_3 precursor composites showed a strong impact on the morphology and porosity of the Fe_2O_3 films. The calcination was performed at temperatures between 300 and 600°C , depending on the type of precursor. It was demonstrated that a great variety of Fe_2O_3 networks could be synthesized and the morphology of their films could be tuned by simple templating with CNCs. The reported synthesis approach is advantageous for the formation of porous homogeneous Fe_2O_3 films on various kinds of substrates [248].

4.3. Miscellaneous Cellulose Templated Porous Metallic Oxides

Natural cellulosic fibers (kapok fibers) were applied as sacrificial templates in the formation of hollow SnO_2 nanotubes by applying the surface sol-gel process followed by calcination at 550°C for 5 h. The prepared nanostructures, consisting of SnO_2 nanoparticles being smaller than 12 nm in size, were hollow nanotubes with a diameter between 50 and 100 nm, while the thickness of the tube wall was estimated to be from 10 to 20 nm. The resulting SnO_2 nanotubes showed a high BET surface area of $185.15\text{ m}^2\text{ g}^{-1}$ and very high aspect ratios. The coulombic efficiencies larger than 97.8% and stable discharge capacities of $\sim 600\text{ mA h g}^{-1}$ were measured by using the current density of 100 mA g^{-1} . The characteristics of the nanostructured SnO_2 particles embedded in the nanotube resulted in high electronic conductivity and high capacity of the electrode. The hollow structure provided enough void space so that the SnO_2 nanoparticles changed a volume without a collapse, causing excellent cycling stability of the electrode. This preparation approach is low-cost, facile, and is suitable for the scale-up production of nanotubular materials that are applicable in gas sensors or in lithium-ion batteries [249].

Cellulose was applied as a template in the preparation of octahedral, face-raised Co_3O_4 crystals to be applied as a catalyst in the selective oxidation of alcohols. Initially, the CoCl_2 precursor and cellulose were mixed in solution, dried, and calcined at 500°C for various times of 2–6 h. The edge length of the prepared Co_3O_4 structures was about 200 nm and they formed microtubes with a width of 2–3 μm and a length of ca. 10 μm . The formation of the Co_3O_4 octahedral structure and assembly process were facilitated by the thermal decomposition and carbonization of cellulose (Figure 11). The face-raised Co_3O_4 octahedral nanocrystals showed higher saturation magnetization and remanence due to smaller grain sizes with higher uniformity compared to the normal Co_3O_4 octahedra. Additionally, the Co_3O_4 octahedra grown by the cellulose-assisted process exhibited both the higher selectivity and higher activity in the catalytic oxidation of alcohols compared to the normal Co_3O_4 octahedra. For example, the reported Co_3O_4 nanocrystals showed a very high catalytic activity after eight cycles, giving them a high potential in heterocatalytic applications [250].

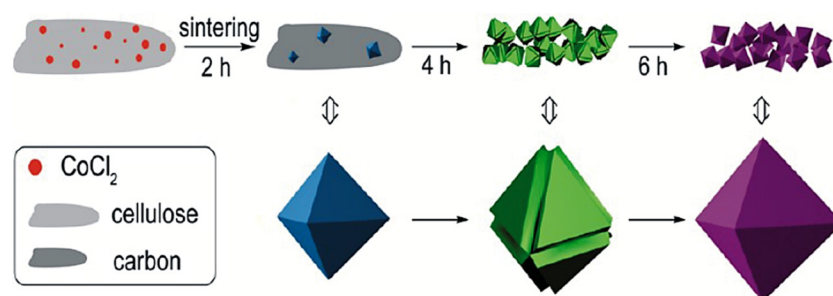


Figure 11. The schematic illustration describing a time-dependent growth of Co_3O_4 . Reprinted with permission from [250]. Copyright 2014 American Chemical Society.

The cellulose/CuO nanocomposites were prepared by an ionic liquid microwave-assisted process from the microcrystalline cellulose solution, CuCl_2 precursor, and BmimBF_4 medium. The reported procedure combined three highly important green chemistry principles: sustainable resources, green solvents, and an environmentally-friendly method. With longer microwave-heating time, the crystallinity of CuO increased and the CuO shape changed from nanosheets to bundles composed of irregular nanosheets, and finally, to regular nanoparticles. The ratio of the cellulose solution to ionic liquid significantly affected the microstructure and morphology of CuO in the nanocomposites. The pure CuO structures with various morphologies and particle sizes were obtained by the calcination of different precursors (cellulose/CuO nanocomposites) at $800\text{ }^\circ\text{C}$ for 3 h. The reported synthetic approach opens a novel path toward the formation of inorganic oxides and to the application of cellulose with a high-added value [251].

Pure ZnO nanoparticles with a wurtzite structure have been prepared by using bacterial cellulose (BC) embedded with zinc acetate as a template and by subsequent calcination. The morphology and average particle size of ZnO nanoparticles were tuned by varying the calcination temperature and the concentration of zinc acetate in an aqueous solution. The presence of BC strongly influenced the size, morphology, and size distribution of the formed ZnO. Highly crystalline ZnO nanostructures with a narrow particle size distribution from 20 to 50 nm and high photocatalytic activity were prepared by using BC as a template containing 1 wt.% zinc acetate and by calcination at $600\text{ }^\circ\text{C}$ for 2 h. The reported process provided an efficient, facile as well as environmentally-friendly approach toward the formation of the highly defined and homogeneously dispersed ZnO nanostructures. The reported process can be applied for the preparation of other nanoscaled metal oxide particles. The only disadvantage of this approach is the rather high calcination temperature, which can cause sintering of the ZnO nanoparticles [252].

Inspired by the unique structural and surface characteristics of cellulose nanocrystals (CNCs), Kong et al. used an evaporation-induced self-assembly process to prepare niobium oxide/CNC composite films (Figure 12) [253]. After the calcination of the CNCs in air at $600\text{ }^\circ\text{C}$, mesoporous $T\text{-Nb}_2\text{O}_5$ films were obtained that were composed of interconnected nanocrystals (size ~ 50 nm). By varying the NbCl_5/CNC mass ratio, it was possible to control the crystallite dimensions (20–50 nm) and the surface area of the Nb_2O_5 nanostructures. When studied as the electrode materials, these $T\text{-Nb}_2\text{O}_5$ nanocrystals showed very high Li^+ intercalation pseudo capacitance, wide temperature adaptability, and excellent cycle performance. The superior charge storage and kinetics benefits of the prepared $T\text{-Nb}_2\text{O}_5$ nanocrystals enabled an innovative approach toward the design of materials providing high energy density and high power density at the same time for electrochemical energy storage applications.

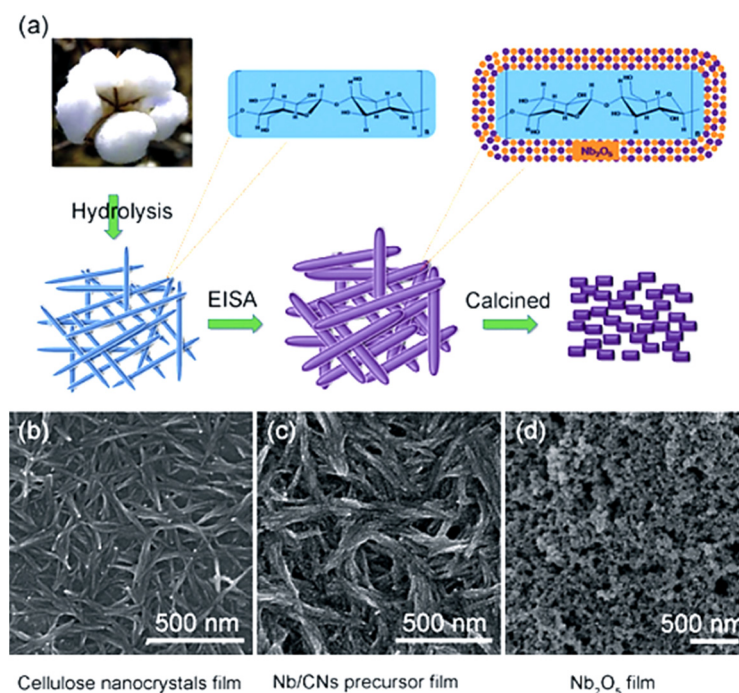


Figure 12. The schematic presentation of the Nb_2O_5 nanostructures prepared by an evaporation-induced self-assembly process directed by CNCs (a), the SEM micrographs of the CN film (b), the CN/ NbCl_5 composite film (c), and the mesoporous film of Nb_2O_5 after calcination (d). Reprinted from [253]. Copyright 2014, with permission from Elsevier B.V.

Europium (Eu^{3+}) doped, chiral nematic, mesoporous luminescent films of ZrO_2 (EDCNMZrO_2) with tunable optical properties were prepared by a hard template process using silica templated by cellulose nanocrystals (CNCs). Chiral nematic SiO_2 films were formed by replicating the chiral nematic structure of CNC using an evaporation-induced self-assembly (EISA) approach, followed by calcination at $600\text{ }^\circ\text{C}$ for 6 h, and subsequent silica etching. The obtained EDCNMZrO_2 showed selective suppression of the spontaneous emission of Eu^{3+} ions as well as the possibility of modulating their luminescence lifetime. This study is a showcase of how the capability of CNC to organize into the liquid crystal nematic phase can be exploited as an indirect template to prepare the inorganic (ZrO_2) photonic material, which has potential application in novel smart optical nanodevices [254].

4.4. Inorganic Nanostructures Supported by Carbon Fibers Formed from Cellulose

A special case represents the carbon nanofibers formed from various cellulose structures by pyrolysis in an inert atmosphere. Such structures are thermally stable and electrically conductive. When bacterial nanocellulose is used, templated carbon networks are obtained. Depending on the raw cellulose material, a whole variety of porous carbon nanostructures can be formed. For example, when wood was first delignified, the resulting cellulose hierarchical structure was exposed to cellulose enzymes to partially degrade its structure to form micro- and nanopores, followed by carbonation at $1000\text{ }^\circ\text{C}$ for 3 h in a N_2 atmosphere, a highly porous hierarchical carbon structure was obtained. Such structures with a high specific surface have been applied as electrodes in supercapacitors with high areal/volumetric energy density and excellent stability [255]. Porous carbon hierarchical structures based on wood cellulose are frequently studied as electrodes in supercapacitors or in batteries [256,257]. Various cellulose raw materials including agro waste can be applied to form porous hierarchical carbon structures [258]. Carbonized cellulose structures have a wide range of potential applications. For example, regenerated cellulose (RC) fibers with low crystallinity have been used as a template for the formation of inorganic hollow structural materials by a simple pyrolysis procedure. The RC- CuO composite fibers were

composed of cellulose fibers and a high concentration of CuO NPs inside the fibers. The obtained heterogeneous system allowed for the specific thermal decomposition mechanism of the cellulose template during the pyrolysis process, involving the migration of the CuO NPs from the center to the fibers' edge (Figure 13). At the end, Cu@C and CuO hollow microfibers with a controllable morphology and size were formed in an argon and air atmosphere, respectively. Aside from the copper-based hollow structures, other metallic hollow structural materials such as the Ni@C as well as the hollow structures of many inorganic oxides (NiO, Fe₂O₃, Mn₂O₃, Fe₃O₄@C, MnO@C) have been prepared through this process. The reported approach to create hollow fibers was demonstrated to be scaled-up easily and the application of elaborated processes as well as expensive starting materials was avoided. The potential applications of the prepared hollow inorganic fibrous materials are in microfluidics, as microreactors, and in catalysis [259].

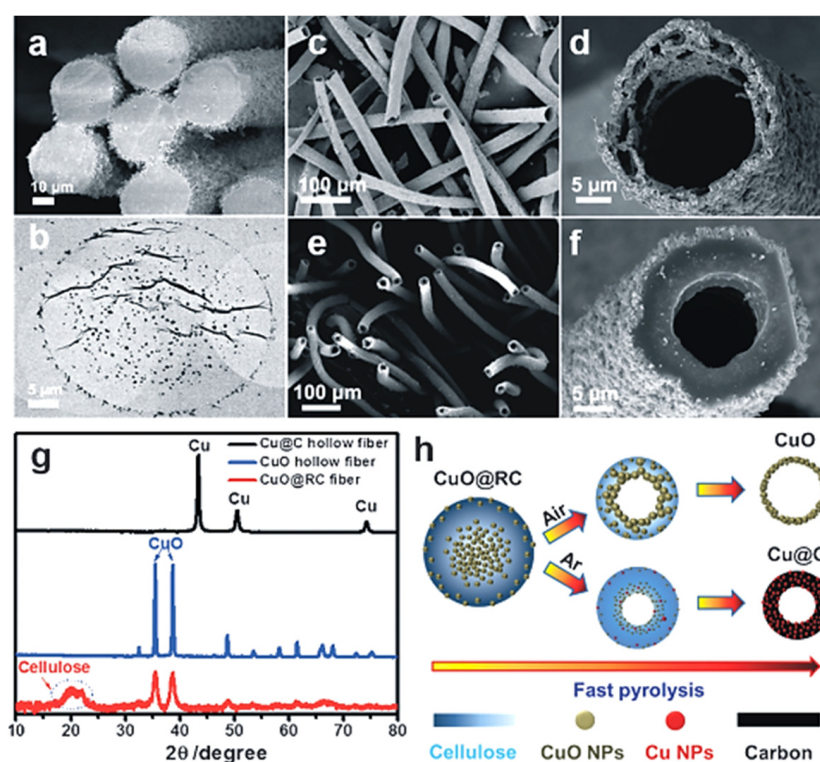


Figure 13. (a) The SEM and (b) TEM images of the CuO–RC filaments. (c,d) SEM images of CuO– and (e,f) SEM images of the Cu@C hollow fibers. (g) The XRD patterns of the CuO–RC fibers, CuO, and Cu–C hollow fibers. (h) The formation of CuO and Cu–C hollow fibers by the fast pyrolysis of CuO–RC filaments. CuO and Cu–C hollow fibers were obtained by the pyrolysis of CuO–RC filaments at 600 °C for 1 h in an air and argon atmosphere, respectively [259]. Copyright 2016 John Wiley & Sons Inc. Reproduced with permission.

Nitrogen-doped carbon networks were formed by carbonizing the polyaniline (PANI) coated BNC at 850 °C for 2 h in a flow of N₂ where the bacterial nanocellulose (BNC) was applied as the precursor and template. The obtained carbon networks functioned as conductive networks for the integration of active electrode materials providing the fast electron transfer and as a support for the preparation of high capacitance electrode materials. MnO₂ was formed on the surface of the activated carbon network by the redox reaction using KMnO₄ as a precursor. The prepared asymmetric supercapacitors, based on activated carbon/carbon-MnO₂, showed a maximum power density of 227 kW kg^{−1} and a high energy density of 63 W h kg^{−1} in an aqueous solution of 1.0 M Na₂SO₄. Their energy density was higher than most values reported for the activated carbon//MnO₂ asymmetric supercapacitors. Additionally, the resulting supercapacitor also showed a formidable cycling performance with a 92% specific capacitance retention after 5000 cycles.

The reported approach represents an environmentally-friendly and low-cost preparation process of electrode materials with potential application in high-performance energy storage devices [260].

The thermal reduction of metallic nanoparticles in the presence of cellulose is questionable due to its rather low thermal stability, but the thermal reduction of metals in an inert atmosphere accompanied with carbonization of the cellulose is possible. For example, metallic Ni nanoparticles deposited on bacterial cellulose-derived carbon fibers (Ni-NPs/BCCF) were synthesized using a simple impregnation-pyrolysis method as efficient electrocatalysts for a two electron oxygen reduction reaction ($2e^-$ ORR). NiCl₂ was first deposited on BC by its immersion in an aqueous solution of the precursor (NiCl₂-conc. = 0.1 mol L⁻¹) for 24 h and subsequently freeze-dried. The resulting material was pyrolyzed first at 360 °C for 2 h and then at 700 °C for an additional 2h both in an Ar atmosphere. After cooling down to RT, the solid product was ground in a mortar, washed several times with deionized water and ethanol, and dried for further use. In 0.1 mol L⁻¹ KOH, the Ni-NPs/BCCF-20.7 sample showed a high electrocatalytic performance toward $2e^-$ ORR, exhibiting a H₂O₂ selectivity of ~90% and an onset potential of 0.75 V vs. the reversible hydrogen electrode (RHE). By applying this catalyst, a high Faradaic efficiency (93.9% ± 4.2% at 0.5 V vs. RHE in bulk ORR electrolysis) and a high H₂O₂ yield rate (162.7 ± 13.7 mmol g_{cat}⁻¹ h⁻¹ at 0.2 V vs. RHE) were achieved. This work provides new insights into the design and development of high efficiency $2e^-$ ORR electrocatalysts for H₂O₂ production [261].

The number of publications on cellulose-templated or cellulose-based carbon fiber supported inorganic structures is quite numerous and they are summarized in Table 4. Table 4 itself is divided into two parts: the first part is devoted to the publications on cellulose-templated porous purely inorganic structures, while the second part comprises the publications on inorganic nanostructures supported by cellulose-based carbon (nano)fibers. The preparation procedures in both cases were similar; that is, the formation of inorganic structures templated by cellulose, followed by thermal treatment of the structure. The difference was only in the type of atmosphere used during the thermal processing. In the first case, the thermal treatment was performed in air, causing the complete degradation of the cellulose structure and leaving predominantly porous inorganic structures, while in the second case, thermal treatment was carried out in an inert atmosphere, causing the carbonization of cellulose and producing carbon fiber supported inorganic structures. The resulting structures were predominantly tested for (photo)catalytical systems, anodes in Li batteries, or electrodes in various sensors.

Table 4. The list of publications on cellulose-templated porous metal oxide structures or metal oxide nanostructures supported by carbon fibers formed from cellulose structures. The list is organized from large cellulose structures (CF and RC) via the microstructured celluloses (MCC and MFC) to the nanostructured celluloses (BNC and CNCs).

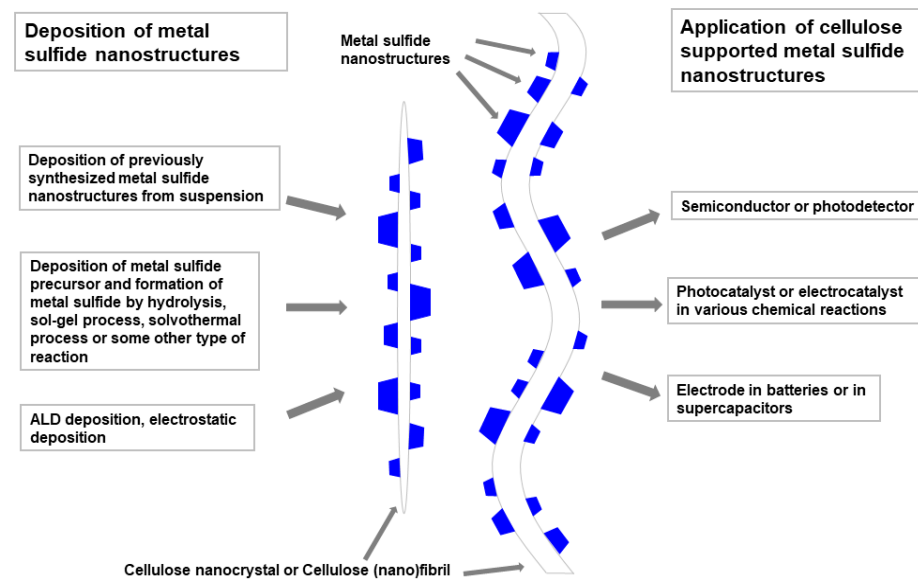
Inorg. Particle (Size—nm)	Cellulose Used	Precursor (Synthetic Path)	Application	Reference
Cellulose Templated Inorganic Oxides				
TiO ₂	MCC	titanium isopropoxide, HNO ₃ , H ₃ PO ₄ , NaOH, urea	Sorbent microextr. of organic compounds	[262]
TiO ₂ nanofibers	CNF	titanium isopropoxide, NH ₃	Photocatalyst—degr. of methylene blue	[263]
TiO ₂ network	CNCs	Ti(N(CH ₃) ₂) ₄ , atomic layer deposition titanium(IV)	Photoelectrochemical water splitting	[250]
TiO ₂	CNCs	ethoxide	Sorbent for microextraction	[264]
TiO ₂	CNCs	Ti-n-butoxide	Photocatalyst—(degradation of methylene blue)	[265]
TiO ₂	CNCs	tetra-n-butyl titanium	Photocatalyst—degradation of Rhodamine B	[266]
α-Fe ₂ O ₃	CF	FeCl ₃ , calcination	Catalyst (oxidation of alcohols with H ₂ O ₂)	[267]
α-Fe ₂ O ₃	CF	FeCl ₃ , calcination	Magnetic materials, catalyst	[268]
α-Fe ₂ O ₃	CF	FeCl ₃ , calcination	—	[269]
Fe ₂ O ₃	RC	FeCl ₂ , NaOH	—	[270]
Fe ₃ O ₄ NPs (10 nm)	BNC	Fe(NO ₃) ₃ , urea, hydrothermal reaction	Electrode in Li batteries	[271]
Fe ₃ O ₄ NPs (10 nm)	BNC	Fe(NO ₃) ₃ , urea, hydrothermal reaction	Flexible electrodes in Li batteries	[272]
Fe ₂ O ₃ NPs	BNC	Fe(NO ₃) ₃ , pyrolysis	Anode in Li-ion batteries	[273]
ZnO	CF	ZnCl ₂ , NaOH, ethylenediamine	Photocatalyst (degradation of methyl orange)	[274]
ZnO	CF	Zn(NO ₃) ₂ , urea, calcination	Photocatalyst (degradation of methyl orange)	[275]
ZnO (500–1000 nm)	MCC	Zn(NO ₃) ₂ , NH ₃ , microwaves, hydrothermal reaction	Photocatalyst (degr. of methylene blue and rhodamine B)	[276]
In ₂ O ₃ –SnO ₂ nanotubular (ITO)	CF	In(III) acetylacetonate, Sn(IV) isopropoxide	Active multilayers in photoanode	[277]
Co ₃ O ₄ NPs (50–100 nm)	RC	CoCl ₂ , calcination	Electrode in Li batteries	[278]
MnO ₂ NPs	MCC	Mn(CH ₃ COO) ₂ , CO(NH ₂) ₂ , KOH, (CH ₂) ₆ N ₄ , NaOH, calcin	—	[279]
Co _{0.5} Cu _{0.5} Fe ₂ O ₄	CF	Fe(NO ₃) ₃ , sol-gel process, calcination	—	[280]
V ₂ O ₅ , V ₂ O ₃ , Fe ₃ O ₄ , WO ₃ (200–1000 nm)	CF	Vanadium(V) oxychloride, tungsten(VI) chloride, iron(III) chloride	—	[281]
CoFe ₂ O ₄ NPs (5–10 nm)	BNC	Fe(NO ₃) ₃ , Co(NO ₃) ₂ , NH ₄ OH	Catalyst in fuel cells	[282]
MnO ₂ NPs	BNC	KMnO ₄ , K ₂ SO ₄ , reduction by C	Electrode in supercapacitors	[283]
MnFe ₂ O ₄	CF	Previously synthesized MnFe ₂ O ₄	Adsorbent for As(III) and As(V)	[284]
LaNiO ₃	MCC	La nitrate, Ni nitrate, NH ₃ , EDTA	Catalyst (steam CO ₂ reforming of methane)	[285]
SnO ₂	CF	(Sn(OiPr) ₄ , sol-gel process, calcination	Electrode Li batteries	[286]
SnO ₂	BNC	SnCl ₂ , pyrolysis	Anode in Li-ion batteries	[287]

Table 4. Cont.

Inorg. Particle (Size—nm)	Cellulose Used	Precursor (Synthetic Path)	Application	Reference
Inorganic Nanostructures Supported by Carbon Fibers Formed from Cellulose				
Ge	BNC	GeBr ₂ , pyrolysis	Anode in Li-ion batteries	[287]
Pd-Al	CF	Pd(NO ₃) ₂ , Al(NO ₃) ₃ (decomposition in a reducing atm. H ₂ /N ₂)	Catalyst—(hydrogenation of cyclohexene)	[288]
Ni	MCC	Ni(OOCCH ₃) ₂ ,	Catalyst (conv. of p-nitrophenol into p-aminophenol)	[289]
Ni/NiO NPs (2–100 nm)	CNCs	Ni(NO ₃) ₂ , glycine, calcination	–	[290]
Ru NPs	BNC	RuCl ₃ , pyrolysis	Electrode in Li–O ₂ batteries	[291]
Fe ₃ C NPs (10–30 nm)	BNC	FeCl ₃ , pyrolysis	Electrode in Li-ion or Na-ion batteries	[292]
MoS ₂ nanoleaves	BNC	Na ₂ MoO ₄ , CS(NH ₂) ₂ , pyrolysis	Anode in Li-ion batteries	[293]
MoS ₂ NPs	BNC	(NH ₄) ₆ Mo ₇ O ₂₄ , CH ₄ N ₂ S, hydrothermal process	Electrocatalyst in H ₂ evolution reaction	[294]
NiCo ₂ S ₄	CF	Ni(NO ₃) ₂ , Co(NO ₃) ₂ , hexamethylenetetramine	Positive electrode in supercapacitors	[295]
BiOBr	CNFs	Bi(NO ₃) ₃ , NaBr, ethylene glycol	Adsorbent for rhodamine B and Cr(VI)	[296]

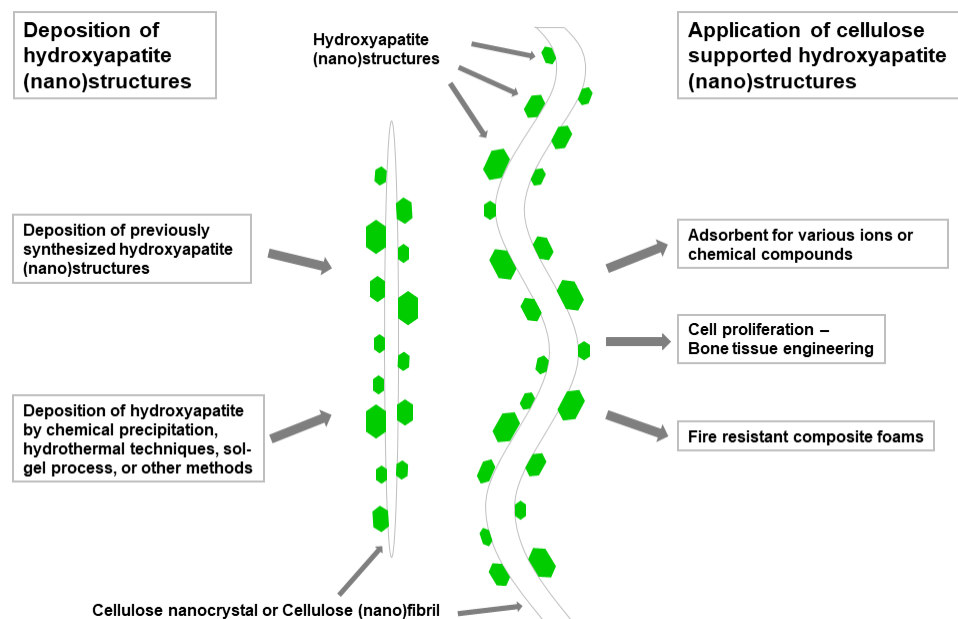
5. Cellulose Supported/Templated Nanostructures of Metal Sulfides, Hydroxyapatites, and Other Inorganic Compounds

The synthesis of cellulose/inorganic nanohybrid materials has become an important topic of research in science and industry since it offers novel and innovative applications in catalysis, energy harvesting, energy conversion and storage, drug delivery, etc. Aside from metallic and metal oxide particles, other inorganic compounds such as various inorganic sulfides, apatites, halides, etc. can be deposited or formed by using cellulose as a support and/or template. Other than metals and metal oxides, cellulose-templated hierarchical structures of other types of inorganic compounds can also be prepared such as various sulfides, halides, carbonates, and phosphates. The formation of cellulose supported metallic sulfides has not been as intensely studied as metals and metal oxides, but there has been a review partially dealing with this topic [297]. Deposition of AgCl on the bacterial cellulose is a simple route to the manufacturing of hydrophilic antimicrobial membranes, which are a promising alternative for antimicrobial wound dressings. Cellulose has been proven to be an alternative universal platform for engineering a variety of functional materials at the nanoscale. Cellulose hydroxyl groups not only anchor metallic ions tightly on the BC nanofibers via the ion–dipole interaction, but also stabilize inorganic nanoparticles by a strong interaction with their surface hydroxyl groups, thus preventing their aggregation. In many cases, the authors have used cationic surfactants to facilitate the synthesis of well-defined semiconductor nanoparticles on the cellulose surface. A special case is represented by decorated cellulose-based materials or surface-coated with carbonates, and especially with various types of hydroxyapatites. The resulting inorganic cellulose-based composites are biocompatible and capable of facilitating the osteoblast cell attachment and growth. Such materials have potential application as bone tissue scaffolds and in other biomedical fields. Additionally, these materials exhibit an effective adsorption of various ions from water solutions. Consequently, they are promising water purification materials distinguished by fast adsorption rates and high capacities. The presentation of the versatility of cellulose substrates, the formation processes of the metal sulfide nanostructures, and the potential applications of these hierarchical structures are shown in Scheme 5.



Scheme 5. The schematic representation of the cellulose/metal sulfide particle nanocomposites, synthetic routes, and the most frequent applications of such materials.

In Scheme 6, the versatility of the cellulose substrates, the formation processes of hydroxyapatite nanostructures, and the possible applications of these hierarchical structures are presented.



Scheme 6. The schematic representation of the cellulose/hydroxyapatite nanocomposites, synthetic routes, and the most frequent applications of these materials.

5.1. Cellulose Supported/Templated Metal Sulfides

By using the porous structure of the regenerated cellulose, the CdS nanostructures were formed from the CdCl_2 solution. The cellulose pores functioned as reaction cavities where the CdS nanoparticles were grown and deposited in the shell composed of the cellulose fibers that prevented the aggregation of forming nanostructures. The CdS nanoparticles (size 6 nm) were homogeneously distributed and tightly adsorbed onto the cellulose structure by the strong intermolecular interaction between the CdS and cellulose fibers, thus preventing their aggregation. The CdS/cellulose composite films showed a substantially

enhanced photocatalytic activity due to the porous structure of the cellulose template and the presence of the CdS nanoparticles. Additionally, for the promotion of H₂ evolution, Pt was applied as a cocatalyst. This was formed in situ on the surface of the CdS–cellulose films by photo deposition using H₂PtCl₆ as a precursor. The cellulose fiber supported CdS nanoparticles showed a high efficiency in the photocatalytic evolution of hydrogen, and as a portable photocatalyst, they were easily recovered, avoiding environmental pollution [298].

An innovative nanocomposite aerogel composed of TEMPO oxidized microfibrillated cellulose embedded in a layer of previously synthesized ultrathin, fire retardant nanosheets of MoS₂ was prepared. The cross linking between Mo⁴⁺ cations and carboxyl (–COOH) as well as hydroxyl (–OH) groups on the cellulose surface caused intense interaction between the MoS₂ nanosheets and the cellulose fibers, thus enabling the formation of an aerogel with a density of 0.00473 g cm^{−3} and a 97.36% porosity. The resulting material showed outstanding self-extinguishing capabilities and fire resistant properties as characterized by cone calorimetry as well as by the vertical burning test. The MoS₂ structure in the aerogel remained unchanged after the vertical burning test, as shown by Raman spectroscopy. This study represents a new approach toward the preparation of fire resistant and lightweight aerogel materials for application in the construction of fire resistant and energy efficient buildings as well as aerospace applications [299].

Various semiconducting sulfide nanostructures such as ZnS, PbS, and CdS have been prepared by using cellulose nanocrystals (CNCs) as supports combined with cationic surfactants as stabilizers. Their synthesis on the CNC surface was carried out by reacting precursor salts such as ZnCl₂, Pb(NO₃)₂, and CdCl₂ with H₂S gas. In the controlled growth of defined semiconductor nanoparticles, the application of a cetyltrimethylammonium bromide (CTAB) cationic surfactant was the crucial factor. The pH of the salt solution and precursor concentration were varied to control the packing density and average particle size of the sulfide semiconductor nanostructures on the CNC surface. This procedure could serve as an innovative universal platform for engineering a variety of nanoscale functional materials for optical and electronic nanodevices [300].

5.2. Cellulose Supported/Templated Hydroxyapatites

Carbonated hydroxyapatite (CHA) modified microfibrillated cellulose (MFC) was studied as an adsorption substrate for Ni²⁺, Cd²⁺, PO₄^{3−}, and NO₃[−] ions from the aqueous solution. The MFC was initially treated with NaOH and CHA was subsequently deposited on its surface by the reaction of CaCl₂ and NaH₂PO₄. The obtained results revealed that the removal of all of the studied ions was not dependent on the pH and was highly effective for Ni²⁺, Cd²⁺, and PO₄^{3−}. Namely, the adsorption efficiency for NO₃[−] removal from an aqueous solution reached more than 50% while the adsorption efficiencies for the other three ions were higher than 90%. The highest observed removal capacities of the studied CHA/MFC adsorbent for the NO₃[−], PO₄^{3−}, Cd²⁺, and Ni²⁺ ions were 0.209, 0.843, 1.224, and 2.021 mmol g^{−1}, respectively. The adsorption kinetics was very fast for all of the studied ions. This study demonstrated that CHA/MFC was an environmentally-friendly and practical adsorbent, exhibiting high removal efficiencies for both the metallic and phosphate ions while the removal efficiency for the nitrate ions was only moderate [301].

A biomimetic approach was applied for the development of hydroxyapatite/bacterial cellulose nanocomposites with bone healing properties. The nucleation of calcium-deficient hydroxyapatite (cdHAp) was initiated by the adsorption of carboxymethyl cellulose (CMC) on two forms of bacterial cellulose (BC) (pellicles and tubes). The dynamic simulated body fluid (SBF) was used in the formation of the cdHAp in vitro over a one-week period. The atomic content of phosphorus and calcium varied from 0.3 to 11.2 atomic % and 0.4 to 7.7 atomic %, respectively, while the Ca/P overall ratio changed from 1.2 to 1.9 and the crystal size of cdHAp decreased with the decrease in the density of bacterial nanocellulose fibrils. The differentiation and morphology of the osteoprogenitor cells were studied through alkaline phosphatase gene expression and fluorescence microscopy to determine the viability of the scaffolds in vitro. The BC surface coated with cdHAp crystals showed

an enhanced cell attachment, indicating that the BC-cdHAp scaffolds were a feasible and promising bone scaffolding material [302].

Cellulose (BC) is a high-strength fibrous and extensively used biomaterial while hydroxyapatite (HAp) has outstanding osteoconductivity and bioactivity. Composite materials composed of cellulose matrices and inorganic nano-hydroxyapatite (n-HA) fillers have received considerable attention in bone engineering, although the brittleness and low strengths limit their application. Therefore, the improvements in the toughness and mechanical strength of aerogel-based biomaterials are necessary. A urea alkali system was applied to disperse and gelate cellulose mixed with silk fibroin (SF) to prepare the composite aerosol. n-HA was prepared by swelling PAA with water for 20 h and then CaCl_2 was added and stirred at 90°C until complete dissolution. Subsequently, the Na_2HPO_4 solution ($\text{Ca}/\text{P} = 1.67$) was admixed into the prepared solution with the pH adjusted to 10 using a NaOH solution. After this, the solution was stirred for 2 h at 90°C followed by aging at RT for 24 h. At the end, the resulting precipitate was freeze-dried and calcined at 800°C to prepare the n-HA. By using uniaxial compression, the composite aerogel material with a density close to that of natural bone was prepared with a high mechanical strength and toughness. When the ratio of the cellulose, n-HA, and SF was 8:1:1, the composite aerogel showed the same mechanical strength range as the cancellous bone. HEK-293T cells, cultured on these composite aerogels, exhibited a high ability of adhesion, differentiation and proliferation. The studied biodegradable composite aerogel has high potential to be applied as a bone tissue substitute in bone-tissue engineering [303].

The one-step electrophoretic deposition process (EPD) was used for the preparation of an innovative bioglass—a cellulose nanocrystal (BG-CNC) bioactive hybrid material—to be applied for the surface coating of orthopedic implants with the purpose to enhance their contact with the bone tissue. The characterization of the prepared materials revealed that the network of CNCs functioned as an in situ template tailoring the mineralization rate and morphology of the formed hydroxyapatite (HA) crystal phase (Figure 14). The BG particles were individually wrapped by a nanoporous CNC layer. A very rapid formation of a HA layer (after 0.5 day) on the BG particles of the deposited BG-CNC coating in the simulated body fluid was observed during in vitro characterization. The cell culture tests using the MC3T3-E1 cell line revealed that the formed BG-CNC hybrid coatings represent a promising platform for the proliferation, accelerated attachment, and differentiation of cells, confirming their potential in biomedical applications as an advanced bone contacting material [304].

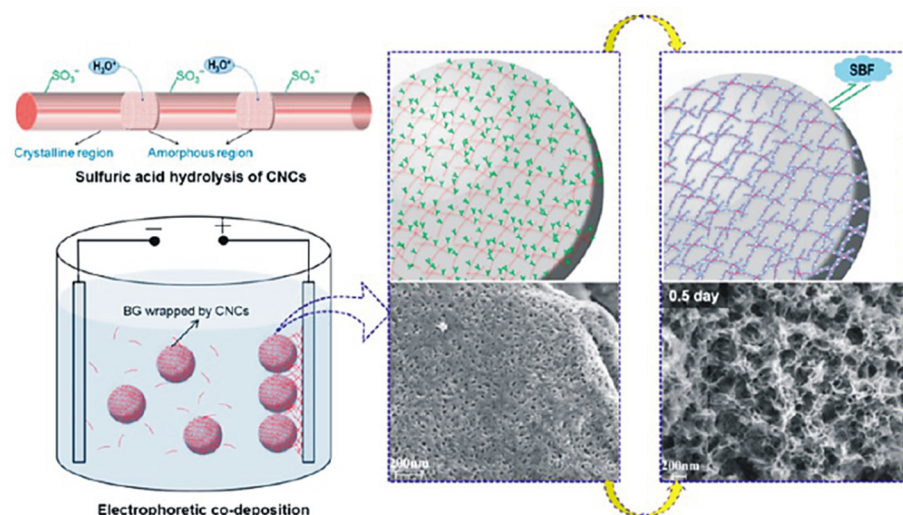


Figure 14. The schematic model describing the interaction between the BG particles and CNCs in the suspension, together with their electrophoretic co-deposition process as well as the mechanism of mineralization by the formation of HAp in the simulated body fluid. Reprinted with permission from [304]. Copyright 2015 American Chemical Society.

5.3. Miscellaneous Cellulose Supported/Templated Inorganic Compounds

Cellulose fibers with UV activity have been prepared by spinning of 8 wt.% α -cellulose solution in *N*-methylmorpholine-*N*-oxide (NMMO) using a dry-wet method and by subsequent surface modification of the fibers by the deposition of the $\text{Gd}_4\text{O}_3\text{F}_6\cdot\text{Eu}^{3+}$ doped with 5 mol % of the Eu^{3+} . During its dissolution process in NMMO, the photoluminescent nanostructures were admixed as a powder into the cellulose matrix. Photoluminescence spectroscopy was used to study the relationships between the emission intensity and the excitation energy as well as the concentration of $\text{Gd}_4\text{O}_3\text{F}_6\cdot\text{Eu}^{3+}$ nanoparticles in the final composite products. About 80% of inorganic particles had a diameter below 300 nm when the samples contained up to 1% of the modifier, and with an increase in the modifier concentration, the agglomeration of the particles was intensified. The obtained cellulose fibers with UV activity have potential application as a security marking for documents, textile, and paper products [305].

Cobalt ferrite (CoFe_2O_4) nanostructures were formed on the surface of the cellulose structures from CoCl_2 and FeSO_4 as precursors in the presence of KNO_3 and NaOH . These inorganic nanoparticles were applied as labels for fine cellulose fibers, representing an approach that allows for the detection of micro- and nanostructured celluloses in paper sheets in combination with various imaging technologies. The addition of nanostructured CoFe_2O_4 as a labeling material during the paper manufacturing process enables imaging in scanning electron microscopy/energy-dispersive X-ray spectroscopy experiments and provides contrast in X-ray microtomography. By combining these two techniques, the fines in the paper sheets were located, evaluated, and quantified. It was demonstrated that the water retention value, the tensile indices, and the air permeability of the handsheets were not changed by the addition of the CoFe_2O_4 labeled fines compared to the sheets where the nonlabeled fines were added. The knowledge about the distribution of nano- and microscale cellulosic structures in a cellulose fiber matrix is important to improve the properties of the existing paper products and in the future, the design of new materials in the paper industry [306].

The number of publications on sulfides, hydroxyapatites, carbonates, halides, and other types of inorganic materials is not as large as in the case of metallic oxides. These are summarized in Table 5. Metallic sulfides are mostly formed on the cellulose by hydrothermal or solvothermal processes using sodium sulfide, thiourea, or thioacetamide as a source of sulfur. Metallic sulfide-cellulose structures are predominantly used as photocatalysts, electrodes in super capacitors, and photoluminescent or fluorescent materials. Ca hydroxyapatites-cellulose structures are mostly prepared by the biological route from $\text{Na}_2\text{H}_2\text{PO}_4$ or $\text{NH}_4\text{H}_2\text{PO}_4$, and CaCl_2 using simulated body fluid. These are used as substrates in bone tissue engineering or as absorbents for heavy metal ions.

Table 5. The list of publications on cellulose supported metal sulfide, hydroxyapatite, and other inorganic nanostructures. The list is organized from large cellulose structures (CF and RC) via the microstructured celluloses (MCC and MFC) to nanostructured celluloses (BNC and CNCs).

Inorg. Particle (Size—nm)	Cellulose Used	Precursor (Synthetic Path)	Application	Reference
Cellulose Supported Metal Sulfides				
CdS	CF	CdCl ₂ , AgNO ₃ , mercaptoacet. acid	Colorimetric paper test stripe for Hg	[307]
ZnS–MoS ₂ (200–1000 nm)	CF	Na ₂ MoO ₄ , ZnCl ₂ , CH ₄ N ₂ S	Flexible Broadband Photodetector	[308]
AgInS ₂ NPs	CF	AgNO ₃ , In(NO ₃) ₃ , NaOH, cysteine	Nanodrug for hepatocellular carcinoma	[309]
CuS	MFC	CuSO ₄ , Na ₂ S, NaOH, NH ₃ , xylan	Paper for ablation of pathogenic microorganisms	[310]
CuS (100–1000 nm)	BNC	CuSO ₄ , Na ₂ S	Electrode in supercapacitors	[311]
CdS	BNC	Cadmium(II) chloride, thiourea	Photocatalyst–methyl orange under UV	[312]
MoS ₂	CF	Na ₂ MoO ₄ , thiourea, MnCl ₂	Photocatalyst–degr. of RhB dye	[313]
ZnS	BNC	Zinc(II) acetate, thioacetamide	Fluorescent material	[314]
Zn _x Cd _y S	BNC	Cd(II) chloride, thiourea	Photocatalyst–H ₂ prod.-visible light	[315]
ZnO–CdS	BNC	Zinc(II) nitrate, Cd(II) sulfate	Photocatalyst–methyl orange–UV	[236]
MoS ₂ NPs (10 nm)	BNC	(NH ₄) ₂ MoS ₄ , N ₂ H ₄	Electrocatalyst in H ₂ evolution react.	[316]
MoS ₂ NPs	BNC	(NH ₄) ₂ MoO ₄ , CH ₄ N ₂ S,	Electrode in Li-ion batteries	[317]
ZnS	CF	Zinc(II) nitrate hexahydrate, sodium sulfide	Photoluminescent material–security paper	[318]
In doped Mo(O,S) ₂	CNFs	MoCl ₅ , InCl ₃ , CH ₃ CSNH ₂ , NH ₂ NH ₂	Photocatalyst for organic dyes	[319]
FeS NPs (10–20 nm)	CF	Iron(II) chloride, sodium sulfide	Uranium(VI) ions immobilization–water purification	[320]
Ni ₃ S ₂ NPs	BNC	NiCl ₂ , CN ₂ H ₄ S, NH ₃	Electrode in supercapacitor	[321]
Cellulose supported hydroxyapatites				
Ca hydroxyapatite	MFC	NaH ₂ PO ₄ , CaCl ₂	Adsorbent for Cr(VI) ions, H ₂ O purification	[322]
Ca hydroxyapatite	BNC	NaH ₂ PO ₄ , CaCl ₂	Cell proliferation–bone tissue engin.	[323]
Ca hydroxyapatite	CF	Ca(NO ₃) ₂ , CO(NH ₂) ₂ (NH ₄) ₂ HPO ₄ , NaOH,	Cell proliferation–bone tissue engin.	[324]
Ca phosphate–Ca hydroxyapatite	CF	CaCO ₃ , P ₂ O ₅ , MgO Ca hydroxyapatite	Injectable bone paste	[325]
Ca hydroxyapatite	CF	Ca(NO ₃) ₂ , (NH ₄) ₂ HPO ₄ , NH ₃	Adsorbent for Hg, H ₂ O purification	[326]
Ca hydroxyapatite	CNFs	Ca(NO ₃) ₂ , (NH ₄) ₂ HPO ₄	Fire resistant composite foams	[327]
Ca nanohydroxyapatite	CNCs	Commercial hydroxyapatite	Cell proliferation–bone tissue engin.	[328]
Ca hydroxyapatite	CNCs	Ca(NO ₃) ₂ , (NH ₄) ₂ HPO ₄	Adsorbent for chlortetracycline	[329]
Cellulose supported miscellaneous inorganic nanostructures				
CaCO ₃ NPs	CF	CaCl ₂ , Na ₂ CO ₃	Biomedical material	[330]
EuF ₃ NPs (250–600 nm)	CF	LiCl, EuF ₃	Phosphor–flexible optical material	[331]
Se NPs	CNCs	H ₂ SeO ₃ , Na ₂ SeO ₃ , sorbitol	-	[332]
Bi NPs (2–10 nm)	CNFs	Bi(NO ₃) ₃ , NaBH ₄	Agent for enhanced radiation therapy	[333]

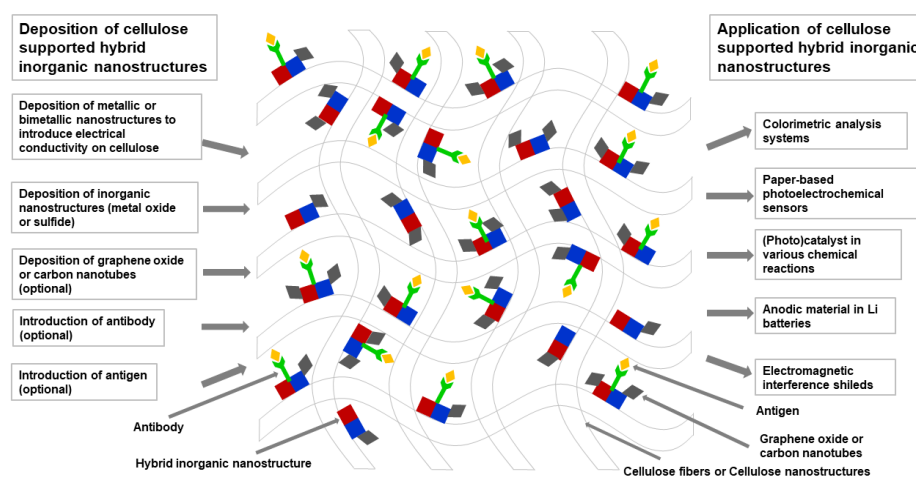
Table 5. Cont.

Inorg. Particle (Size—nm)	Cellulose Used	Precursor (Synthetic Path)	Application	Reference
Cellulose supported miscellaneous inorganic nanostructures				
Ni(OH) ₂ NPs	BNC	NiSO ₄ , NH ₄ F, NH ₃	Electrode in supercapacitors	[334]
AgCl NPs	CF	AgNO ₃ , NaCl	Antibacterial agent	[335]
AgCl/Ag (~1200 nm)	CF	AgNO ₃ , AlCl ₃ , NaOH	Photocatalyst, antibacterial agent	[336]
FeOOH	BNC	-	Flexible electrode-supercapacitors	[337]

6. Cellulose Supported or Templated Hybrid Inorganic Nanostructures

Aside from metallic, metal oxide, or other inorganic nanoparticles, various complex hybrid nanostructures have also been formed on the cellulose surface. The specific fibrous structure and high number of hydrogen bonds give the cellulose sufficient porosity and high specific surface area, which can serve as a matrix to support other functionalized materials and as a template to form various inorganic hierarchical nanostructures. New materials with interesting combinations of properties and functions have been prepared by combining different inorganic nanostructures and polymer chains with various cellulose structures. Other than cellulose supported or templated inorganic compounds, more complex hybrid modifications or decorations of the cellulose structures have also been studied and reported. Complex hybrid cellulose materials have a wide variety of potential applications (e.g., in medicine, pharmaceutical technology, chemical catalysis, electronics, and energy conversion [1,3,338–340]). The development of complex cellulose-based structures aims at the formation of hierarchical nanoparticle structures with specific tailored combinations of properties for various applications such as the optimization of the catalytic activity through a combination of two catalytic materials or the optimization of the antibacterial activity of wound dressings through a combination of two antibacterial agents. In addition, combinations of three or even more components with cellulose have been reported. For example, MnO₂, polypyrrole, and cellulose nanocrystals were applied to form lightweight, highly porous, and flexible hybrid (inorganic–organic) materials based on the cellulose aerogel for super capacitive application. Supercapacitors are a highly propulsive area of research and have already found commercial application [1]. A complex combination of cellulose nanocrystals, Fe₃O₄, cationic polymer, SiO₂, poly(vinylpyrrolidone), and cyclodextrine was studied and its potential application in the separation of pharmaceutical compounds was demonstrated. Similarly, the CNC/Fe₃O₄/Au (CNFeAu) nanocomposite was used as a support matrix for the immobilization and separation of papain from the reaction solution with a high enzyme loading; the conjugated biomolecules retained their high enzyme activity and exhibited high stability and reusability. Inorganic nanostructures can be synthesized in situ on the surface of the cellulose fibrillar structure or they can be admixed to the cellulose. In this way, ZnO nanoparticles were formed in the presence of various saccharides, and such saccharide capped ZnO nanostructures were further deposited on the pine cellulose fibers that were subsequently incorporated into the alginic acid sheets, producing paper materials with a high degree of immobilization of biomolecules for the detection of blood type. Instead of chemical methods, physical methods of nanostructure formation can also be applied. For example, cellulose–Cu and Al₂O₃ sandwich nanostructures were prepared by magnetron sputtering and RF reactive sputtering, producing promising materials for EMI shielding applications. Recently, cellulose paper substrates have attracted tremendous interest from both academia and industry as a platform for biosensing applications. Cellulose fibers have an interesting combination of features that makes this substrate advantageous or even ideal for conducting chemical and biological analyses comprising the passive transport of fluids through their capillary wicking, excellent biocompatibility and biodegradability, large surface-to-volume ratio,

porous structure, high abundance, and most importantly, their low-cost [339,341]. Since most of these hybrid structures contain biological molecules (proteins or DNA), doubt about the stability of the reported sensing devices over time has risen because in most cases, it was not studied. In Scheme 7, the versatility of cellulose substrates, the formation processes of hybrid cellulose/metallic or metal oxide particles, and the application possibilities of these complex hierarchical structures are presented.



Scheme 7. The schematic representation of hybrid cellulose/metallic or metal oxide particle nanocomposites, the synthesis or preparation procedures, and the most frequent applications of these materials.

6.1. Cellulose Supported Metallic Hybrid Nanostructures

A sensitive paper-based electrochemiluminescence origami device (PECLOD) for the detection of the human immunoglobulin G (H-IgG) antigen based on the rolling circle amplification (RCA) using the Au-paper working electrode (Au-PWE) was developed (Figure 15). The Au-PWE functionalized with the Ab1 antibodies provided a suitable environment for the efficient capture of H-IgG and played a significant role in electrochemiluminescence (ECL) amplification due to its 3D macroporous structure. Carbon dot (CD)-tagged RCA amplified DNA as a signal amplification device significantly increased the sensitivity and offered a high ratio of signal labels. The prepared PECLOD demonstrated the ultrahigh sensitivity, acceptable reproducibility, and broad dynamic range with very limited non-specific adsorption under optimal conditions by applying H-IgG as a model protein. The designed PECLOD showed a dynamic response to H-IgG ranging from 1.0 fM to 25 pM with a very low detection limit of 0.15 fM. Additionally, the reported approach showed a potential to be extended for the detection of other biomarkers or proteins [342].

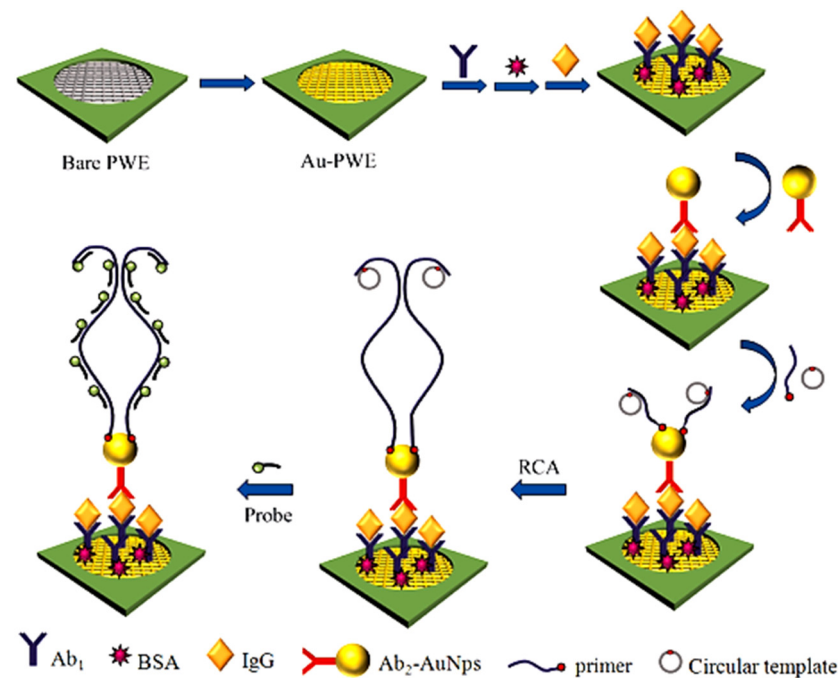


Figure 15. The schematic presentation of the fabrication procedures for the paper-based electrochemiluminescence origami device (PECLOD), (IgG—human immunoglobulin G protein; Ab—capture antibodies of IgG; BSA—bovine serum albumin; Ab₂—monoclonal antihuman IgG antibodies; Au Nps—gold nanoparticles; primer—primer DNA; circular template—circular template DNA; probe—carbon dots-DNA probe; RCA—rolling circle amplification). Reprinted from [342]. Copyright 2015, with permission from Elsevier B.V.

Ordinary filter paper with a 6 μm pore size was applied as a solid support that facilitated the impregnation with europium tetrakis dibenzoylmethide triethylammonium (EuD_4TEA) and with gold nanoparticles that provided durability. This impregnated paper-based sensor platform was applied for the development of the fluorescence turn-on cyanide (CN^-) assay in aqueous media. The detection mechanism was based on two processes: (a) Ligand exchange of TEA with the CN^- ion stimulating the enhancement of cyanide specific fluorescence, and (b) the dissolution of gold nanoparticles, causing the recovery of fluorescence. The described CN^- assay demonstrated a visible transition of color as a function of CN^- exposure in the concentration range from 10^{-2} to 10^{-12} M. Additionally, an algorithm of image processing was developed that enabled the color change calibration and quantification of the CN^- concentration. The reported algorithm was applicable to an Android smart phone, thus transforming it into a quantitative detector of CN^- ions. The reported approach enabled sensitive, fast, and simple instrument free CN^- ion detection in water as well as the possibility of remote water monitoring and controlling in the laboratory [343].

By using cellulose nanocrystals (CNC) as a template, mesoporous silica (SiO_2) films with chiral nematic ordering were prepared and further applied as a hard template for the formation of silver nanoparticles (AgNPs) from AgNO_3 by reduction with NaBH_4 . The resulting SiO_2 films deposited with the Ag NPs showed optical activities in the vicinity of the surface plasmon resonance (SPR) of the Ag NPs, as shown by the circular dichroism (CD) measurements. By conducting the experiments with three different SiO_2 hard templates loaded with AgNPs dried and soaked with water, it was shown that the optical activities only originated from the long-range organization of the Ag NPs in the nematic chiral silica template. Since the SPR of metallic NPs is important in biosensing, the application of the response based on the chiral organization of metallic AgNPs embedded in a chiral mesoporous host will lead to the development of new biosensors. This is a showcase of

the indirect application of CNC nematic liquid crystals in the formation of optically active inorganic structures [344].

Additionally, cellulose fibers (paper) have been used for the preparation of large surface area bioactive hybrid scaffolds by exploiting the self-assembly and adsorption of the previously formed oxidized nickel (Ni/NiO) nanoparticles (NPs). The Ni/NiO NPs enabled the oriented binding of functional His-tagged protein G to the cellulose surface as it was confirmed by the subsequent binding of fluorescent antibodies. It was shown that the interaction between the polyhistidine-tagged protein and the nickel substrate was chemically inert and highly resilient. The targeted conjugation of His-tagged protein G enabled the oriented binding of anti-Salmonella antibodies, enabling the attachment of Salmonella bacteria to the substrate (Figure 16). This simple approach opens the way for the application of other paper-supported metallic NPs as docking sites for a variety of biomolecules—nucleic acids or proteins. The reported strategy is based on the high surface area of the fibrillar cellulose structure, which enables a higher potential of protein capture, causing a large increase in the signal detection and improved assay sensitivity [345].

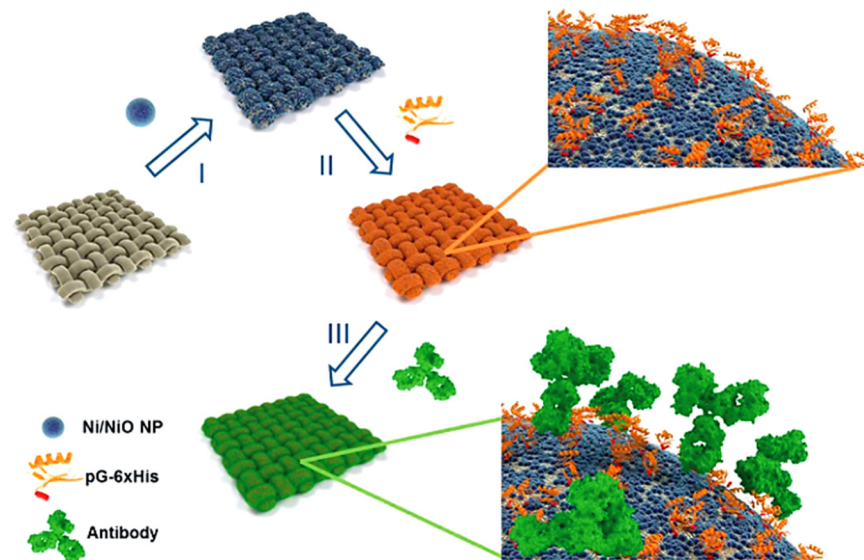


Figure 16. The schematic presentation of the bioactive scaffold preparation: (I) adsorption of Ni/NiO NPs on cellulose fiber-filter paper, (II) targeted immobilization of the polyhistidine-tagged protein G (pG-6xHis), and (III) protein G-mediated capture of antibodies. Protein G is presented by the protein G B1 domain (PDB: 1GB1, orange) bearing a 6xHis at its C-terminus (red). The antibody is an IgG2a immunoglobulin (PDB: 1IGT, green). Reprinted with permission from [345]. Copyright 2014 American Chemical Society.

α -Cellulose was applied as a support in the formation of hybrid zinc oxide/silver (ZnO/Ag) nanostructures on its surface by the microwave solvothermal synthesis using $\text{Zn}(\text{OOCCH}_3)_2$ and AgNO_3 as precursors and hexamethylenetetramine as the precipitating and reducing agent. Before synthesis, the surface of cellulose was activated by H_2O_2 with a relatively mild effect on the contact angle with H_2O . The formed ZnO/Ag nanostructure was a nanodispersed semiconductor/metal hybrid with an exceptional collective plasmonic structure never previously observed. The experiments with a single precursor solution enabled the separate study of the interaction of Zn^{2+} and Ag^+ ions with the cellulose surface and in this way, the reaction mechanism in the mixed precursor solution was explained. A specific interaction between the Zn^{2+} and the cellulose substrate was confirmed while no specific non-thermal effects of microwave heating were detected [346].

6.2. Cellulose Supported Metal Oxide Hybrid Nanostructures

For the antibody immobilization, pine cellulose fiber sheets decorated with saccharide capped-ZnO nanoparticles have been applied as a bioactive substrate. Initially, ZnO nanoparticles were formed in the presence of starch and alginic acid as well as sucrose and glucose. The fibers of pine cellulose were subsequently surface modified by the prepared saccharide capped ZnO nanoparticles that were finally incorporated into sheets of alginic acid. The immobilization of antibodies on the surface of the fibers was significantly enhanced by the adsorbed ZnO nanoparticles. The observed retention of antibodies was about 95% after rewetting the ZnO–alginic acid modified sheets with the saline solution. For the possible application of bioactive- or biosensing-papers for the detection of blood types, a high degree of the biomolecule immobilization is an important characteristic. The possibility of detecting blood types was successfully demonstrated by using A-, B-, and D-antibodies. Additionally, the ZnO nanoparticles introduced a strong activity against bacteria (*S. aureus* and *E. coli*) as well as strong resistance toward cellulase producing fungus *G. trabeum* [347].

Natural cellulose was applied to template the TiO₂ and to prepare a bioinspired nanocomposite composed of nanotubular TiO₂ and platinum quantum dots. TiO₂ nanotubes were formed by calcination at 450 °C where the cellulose structure played the role of a sacrificial template. The studied composites were composed of three-dimensional hierarchical structures of TiO₂ and metallic ultrafine Pt quantum dots with sizes of app. 2 nm being uniformly formed on the surface of the TiO₂ nanotubes by a photo deposition process. Complex nanocomposite structures with 1.06 wt.% of Pt content demonstrated the maximum photocatalytic hydrogen production of 16.44 mmol h⁻¹ g⁻¹ from water-splitting, while higher concentrations of Pt caused a decrease in the photocatalytic activity. The sufficient photocatalytic stability was a result of the structural integrity of the nanocomposite during cyclic water-splitting processes. The introduction of cellulose supported hierarchical nanomaterials into photocatalytic systems is an innovative approach to the design and production of new photocatalytic systems [348].

ZnO nanorod arrays (NRAs) were formed on the CuO nanospindle (CuO NS)/paper by using a hydrothermal process to prepare the cellulose supported p–n junction device. Soaking with an aqueous solution of Cu(NO₃)₂ and hexamethylenetetramine and thermal treatment at 75 °C for 6 h produced cellulose fibers decorated with CuO NSs. The resulting CuO NSs/paper was coated with ZnO seeds and subsequently transformed into ZnO NRAs through hydrothermal synthesis at 85–90 °C for 3 h. The prepared device exhibited the I–V characteristics with rectifying behavior at 0.93 V of the turn-on voltage. This simple process for the ZnO NRA formation on the CuO NS-modified paper proved to be a useful strategy toward the formation of paper-based nanostructures for applications in electronic devices [349].

EMI shielding-based sandwich nanomaterials were prepared by functionalizing the bacterial cellulose with Cu and Al₂O₃ nanoparticles by using the magnetron sputtering and RF reactive sputtering method. To optimize the material properties, the ratio of the Cu and Al₂O₃ nanostructure films was explored by applying the P–B ratio theory. The addition of Al₂O₃ nanosheets enhanced the EMI shielding and anti-oxidation properties of the Al₂O₃/Cu/BC nanocomposite materials (Figure 17). The as-prepared sandwich nanomaterials thus demonstrated high EMI shielding properties (65.3 dB), high hydrophobicity, and good mechanical properties (41.3 MPa). The reported innovative topological composite cellulose structure proved to be a promising material for commercial applications in the area of EMI shielding [350].

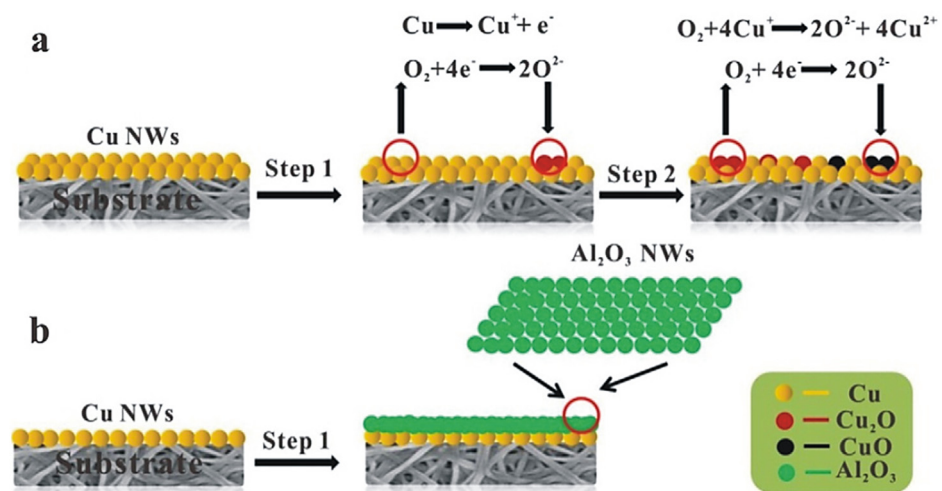


Figure 17. The schematic diagram of the anti-oxidation mechanism of the Cu nanostructure layers (a) in the absence and (b) presence of Al₂O₃ layers. Reprinted from [350]. Copyright 2016, with permission from Elsevier Ltd.

Fe₃O₄ nanoparticles were formed in situ on the bacterial cellulose (BC) modified with fluoroalkyl silane (FAS) under moderate reaction conditions to prepare the magnetic flexible hybrid membranes with an amphiphobic surface. The surface chemical properties of the BC nanofibers (ether and hydroxyl groups) and the ultrafine network architecture both functioned as effective nanoreactor cavities for the formation of magnetite nanostructures. The FS10 sample with homogeneously dispersed magnetite nanoparticles on the BC showed the maximal amphiphobicity with an oil contact angle of 112° and a water contact angle of 130°. It also showed the excellent superparamagnetic properties (M_s of 8.03 emu g⁻¹) as well as the highest tensile strength (186 MPa) among the fluorinated magnetic membranes, and magnetic actuation was also demonstrated. This is an effective process in which to prepare self-cleaning, magnetic, and flexible BC membranes that can find potential application in EMI shielding, information storage, magnetographic printing, or as electronic actuators [351].

A simple aqueous sol–gel process was developed which comprised mixing, freezing, and freeze-drying to entangle one of the three types of capacitive nanoparticles with different dimensions, shapes, and chemistries within chemically modified CNC networks composed of aldehyde modified CNCs and hydrazine modified CNCs. Capacitive structures such as MnO₂ nanoparticles, polypyrrole-nanofibers, and polypyrrole coated carbon nanotubes were synthesized separately and subsequently deposited into the 3D cellulose aerogel structure in one step during the aerogel assembly, providing a huge accessible surface area of the capacitive material, thus enhancing the charge storage (Figure 18). Because of the high mass ratio of the active material to the total electrode mass, excellent capacitance retention at high charge–discharge rates was observed. Multiple channels in the aerogels formed a higher number of electronic and ionic diffusion paths, producing a CNC-based material with the lowest internal resistance for nanocellulose supercapacitors. The preparation and supercapacitive performance of highly porous, lightweight, and flexible hybrid (inorganic–organic) materials based on CNC aerogels have been demonstrated [352].

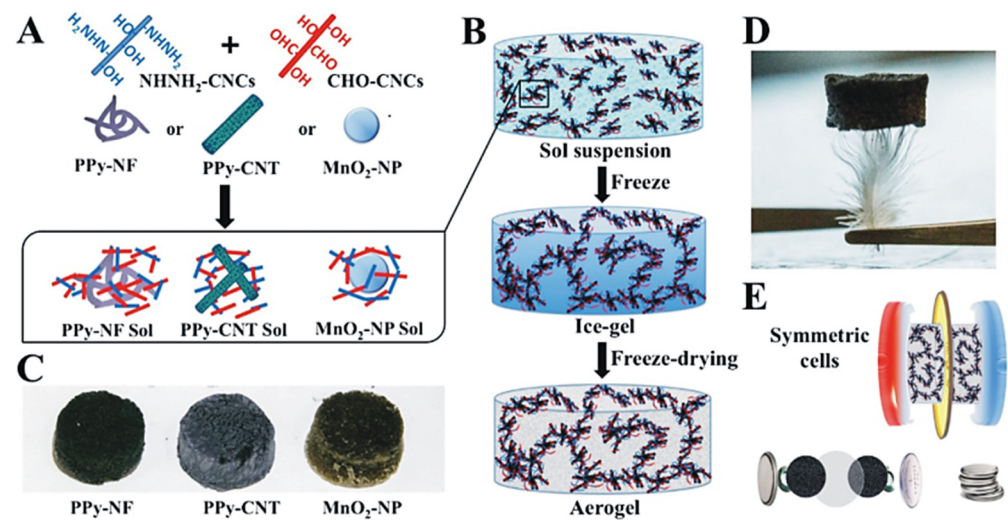


Figure 18. (A) The schematic presentation of the aerogel components including functionalized CNCs and capacitive nanoparticles, which form the initial suspension of cross-linked clusters. (B) The sol-gel process used to prepare aerogels. (C) Photograph of the final hybrid aerogels with a diameter of 1.5 cm. (D) Photograph emphasizing the lightweight nature of a hybrid aerogel resting on the top of a feather. (E) Schematic presentation showing the fabrication of symmetric supercapacitor cells in the CR2032-type coin-cell cases with two hybrid aerogels separated by a porous polyethylene membrane in a saturated Na_2SO_4 aqueous electrolyte [352]. Copyright 2015 John Wiley & Sons Inc. Reproduced with permission.

Some authors have combined cellulose structures, inorganic nanoparticles, and various polymers to obtain materials with highly complex structures and specific functions. For example, Chen et al. reported on a six-stage modification of CNCs [353]. The first stage was the surface deposition of poly(diallyldimethyl ammonium chloride) followed by the surface decoration with Fe_3O_4 nanoparticles (Figure 19). Subsequently, PVP was deposited on the surface of Fe_3O_4 decorated CNCs, followed by embedding the whole structure into SiO_2 (Figure 19). The silica coating significantly increased the CNCs' thermal stability since the onset decomposition temperature was shifted by 60°C toward higher temperatures while Fe_3O_4 introduced magnetic properties into the system. On the surface of the final SiO_2 layer, cyclodextrin molecules were finally grafted, which provided functionality to these complex structures (Figure 19). The as-prepared CNC/ Fe_3O_4 / SiO_2 / β -CD hybrids showed interesting magnetic properties and effective adsorption properties toward two pharmaceutical molecules as model compounds. Consequently, they were highly effective in the magnetic separation of imipramine hydrochloride and procaine hydrochloride from the water solution. The developed process has the potential to be used for the formation of other organic–inorganic nanocomposites by applying CNCs as a template and support.

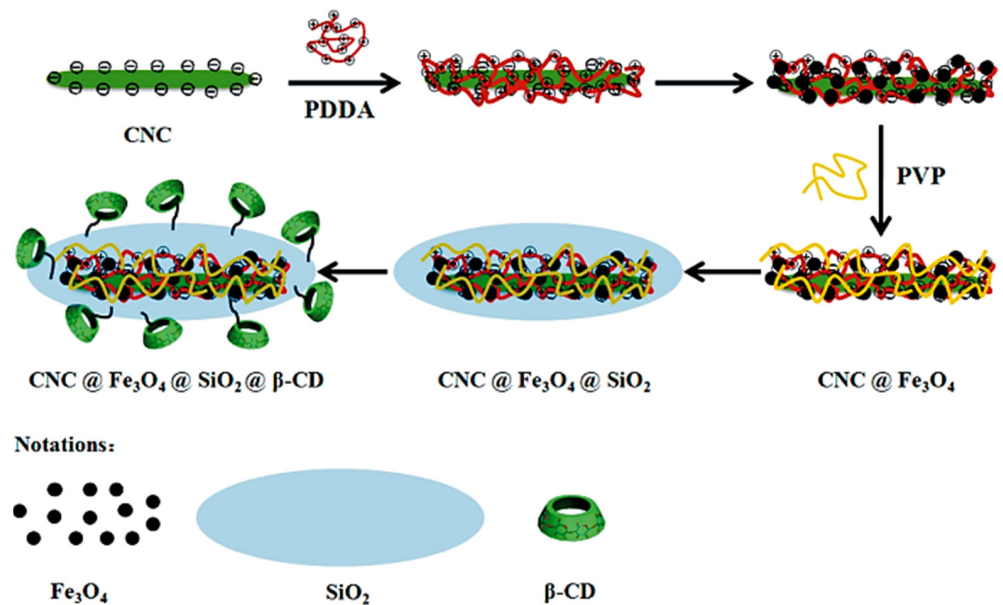


Figure 19. The schematic presentation for the synthesis of the $\text{CNC} @ \text{Fe}_3\text{O}_4 @ \text{SiO}_2 @ \beta\text{-CD}$ ^a. Reprinted with permission from [353]. Copyright 2014 American Chemical Society. ^aCNC: cellulose nanocrystal. PDDA: poly(diallyldimethylammonium chloride). PVP: polyvinylpyrrolidone. $\beta\text{-CD}$: β -cyclodextrin.

The synthesis and characterization of Fe_3O_4 NPs and Au NPs immobilized on CNCs was reported. The $\text{CNC} / \text{Fe}_3\text{O}_4 \text{ NPs} / \text{Au NPs}$ (CNFeAu) nanocomposite was developed as a support for the adsorption and separation of papain, having a maximum loading of $186 \text{ mg protein g}^{-1}$ on the CNFeAu from the reaction solution (Figure 20). The conjugated papain molecules exhibited high stability and reusability and their high enzymatic activity was preserved. The enzyme adsorbed on CNFeAu retained more than 83% of the original activity, with high thermal tolerance and reusability compared to the nonadsorbed reference, as shown by the electrochemical detection and conventional spectrophotometric assay of the specific enzyme binding to the Thc-Fca-Gly-Gly-Tyr-Arg inhibitory film. The magnetic CNFeAu proved to be an effective support matrix with the potential for the magnetic separation of molecules as well as in immobilizing proteins, enzymes, and other biomolecules [354].

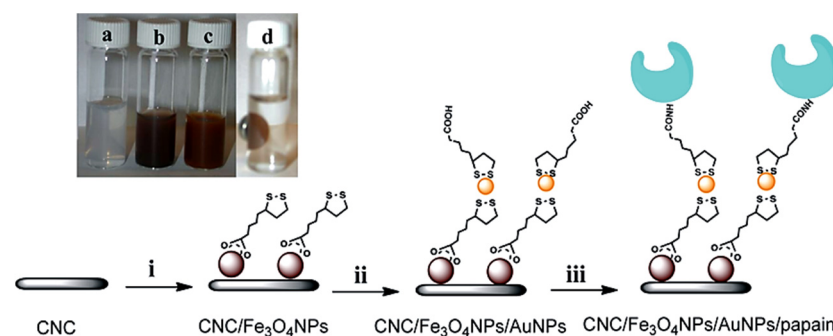


Figure 20. The schematic presentation of the stepwise formation of the conjugate of $\text{CNC} / \text{Fe}_3\text{O}_4 \text{ NPs} / \text{Au NPs} / \text{Papain}$ —(i) FeCl_3 , FeCl_2 , thioctic acid; (ii) HAuCl_4 , α -cyclodextrin, NaBH_4 , thioctic acid; (iii) EDC, NHS, papain. Inset shows photographs of (a) pristine CNC; (b) $\text{CNC} / \text{Fe}_3\text{O}_4 \text{ NPs}$; (c) $\text{CNC} / \text{Fe}_3\text{O}_4 \text{ NPs} / \text{Au NPs}$; and (d) $\text{CNC} / \text{Fe}_3\text{O}_4 \text{ NPs} / \text{Au NPs}$ attracted to the sidewall with a permanent magnet. Reprinted with permission from [354]. Copyright 2013 American Chemical Society.

Mesoporous TiO_2 containing a replica of a chiral nematic structure was synthesized by preparing a titania aqueous sol using a titanium isopropoxide precursor and acetic acid and

subsequently mesoporous TiO₂ with a chiral nematic structure (CNTiO₂) was formed by dipping the previously prepared CNC photonic films, prepared by an evaporation-induced self-assembly (EISA) method, into the TiO₂ sol. CNC photonic films acted as a chiral biotemplate, which was removed by calcination at 500 °C for 4 h and mesoporous chiral TiO₂ film was formed. The stopband of the TiO₂ photonic films was controlled by the quantity of D-glucose added to the system. Finally, mesoporous TiO₂ was decorated with Au nanoparticles using HAuCl₄ as a precursor and NaBH₄ as a reducing agent to increase its photocatalytic activity. The prepared mesoporous chiral TiO₂/Au hybrid films were tested as catalysts in the photocatalytic splitting of water for the production of H₂. It was demonstrated that the photo generation of H₂ was more than eight times higher compared to the conventional mesoporous TiO₂ loaded with Au nanoparticles [355].

The number of publications on cellulose supported or templated hybrid inorganic nanostructures is extensive due to the large number of hybrid combinations and potential applications. These are summarized in Table 6 to concentrate the information in the smallest possible space. The majority of publications in Table 6 reported on the formation of cellulose fiber (paper)–Au or other noble metal based electrodes, constituting various medical and environmental sensors. Noble metals predominate due to their stability and resistance to corrosion. Usually, metallic nanoparticles are formed in two stage process: First, the formation of seeds or nuclei, followed by the seeded growth of nanostructures that completely cover the cellulose surface and form conductive electrodes. The most commonly used precursors are HAuCl₄, H₂PtCl₆, AgNO₃, or H₂PdCl₄ while the most frequently used reducing agents are NaBH₄, Na citrate, or ascorbic acid. The most frequently used process for the growth of Au nanorods is the one reported by Busbee et al. [356]. The most important area of their application is in medical diagnostics and environmental monitoring. The most predominantly applied cellulose substrate is paper—cellulose fibers but bacterial nanocellulose (BNC) and cellulose nanocrystals (CNCs) are also used.

Table 6. The list of publications on cellulose supported/templated inorganic hybrid nanostructures. The list is organized from large cellulose structures (CF and RC) via the microstructured celluloses (MCC and MFC) to nanostructured celluloses (BNC and CNCs).

Inorg. Particle (Size—nm)	Cellulose Used	Precursor (Synthetic Path)	Application	Reference
Cellulose Supported Metallic Hybrid Nanostructures				
Au (~100 nm)	CF	HAuCl ₄ , cetyltrimethyl ammonium chloride, H ₂ O ₂	Flexible electrode in environmental and biosensors	[357]
Au nanorods, Ag NPs, ZnO	CF	HAuCl ₄ , H ₂ NOH.HCl, Zn(NO ₃) ₂ , NH ₃ , AgNO ₃ , ethylene glycol	Electrode in electrochemical immunosensor	[358]
Au NPs (50–100 nm)	CF	HAuCl ₄ , NaBH ₄ , Na citrate, reduction	Flexible electrode sensor-oligonucleotides	[359]
Au NPs (30–100 nm)	CF	HAuCl ₄ , trisodium citrate	Flexible plasmonic immunosensor for detection of sepsis	[360]
Au NPs, ZnO nanorods	CF	HAuCl ₄ , cetyltrimethyl ammonium chloride, H ₂ O ₂ ; Zn(NO ₃) ₂ , (CH ₂) ₆ N ₄ ,	Photoelectrochemical immunosensor-carcinoembryonic antigen antibodies	[361]
Au NPs, Mn ₂ O ₃	CF	HAuCl ₄ , ascorbic acid, Mn(NO ₃) ₂ , glucose	Paper-based biosensor for Pb ²⁺ detection	[362]
Au-Ag NPs	CF	HAuCl ₄ , AgNO ₃ , NH ₃ , ascorbic acid, reduction	Electrode in electrochemical immunosensor-carbohydrate antigen	[363]
Pt NPs (100–200 nm)	CF	H ₂ PtCl ₆ , ascorbic acid, reduction	Electrode in electrochemical immunodevice-tumor biomarker	[364]

Table 6. Cont.

Inorg. Particle (Size—nm)	Cellulose Used	Precursor (Synthetic Path)	Application	Reference
Cellulose Supported Metallic Hybrid Nanostructures				
Pt NPs–ZnO nanorods	CF	H ₂ PtCl ₆ , NaBH ₄ , reduction; Zn(NO ₃) ₂ , CH ₃ COONH ₄ , ethylenediamine	Electrode in H ₂ O ₂ sensor–tumor cells detection	[365]
Pt NPs	CF	H ₂ PtCl ₆ , NaBH ₄ , H ₂ PtCl ₆ , ascorbic acid, reduction;	Electrode in electrochemical sensor-DNA	[366]
Pt NPs	CF	H ₂ PtCl ₆ , ascorbic acid, reduction	Electrode in H ₂ O ₂ sensor–cancer cells monitoring	[367]
Ag NPs	CF	AgNO ₃ , ascorbic acid, reduction	Electrode in electrochemiluminescence sensor-antibodies	[368]
Ag NPs (20–100 nm)	CF	AgNO ₃ , ascorbic acid, reduction	Electrode in immunodevice–cancer antigens	[369]
Ag NPs	CF	AgNO ₃ , H ₂ O ₂ , NaOH, trisodium citrate	Self-healing superhydrophobicity	[370]
Pd-Au NPs (20–50 nm)	CF	Na ₂ PdCl ₄ and HAuCl ₄ , ascorbic acid, reduction	Electrode in H ₂ O ₂ sensor–cancer cells monitoring	[371]
Au-Ag (100–500 nm)	CF	HAuCl ₄ and AgNO ₃ , hydroxylammonium chloride, reduction	Electrode in cyto-device–glycan expression	[372]
Au-Pt (50–100 nm)	CF	HAuCl ₄ and H ₂ PtCl ₆ , ascorbic acid, reduction	Electrode in photoelectrochemical immunodevice–carcinoembryonic antigen	[373]
Pd-Au	CF	H ₂ PdCl ₄ and HAuCl ₄ , ascorbic acid, reduction	Electrode in electrochemical immunodevice–carcinoembryonic antigen	[374]
Ag NPs	CF	Previously formed Ag NPs, AgNO ₃ , Na citrate	Paper-Based SERS Sensor for Pesticide Detection	[375]
Ag NPs	CF	AgNO ₃ , NaOH	Colorimetric assay for Hg ²⁺ detection	[376]
Ag NPs	CF	AgNO ₃ , dopamine hydrochloride	Antibacterial CA/TiO ₂ /Ag NPs material	[377]
Au NPs (10–30 nm)	CF	HAuCl ₄ , NaOH	Fluorescent probe for the detection of Hg(II) ions	[378]
Au-Pt NPs	CF	HAuCl ₄ and H ₂ PtCl ₆ , ascorbic acid, reduction	Electrode in cyto-device–H ₂ S from cancer cells	[379]
Au NPs	CF	HAuCl ₄ , NH ₃ , trisodium citrate	Electrode in electrochemical biosensor for Pb ²⁺ ions	[380]
Au NPs	CF	HAuCl ₄ , cetyltrimethyl ammonium chloride, H ₂ O ₂	Electrode in photoelectrochemical sensor-pentachlorophenol	[381]
Au NPs	BNC	-	Electrode in bioenzymatic sensor-glucose	[382]
Cellulose Supported Metal Oxide or Sulfide Hybrid Nanostructures				
ZnO platelet-superstructure	CF	Zn(NO ₃) ₂ , trisodium citrate, NaOH	Electrode in photoelectrochemical immunodevice–carcinoembryonic antigen	[383]
ZnO nanorods	CF	Zn acetate, Zn(NO ₃) ₂ , hexamethylenetetramine	Electrode in electrochemical immunosensor— α -fetoprotein	[384]

Table 6. Cont.

Inorg. Particle (Size—nm)	Cellulose Used	Precursor (Synthetic Path)	Application	Reference
Cellulose Supported Metal Oxide or Sulfide Hybrid Nanostructures				
ZnO platelets, CuS NPs	CF	Zn(NO ₃) ₂ , KCl, electrodeposition; Cu(NO ₃) ₂ , Na ₂ S	Electrode in photoelectrochemical (PEC) immunosensor-carcinoembryonic antigen	[385]
ZnO nanorods	CF	Pulsed laser deposition	Electrode in LED-photoelectrochemical immunoassay	[386]
SnO ₂ NPs	CF	SnCl ₄ , graphene oxide	Electrode in chemiluminescence photoelectrochemical aptamer device	[387]
MnO ₂ nanowires	CF	MnSO ₄ , Na ₂ SO ₄ , electrodeposition	Electrode in electrochemical immunosensor-prostate protein antigen	[388]
CdS NPs (~5 nm)	CF	CdCl ₂ , Na ₂ S, thioglycolic acid	Electrode in photoelectrochemical analytical device-adenosine triphosphate	[389]
Cu _{1.3} Mn _{1.7} O ₄ NPs (~50 nm)	CF	Cu(NO ₃) ₂ , Mn(NO ₃) ₂ , sol-gel process	Li-ion batteries	[390]
MoO ₃ (100–1000 nm)	CF	Previously prepared MoO ₃ , (NH ₄) ₆ Mo ₇ O ₂₄ , calcination	Colorimetric analysis system for Fe(III) ions	[391]
CoS NPs	BNC	Co(NO ₃) ₂ , Na ₂ S	Flexible electrodes-supercapacitors	[392]
FeOOH (5–50 nm)	CNCs	FeCl ₃ , NaOH	Water defluoridation	[393]
ZnO-Ag	CNCs	Zn(OOCCH ₃) ₂ , AgNO ₃ , NaOH	Antibacterial agent	[394]
SnO ₂ -Ag	CF	(Sn(OiPr) ₄ , AgNO ₃ , NH ₃ , NaOH	Anodic material in Li-ion batteries	[395]
Co(Ac) ₂ -Fe ₃ O ₄	CNF	FeCl ₃ , NH ₃ , Co acetate	Nanocatalyst for 4H-pyrene and pyranopyrazole	[396]
TiO ₂ nanorods–Au NPs	CNCs	TiCl ₄ , Ti(OBu) ₄ , HCl, Au(Ac) ₃ , 1-octadecene	Photocatalyst for degr. of Rhodamine B	[397]
AgNW-Fe ₃ O ₄	CNF	AgNO ₃ , ethylene glycol, PVP, FeCl ₃ , FeCl ₂ , NaOH	Electromagnetic interference shielding	[398]

7. Discussion, Conclusions, and Perspectives

7.1. Discussion

By intensifying the global climate changes and shortages in natural resources, increased attention has been devoted in recent years to sustainable resources and environmentally-friendly solutions. Cellulose is the most abundant natural polymer on the Earth, with an annual production of ~1.5.10¹² tons, which is comparable to the reserves of the main fossil and mineral resources on our planet. Cellulose, with its fibrillary structure, contributes greatly to the diversity in the field of the synthesis and application of hierarchical inorganic nanostructures with additional alternatives. Based on the large number of hydroxyl groups on its surface, it influences the formation of inorganic nanomaterials. It serves as a support or template, it can control crystallization or act as a nanoreactor for in situ precipitation, and it can also prevent their aggregation and agglomeration to a large extent. Cellulose in any form enables the formation of hierarchically organized organic/inorganic hybrid nanostructures that cannot be obtained otherwise.

There are two types of cellulose/inorganic composite structures: (i) Cellulose supported inorganic composite materials and (ii) pure inorganic materials with cellulose templated porosities. In the first type, cellulose is present in the final composite material

while in the second case, it serves as a sacrificial template and is removed by calcination, leaving the pure inorganic material. The inorganic component can be synthesized or formed in situ on the surface of the cellulose or it can be synthesized *ex situ*, and subsequently deposited on the cellulose. In the first case, cellulose serves as a template and support, while in the second case, it only serves as a support. When the inorganic (nano)structures are formed or grown on the surface of the cellulose, its surface characteristics (surface morphology, concentration, and reactivity of hydroxyl groups and the space dimensions between the cellulose fibrils) affect and control their formation. On the other hand, when the cellulose is removed by calcination and a porous inorganic material is obtained, then the dimensions of the cellulose structures become important since they directly or indirectly define the dimensions of the pores in the inorganic matrix. The cellulose aerogel, as an example, acting as a support, produces lightweight, highly flexible, porous, mechanically resistant, and environmentally-friendly structures accompanied with interesting catalytic, electronic, optical, magnetic, and antibacterial properties. The potential areas of applications are very broad (i.e., antimicrobial agents in medicine, heterogeneous catalysis in chemical technology, energy conversion and storage, selective adsorption of metallic ions or organic compounds for water purification, as well as sensors in electronics and medical diagnostics).

The most widely studied area of application is medicine, where hydrophilic cellulose aerogels are combined with metallic Ag or/and ZnO nanoparticles to achieve the antibacterial effect. There are numerous publications reporting on the enhanced inhibiting effect on the bacterial or fungal growth. In many cases, the cellulose supported nanoparticles showed higher antibacterial activities compared to the neat nanoparticles, thus presenting a highly promising alternative for antimicrobial wound dressings or antimicrobial packaging materials. Highly promising biomaterials are cellulose/hydroxyapatite hybrid materials used as bone-tissue scaffolds for bone healing.

Heterogeneous catalysis is another application area of cellulose-templated inorganic nanostructures. Metallic or metal oxide nanoparticles immobilized on the cellulose structures show superior catalytic activities compared to conventional catalytic systems while the removal of a catalyst is not the issue, since nanoparticles are attached to cellulose structures. Cellulose templated pure inorganic materials also showed enhanced activities in heterogeneous catalysis due to their porosity and high specific surface area. The highly important growing area comprises catalytic systems in alternative energy sources such as fuel cells and high capacity batteries.

Supercapacitors based on nanocellulose supports with high charge storage, excellent capacitance retention, and very low internal resistance represent another fast growing application field of cellulose supported inorganic or hybrid nanostructures.

The selective and efficient adsorption of toxic metallic ions such as As^{5+} , Pb^{2+} , Cd^{2+} , Cr^{6+} , Mn^{2+} , etc. from the aqueous medium gives the cellulose supported inorganic structures a high potential for use as a water decontaminant, and also in the purification of water or air from various organic chemicals.

Another highly promising area of application includes fast response humidity, chemical, and biomedical sensors, where the porous structure of cellulose-based paper with a high specific surface area certainly has advantages over conventional materials. The rapidly growing subfield of microfluidic cellulose fiber (paper)-based analytical devices is a highly promising approach toward simple, portable, disposable, and low-cost devices for molecular analysis, environmental detection, and health monitoring.

7.2. Conclusions

A comprehensive review on the application of cellulose in all of its forms as a support or template for various inorganic materials demonstrates the role of cellulose as a highly versatile support and template for the formation of inorganic nanostructures as well as for bioinspired hierarchical structures and assemblies with interesting combinations of properties. Cellulose, as a fibrillar and functional biomaterial support or template, offers new

approaches and pathways to the nucleation and controlled growth of inorganic nanoparticles with a defined shape and porosity as well as to hierarchically organized nanostructures that are difficult or even impossible to prepare through conventional processes. Cellulose, and especially cellulose nanostructures with abundant hydroxyl functionalities on their surface, can intensively interact with various metallic ions.

Cellulose thus influences the formation mechanism of metallic and metal oxide nanoparticles and serves as a templating agent, which enables the preparation of (nano)structures that cannot be obtained by conventional methods. Due to the strong interactions of hydroxyl groups with inorganic ions, cellulose prevents the aggregation and agglomeration of growing inorganic nanostructures, indicating a higher interaction energy of these structures with the cellulose surface compared to the driving energy of particle aggregation and Ostwald ripening. Since the cellulose-supported nanostructures do not agglomerate and grow into larger structures, they retain their nanodimensional size and extremely large specific area, which is highly important in the heterogeneous catalysis of various chemical reactions.

However, the formation and growth of inorganic nanostructures should be performed in a more sustainable way to reduce the use of toxic compounds and waste generation as well as by applying low temperature aqueous solution synthetic protocols, thereby reducing the production costs and enhancing manufacturing safety. Additionally, the implementation of such structures may cause some environmental issues associated with their application. The environmental impact should be assessed from many different aspects (waste, biomagnification in the food chain, transport, etc.) including their potential toxicity when released into ecosystems or the human body. The application of cellulose in any form offers answers to the majority of the previously mentioned issues.

The review of publications up to the present shows that research in this area is heading away from the simple deposition of one type of inorganic nanostructure onto the (nano)cellulose structure toward the deposition of hybrid structures combining metallic, metal oxide, or sulfide with carbon nanotubes or graphene oxide or conducting polymers. These cellulose-supported hybrid inorganic materials form functional hierarchical (nano)structures with targeted applications in (photo)catalysis, Li-batteries, bone tissue engineering, supercapacitors, wound healing, waste water cleaning, colorimetric analysis systems, in sensing, or in other areas of electronics.

Recent advances in the preparation of cellulose-based inorganic nanostructures suggest that the cellulose application will facilitate overcoming the major drawbacks of traditional synthetic methodologies. This review provides an insight into a rather specific area of cellulose-based inorganic (nano)structures and the trends of their exploitation in specific applications, demonstrating their huge potential to become as important as other well-known cellulose applications such as a bioreplacement for fossil fuels, organic chemicals, and/or organic materials based on fossil fuels. A large number (~500) of publications on this topic in the last ten years, mostly in the high impact scientific literature, strongly supports the growing importance of cellulose-based inorganic (nano)structures in materials, technologies, and applications of the future.

7.3. Perspectives

Biomaterials based on cellulose are emerging as highly promising solutions to a number of technological challenges. Cellulose and cellulose-based materials are abundant and biocompatible but also possess structures for transformative device performance. A special case is that of cellulose–inorganic hierarchical nanostructures, since this scientific field is a combination of nanotechnology and environmental science. Currently, a substantial number of promising devices and applications of hybrid cellulose–inorganic structures have been demonstrated, but there are still important challenges in the basic scientific research and understanding to bring cellulose-based hybrid materials to a commercial reality in many innovative applications such as: energy saving and transformation applications, sustainable catalytical systems, green electronics, innovative low-cost sensors or detectors, and biological or biocompatible devices. These challenges comprise (i) low-cost solutions

in the extraction of cellulose structures from wood or other cellulose resources and in the production of either components or devices; (ii) high performance cellulose–inorganic hierarchical nanomaterials and devices based on these materials with suitable lifetime and durability; and (iii) the integration of systems composed of multiple devices.

Innovative developments using cellulose–inorganic hybrid materials elaborated in this review, especially those based on nanocellulose, will generate new solutions influencing our everyday life in the future. To cope with the emerging global challenges, environmentally-friendly and forward-thinking strategies are expected to sustain the research initiatives, and cellulose and cellulose–inorganic hierarchical materials will certainly play an important and decisive role in this demanding task.

Author Contributions: Conceptualization, A.A.; writing—original draft preparation, A.A.; writing—review and editing, A.A. and E.Ž.; supervision, E.Ž.; funding acquisition, E.Ž. All authors have read and agreed to the published version of the manuscript.

Funding: The authors acknowledge the financial support from the Slovenian Research Agency (research core funding No. P2-0145).

Institutional Review Board Statement: Not applicable.

Informed Consent Statement: Not applicable.

Data Availability Statement: No new data were created or analyzed in this study. Data sharing is not applicable to this article.

Conflicts of Interest: The authors declare no conflict of interest.

References

1. Pérez-Madrugal, M.M.; Edo, M.G.; Alemán, C. Powering the future: Application of cellulose-based materials for supercapacitors. *Green Chem.* **2016**, *18*, 5930–5956. [[CrossRef](#)]
2. Wu, Y.D.; He, J.M.; Huang, J.D.; Wang, F.W.; Tang, F. Oxidation of Regenerated Cellulose with Nitrogen Dioxide/Carbon Tetrachloride. *Fibers Polym.* **2012**, *13*, 576–581. [[CrossRef](#)]
3. Zhu, H.; Luo, W.; Ciesielski, P.N.; Fang, Z.; Zhu, J.Y.; Henriksson, G.; Himmel, M.E.; Hu, L. Wood-Derived Materials for Green Electronics, Biological Devices, and Energy Applications. *Chem. Rev.* **2016**, *116*, 9305–9374. [[CrossRef](#)] [[PubMed](#)]
4. Lin, Z.; Li, S.; Huang, J. Natural Cellulose Substance Based Energy Materials. *Chem. Asian J.* **2021**, *16*, 378–396. [[CrossRef](#)] [[PubMed](#)]
5. Mendonça Cidreira, A.C.; Cappuccio de Castro, K.; Hatami, T.; Linan, L.Z.; Innocentini Mei, L.H. Cellulose nanocrystals-based materials as hemostatic agents for wound dressings: A review. *Biomed. Microdevices* **2021**, *23*, 43. [[CrossRef](#)] [[PubMed](#)]
6. De Amorim, J.D.P.; de Souza, K.C.; Duarte, C.R.; da Silva Duarte, I.; de Assis Sales Ribeiro, F.; Silva, G.S.; de Farias, P.M.A.; Stingl, A.; Costa, A.F.S.; Vinhas, G.M.; et al. Plant and bacterial nanocellulose: Production, properties and applications in medicine, food, cosmetics, electronics and engineering. A review. *Environ. Chem. Lett.* **2020**, *18*, 851–869. [[CrossRef](#)]
7. Kalita, E.; Nath, B.K.; Deb, P.; Agan, F.; Islam, M.R.; Saikia, K. High quality fluorescent cellulose nanofibers from endemic rice husk: Isolation and characterization. *Carbohydr. Polym.* **2015**, *122*, 308–313. [[CrossRef](#)]
8. Liu, Y.; Liu, A.; Ibrahim, S.A.; Yang, H.; Huang, W. Isolation and characterization of microcrystalline cellulose from pomelo peel. *Int. J. Biol. Macromol.* **2018**, *111*, 717–721. [[CrossRef](#)]
9. Zhang, H.; Tang, X.; Gao, X.; Chen, K. Fabrication and Comparative Evaluation of Regenerated Cellulose Films using Pulp fines and Pith from Corn Stalk in DMAc/LiCl Solvent System. *BioResources* **2019**, *14*, 6421–6432. [[CrossRef](#)]
10. Jiang, W.; Sun, L.; Hao, A.; Chen, J.Y. Regenerated cellulose fibers from waste bagasse using ionic liquid. *Text. Res.* **2011**, *81*, 1949–1958. [[CrossRef](#)]
11. Habibi, Y. Key advances in the chemical modification of nanocelluloses. *Chem. Soc. Rev.* **2014**, *45*, 1519–1542. [[CrossRef](#)] [[PubMed](#)]
12. Heinze, T. Cellulose: Structure and Properties. *Adv. Polym. Sci.* **2016**, *271*, 1.
13. Tingaut, P.; Zimmermann, T.; Sebe, G. Cellulose nanocrystals and microfibrillated cellulose as building blocks for the design of hierarchical functional materials. *J. Mater. Chem.* **2012**, *22*, 20105–20111. [[CrossRef](#)]
14. Hassan, N.S.; Jalil, A.A.; Vo, D.V.N.; Nabgan, W. An overview on the efficiency of biohydrogen production from cellulose. *Biomass Convers. Biorefin.* **2020**, 1–23. [[CrossRef](#)]
15. Ivanova, A.; Fattakhova-Rohlfing, D.; Kayaalp, B.E.; Rathouský, J.; Bein, T. Tailoring the Morphology of Mesoporous Titania Thin Films through Biotemplating with Nanocrystalline Cellulose. *J. Am. Chem. Soc.* **2014**, *136*, 5930–5937. [[CrossRef](#)] [[PubMed](#)]
16. Padalkar, S.; Capadona, J.R.; Rowan, S.J.; Weder, C.; Won, Y.H.; Stanciu, L.A.; Moon, R.J. Natural Biopolymers: Novel Templates for the Synthesis of Nanostructures. *Langmuir* **2010**, *26*, 8497–8502. [[CrossRef](#)] [[PubMed](#)]

17. Wang, Z.; Tammela, P.; Strømme, M.; Nyholm, L. Cellulose-based Supercapacitors: Material and Performance Considerations. *Adv. Energy Mater.* **2017**, *7*, 1700130. [[CrossRef](#)]
18. French, A.D. Glucose, not cellobiose, is the repeating unit of cellulose and why that is important. *Cellulose* **2017**, *24*, 4605–4609. [[CrossRef](#)]
19. French, A.D. Idealized powder diffraction patterns for cellulose polymorphs. *Cellulose* **2014**, *21*, 885–896. [[CrossRef](#)]
20. Habibi, Y.; Lucia, L.A.; Rojas, O.J. Cellulose Nanocrystals: Chemistry, Self-Assembly, and Applications. *Chem. Rev.* **2010**, *110*, 3479–3500. [[CrossRef](#)]
21. Anžlovar, A.; Kunaver, M.; Krajnc, A.; Žagar, E. Nanocomposites of LLDPE and Surface-Modified Cellulose Nanocrystals Prepared by Melt Processing. *Molecules* **2018**, *23*, 1782. [[CrossRef](#)] [[PubMed](#)]
22. Anžlovar, A.; Krajnc, A.; Žagar, E. Silane modified cellulose nanocrystals and nanocomposites with LLDPE prepared by melt processing. *Cellulose* **2020**, *27*, 5785–5800. [[CrossRef](#)]
23. Anžlovar, A.; Švab, I.; Krajnc, A.; Žagar, E. Composites of polystyrene and surface modified cellulose nanocrystals prepared by melt processing. *Cellulose* **2021**, *28*, 7813–7827. [[CrossRef](#)]
24. Nishiyama, Y.; Langan, P.; Chanzy, H. Crystal Structure and Hydrogen-Bonding System in Cellulose I β from Synchrotron X-ray and Neutron Fiber Diffraction. *J. Am. Chem. Soc.* **2002**, *124*, 9074–9082. [[CrossRef](#)] [[PubMed](#)]
25. Campelo, J.M.; Luna, D.; Luque, R.; Marinas, J.M.; Romero, A.A. Sustainable Preparation of Supported Metal Nanoparticles and Their Applications in Catalysis. *ChemSusChem* **2009**, *2*, 18–45. [[CrossRef](#)] [[PubMed](#)]
26. Eichhorn, S.J. Cellulose nanofibres for photonics and plasmonics. *Curr. Opin. Green Sustain. Chem.* **2018**, *12*, 1–7. [[CrossRef](#)]
27. Sun, Z.; Duan, X.; Gnanasekar, P.; Yan, N.; Shi, J. Review: Cascade reactions for conversion of carbohydrates using heteropolyacids as the solid catalysts. *Biomass Convers. Biorefin.* **2022**, *12*, 2313–2331. [[CrossRef](#)]
28. Zinge, C.; Kandasubramanian, B. Nanocellulose based biodegradable polymers. *Eur. Polym. J.* **2020**, *133*, 109758. [[CrossRef](#)]
29. Kalita, R.D.; Nath, Y.; Ochubiojo, M.E.; Buragohain, A.K. Extraction and characterization of microcrystalline cellulose from fodder grass; *Setaria glauca* (L.) P. Beauv, and its potential as a drug delivery vehicle for isoniazid, a first line antituberculosis drug. *Colloids Surf. B* **2013**, *108*, 85–89. [[CrossRef](#)]
30. Chakraborty, I.; Rongpipi, S.; Govindaraju, I.; Rakesh, B.; Mal, S.S.; Gomez, E.W.; Gomez, E.D.; Kalita, R.D.; Nath, Y.; Mazumder, N. An insight into microscopy and analytical techniques for morphological, structural, chemical, and thermal characterization of cellulose. *Microsc. Res. Tech.* **2022**, *85*, 1990–2015. [[CrossRef](#)]
31. Reddy, K.O.; Maheswari, C.U.; Dhlamini, M.S.; Mothudi, B.M.; Kommul, V.P.; Zhang, J.; Zhang, J.; Rajulu, A.V. Extraction and characterization of cellulose single fibers from native African napier grass. *Carbohydr. Polym.* **2018**, *188*, 85–91. [[CrossRef](#)] [[PubMed](#)]
32. Li, F.; Wang, W.; Wang, X.; Yu, J. Changes of structure and property of alkali soluble hydroxyethyl celluloses (HECs) and their regenerated films with the molar substitution. *Carbohydr. Polym.* **2014**, *114*, 206–212. [[CrossRef](#)] [[PubMed](#)]
33. Wang, S.; Lu, A.; Zhang, L. Recent advances in regenerated cellulose materials. *Prog. Polym. Sci.* **2016**, *53*, 169–206. [[CrossRef](#)]
34. Wang, H.; Gurau, G.; Rogers, R.D. Ionic liquid processing of cellulose. *Chem. Soc. Rev.* **2012**, *41*, 1519–1537. [[CrossRef](#)] [[PubMed](#)]
35. Kale, R.D.; Bansal, P.S.; Gorade, V.G. Extraction of Microcrystalline Cellulose from Cotton Sliver and Its Comparison with Commercial Microcrystalline Cellulose. *J. Polym. Environ.* **2018**, *26*, 355–364. [[CrossRef](#)]
36. Yi, T.; Zhao, H.; Mo, Q.; Pan, D.; Liu, Y.; Huang, L.; Xu, H.; Hu, B.; Song, H. From Cellulose to Cellulose Nanofibrils—A Comprehensive Review of the Preparation and Modification of Cellulose Nanofibrils. *Materials* **2020**, *13*, 5062. [[CrossRef](#)]
37. Chandra, C.S.J.; George, N.; Narayanankutty, S.K. Isolation and characterization of cellulose nanofibrils from arecanut husk fibre. *Carbohydr. Polym.* **2016**, *142*, 158–166.
38. Chaker, A.; Mutje, P.; Rei Vilar, M.; Boufi, S. Agriculture crop residues as a source for the production of nanofibrillated cellulose with low energy demand. *Cellulose* **2014**, *21*, 4247–4259. [[CrossRef](#)]
39. Nasir, M.; Aziz, M.A.; Zubair, M.; Manzar, M.S.; Ashraf, N.; Mu'azu, N.D.; Al-Harhi, M.A. Recent review on synthesis, evaluation, and SWOT analysis of nanostructured cellulose in construction applications. *J. Build. Engin.* **2022**, *46*, 103747. [[CrossRef](#)]
40. Tajima, K.; Imai, T.; Yui, T.; Yao, M. Cellulose-synthesizing machinery in bacteria. *Cellulose* **2022**, *29*, 2755–2777. [[CrossRef](#)]
41. Klemm, D.; Kramer, F.; Moritz, S.; Lindstroem, T.; Ankerfors, M.; Gray, D.; Dorris, A. Nanocelluloses: A New Family of Nature-Based Materials. *Angew. Chem. Int. Ed.* **2011**, *50*, 5438–5466. [[CrossRef](#)] [[PubMed](#)]
42. Kos, T.; Anžlovar, A.; Kunaver, M.; Huskić, M.; Žagar, E. Fast preparation of Nanocrystalline cellulose by microwave-assisted hydrolysis. *Cellulose* **2014**, *21*, 2579–2585. [[CrossRef](#)]
43. Kunaver, M.; Anžlovar, A.; Žagar, E. The fast and effective isolation of nanocellulose from selected cellulosic feedstocks. *Carbohydr. Polym.* **2016**, *148*, 251–258. [[CrossRef](#)] [[PubMed](#)]
44. Dufresne, A. Nanocellulose: A new ageless bionanomaterial. *Mater. Today* **2013**, *16*, 220–227. [[CrossRef](#)]
45. Gan, I.; Chow, W.S. Tailoring Chemical, Physical, and Morphological Properties of Sugarcane Bagasse Cellulose Nanocrystals via Phosphorylation Method. *J. Nat. Fibers* **2021**, *18*, 1448–1460. [[CrossRef](#)]
46. Su, H.; Wang, B.; Sun, Z.; Wang, S.; Feng, X.; Mao, Z.; Sui, X. High-tensile regenerated cellulose films enabled by unexpected enhancement of cellulose dissolution in cryogenic aqueous phosphoric acid. *Carbohydr. Polym.* **2022**, *277*, 118878. [[CrossRef](#)]
47. Jordan, J.H.; Easson, M.W.; Condon, B.D. Cellulose hydrolysis using ionic liquids and inorganic acids under dilute conditions: Morphological comparison of nanocellulose. *RSC Adv.* **2020**, *10*, 39413. [[CrossRef](#)]

48. Huang, J.; Hou, S.; Chen, R. Ionic Liquid-assisted Fabrication of Nanocellulose from Cotton Linter by High Pressure Homogenization. *BioResources* **2019**, *14*, 7805–7820.
49. Babicka, M.; Wozniak, M.; Szentner, K.; Bartkowiak, M.; Peplinska, B.; Dwiecki, K.; Borysiak, S.; Ratajczak, I. Nanocellulose Production Using Ionic Liquids with Enzymatic Pretreatment. *Materials* **2021**, *14*, 3264. [[CrossRef](#)]
50. Shen, X.; Shamshina, J.L.; Berton, P.; Gurauc, G.; Rogers, R.D. Hydrogels based on cellulose and chitin: Fabrication, properties, and applications. *Green Chem.* **2016**, *18*, 53–75. [[CrossRef](#)]
51. Chin, S.F.; Jong, S.J.; Yeo, Y.J. Optimization of Cellulose-Based Hydrogel Synthesis Using Response Surface Methodology. *Biointerface Res. Appl. Chem.* **2022**, *12*, 7136–7146.
52. Xu, K.; Wang, Y.; Zhang, B.; Zhang, C.; Liu, T. Stretchable and self-healing polyvinyl alcohol/cellulose nanofiber nanocomposite hydrogels for strain sensors with high sensitivity and linearity. *Compos. Commun.* **2021**, *24*, 100677. [[CrossRef](#)]
53. Li, M.; Chen, D.; Xia Sun, X.; Xu, Z.; Yang, Y.; Song, Y.; Jiang, F. An environmentally tolerant, highly stable, cellulose nanofiber-reinforced, conductive hydrogel multifunctional sensor. *Carbohydr. Polym.* **2022**, *284*, 119199. [[CrossRef](#)]
54. Cheng, Y.; Zang, J.; Zhao, X.; Wang, H.; Hu, Y. Nanocellulose-enhanced organohydrogel with high-strength, conductivity, and anti-freezing properties for wearable strain sensors. *Carbohydr. Polym.* **2022**, *277*, 118872. [[CrossRef](#)] [[PubMed](#)]
55. Zong, Y.; Li, H.; Li, X.; Lou, J.; Ding, Q.; Liu, Z.; Jiang, Y.; Han, W. Bacterial cellulose-based hydrogel thermocells for low-grade heat harvesting. *Chem. Engin. J.* **2022**, *433*, 134550. [[CrossRef](#)]
56. Nabipour, H.; Shi, H.; Wang, X.; Hu, X.; Song, L.; Hu, Y. Flame Retardant Cellulose-Based Hybrid Hydrogels for Firefighting and Fire Prevention. *Fire Technol.* **2022**, 1–15. [[CrossRef](#)]
57. Jiang, X.; Zeng, F.; Yang, X.; Jian, C.; Zhang, L.; Yu, A.; Lu, A. Injectable self-healing cellulose hydrogel based on host-guest interactions and acylhydrazone bonds for sustained cancer therapy. *Acta Biomater.* **2022**, *141*, 102–113. [[CrossRef](#)]
58. Piloto, A.M.L.; Ribeiro, D.S.M.; Rodrigues, S.S.M.; Santos, J.M.L.; Sampaio, P.; Ferreira Sales, M.G. Cellulose-based hydrogel on quantum dots with molecularly imprinted polymers for the detection of CA19-9 protein cancer biomarker. *Microchim. Acta* **2022**, *189*, 134. [[CrossRef](#)]
59. Gao, J.; Yuan, Y.; Yu, Q.; Yan, B.; Qian, Y.; Wen, J.; Ma, C.; Jiang, S.; Wang, X.; Wang, N. Bio-inspired antibacterial cellulose paper–poly(amidoxime) composite hydrogel for highly efficient uranium(VI) capture from seawater. *Chem. Commun.* **2020**, *56*, 3935–3938. [[CrossRef](#)]
60. Lin, N.; Huang, J.; Dufresne, A. Preparation, properties and applications of polysaccharide nanocrystals in advanced functional nanomaterials: A review. *Nanoscale* **2012**, *4*, 3274–3294. [[CrossRef](#)]
61. Vu, P.V.; Doan, T.D.; Tu, G.C.; Do, N.H.N.; Le, K.A.; Le, P.K. A novel application of cellulose aerogel composites from pineapple leaf fibers and cotton waste: Removal of dyes and oil in wastewater. *J. Porous Mater.* **2022**, 1–11. [[CrossRef](#)]
62. Gan, S.; Zakaria, S.; Chia, C.H.; Chen, R.S.; Ellis, A.V.; Kaco, H. Highly porous regenerated cellulose hydrogel and aerogel prepared from hydrothermal synthesized cellulose carbamate. *PLoS ONE* **2017**, *12*, e0173743. [[CrossRef](#)] [[PubMed](#)]
63. Chen, Y.; Li, S.; Li, X.; Mei, C.; Zheng, J.; Shiju, E.; Duan, G.; Liu, K.; Jiang, S. Liquid Transport and Real-Time Dye Purification via Lotus Petiole-Inspired Long-Range-Ordered Anisotropic Cellulose Nanofibril Aerogels. *ACS Nano* **2021**, *15*, 20666–20677. [[CrossRef](#)] [[PubMed](#)]
64. Hosseini Talari, M.; Salman Tabrizi, N.; Babaeipour, V.; Halek, F. Adsorptive removal of organic pollutants from water by carbon fiber aerogel derived from bacterial cellulose. *J. Sol-Gel Sci. Technol.* **2022**, *101*, 345–355. [[CrossRef](#)]
65. Mo, L.; Tan, Y.; Shen, Y.; Zhang, S. Highly compressible nanocellulose aerogels with a cellular structure for high-performance adsorption of Cu(II). *Chemosphere* **2022**, *291*, 132887. [[CrossRef](#)]
66. Cheng, H.; Gu, B.; Pennefather, M.P.; Nguyen, T.X.; Phan-Thien, N.; Duong, H.M. Cotton aerogels and cotton-cellulose aerogels from environmental waste for oil spillage cleanup. *Mater. Des.* **2017**, *130*, 452–458. [[CrossRef](#)]
67. Wang, C.; Liu, W.; Cao, H.; Jia, L.; Liu, P. Cellulose nanofibers aerogels functionalized with AgO: Preparation, characterization and antibacterial activity. *Int. J. Biol. Macromol.* **2022**, *194*, 58–65. [[CrossRef](#)]
68. Wan, C.; Li, J. Cellulose aerogels functionalized with polypyrrole and silver nanoparticles: In-situ synthesis, characterization and antibacterial activity. *Carbohydr. Polym.* **2016**, *146*, 362–367. [[CrossRef](#)]
69. Zou, Y.; Zhao, J.; Zhu, J.; Guo, X.; Chen, P.; Duan, G.; Liu, X.; Li, Y. A Mussel-Inspired Polydopamine-Filled Cellulose Aerogel for Solar- Enabled Water Remediation. *ACS Appl. Mater. Interfaces* **2021**, *13*, 7617–7624. [[CrossRef](#)]
70. Chen, Y.; Zhang, L.; Mei, C.; Li, Y.; Gaigai Duan, G.; Agarwal, S.; Greiner, G.; Ma, C.; Jiang, S. Wood-Inspired Anisotropic Cellulose Nanofibril Composite Sponges for Multifunctional Applications. *ACS Appl. Mater. Interfaces* **2020**, *12*, 35513–35522. [[CrossRef](#)]
71. Li, Y.; Chen, Y.; Huang, X.; Jiang, S.; Wang, G. Anisotropy-functionalized cellulose-based phase change materials with reinforced solar-thermal energy conversion and storage capacity. *Chem. Engin. J.* **2021**, *415*, 129086. [[CrossRef](#)]
72. Krishnan, P.D.; Banas, D.; Durai, R.D.; Kabanov, D.; Hosnedlova, B.; Kepinska, M.; Fernandez, C.; Ruttikay-Nedecky, B.; Nguyen, H.V.; Farid, A.; et al. Nanomaterials for Wound Dressing Applications. *Pharmaceutics* **2020**, *12*, 821. [[CrossRef](#)] [[PubMed](#)]
73. Van Rie, J.; Thielemans, W. Cellulose–gold nanoparticle hybrid materials. *Nanoscale* **2017**, *9*, 8525–8554. [[CrossRef](#)] [[PubMed](#)]
74. Zhou, J.; Hu, Z.; Zabihi, F.; Chen, Z.; Zhu, M. Progress and Perspective of Antiviral Protective Material. *Adv. Fiber Mater.* **2020**, *2*, 123–139. [[CrossRef](#)]
75. Kaushik, M.; Moores, A. Review: Nanocelluloses as versatile supports for metal nanoparticles and their applications in catalysis. *Green Chem.* **2016**, *18*, 622–637. [[CrossRef](#)]

76. Deeksha, B.; Sadanand, V.; Hariram, N.; Rajulu, A.V. Preparation and properties of cellulose nanocomposite fabrics with in situ generated silver nanoparticles by bioreduction method. *J. Bioresour. Bioprod.* **2021**, *6*, 75–81. [[CrossRef](#)]
77. Ashraf, S.; ur-Rehman, S.; Sher, F.; Khalid, Z.M.; Mehmood, M.; Hussain, I. Synthesis of cellulose–metal nanoparticle composites: Development and comparison of different protocols. *Cellulose* **2014**, *21*, 395–405. [[CrossRef](#)]
78. Hamoud, T.; Ibrahim, H.M.; Kafafy, H.H.; Mashaly, H.M.; Mohamed, N.H.; Aly, N.M. Preparation of cellulose-based wipes treated with antimicrobial and antiviral silver nanoparticles as novel effective high-performance coronavirus fighter. *Int. J. Biol. Macromol.* **2021**, *181*, 990–1102. [[CrossRef](#)]
79. Li, Y.; Xu, L.; Xu, B.; Mao, Z.; Xu, H.; Zhong, Y.; Zhang, L.; Wang, B.; Sui, X. Cellulose Sponge Supported Palladium Nanoparticles as Recyclable Cross-Coupling Catalysts. *ACS Appl. Mater. Interfaces* **2017**, *9*, 17155–17162. [[CrossRef](#)]
80. Li, S.M.; Jia, N.; Zhub, J.F.; Ma, M.G.; Xua, F.; Wanga, B.; Sun, R.C. Rapid microwave-assisted preparation and characterization of cellulose–silver nanocomposites. *Carbohydr. Polym.* **2011**, *83*, 422–429. [[CrossRef](#)]
81. Farag, S.; Ibrahim, H.M.; Asker, M.S.; Amr, A.; El-Shafae, A. Impregnation of silver nanoparticles into bacterial cellulose: Green synthesis and cytotoxicity. *Int. J. ChemTech Res.* **2015**, *8*, 651–661.
82. Lu, Z.; Jasinski, J.B.; Handa, S.; Hammond, G.B. Recyclable cellulose-palladium nanoparticles for clean cross-coupling chemistry. *Org. Biomol. Chem.* **2018**, *16*, 2748. [[CrossRef](#)] [[PubMed](#)]
83. Zhang, T.; Wang, W.; Zhang, D.; Zhang, X.; Ma, Y.; Zhou, Y.; Qi, L. Biotemplated Synthesis of Gold Nanoparticle–Bacteria Cellulose Nanofiber Nanocomposites and Their Application in Biosensing. *Adv. Funct. Mater.* **2010**, *20*, 1152–1160. [[CrossRef](#)]
84. Yan, W.; Chen, C.; Wang, L.; Zhang, D.; Li, A.J.; Yao, Z.; Shi, L.Y. Facile and green synthesis of cellulose nanocrystal-supported gold nanoparticles with superior catalytic activity. *Carbohydr. Polym.* **2016**, *140*, 66–73. [[CrossRef](#)] [[PubMed](#)]
85. Alahmadi, N.S.; Betts, J.W.; Cheng, F.; Francesconi, M.G.; Kelly, S.M.; Kornherr, A.; Priora, T.J.; Wadhawan, J.D. Synthesis and antibacterial effects of cobalt–cellulose magnetic nanocomposites. *RSC Adv.* **2017**, *7*, 20020. [[CrossRef](#)]
86. Musa, A.; Ahmad, M.B.; Hussein, M.Z.; Saiman, M.I.; Sani, H.A. Preparation, characterization and catalytic activity of biomaterial-supported copper nanoparticles. *Res. Chem. Intermed.* **2017**, *43*, 801–815. [[CrossRef](#)]
87. Dhar, P.; Kumar, A.; Katiyar, V. Fabrication of cellulose nanocrystal supported stable Fe(0) nanoparticles: A sustainable catalyst for dye reduction, organic conversion and chemo-magnetic propulsion. *Cellulose* **2015**, *22*, 3755–3771. [[CrossRef](#)]
88. Ishida, T.; Watanabe, H.; Bebeko, T.; Akita, T.; Haruta, M. Aerobic oxidation of glucose over gold nanoparticles deposited on cellulose. *Appl. Catal. A Gen.* **2010**, *377*, 42–46. [[CrossRef](#)]
89. Wu, J.; Zhao, N.; Zhang, X.; Xu, J. Cellulose/silver nanoparticles composite microspheres: Eco-friendly synthesis and catalytic application. *Cellulose* **2012**, *19*, 1239–1249. [[CrossRef](#)]
90. Koga, H.; Tokunaga, E.; Hidaka, M.; Umemura, Y.; Saito, T.; Isogai, A.; Kitaoka, T. Topochemical synthesis and catalysis of metal nanoparticles exposed on crystalline cellulose nanofibers. *Chem. Commun.* **2010**, *46*, 8567–8569. [[CrossRef](#)]
91. Hsieh, M.C.; Kim, C.; Nogi, M.; Saganuma, K. Electrically conductive lines on cellulose nanopaper for flexible electrical devices. *Nanoscale* **2013**, *5*, 9289–9295. [[CrossRef](#)] [[PubMed](#)]
92. Azetsu, A.; Koga, H.; Isogai, A.; Kitaoka, T. Synthesis and Catalytic Features of Hybrid Metal Nanoparticles Supported on Cellulose Nanofibers. *Catalysts* **2011**, *1*, 83–96. [[CrossRef](#)]
93. Oracion, J.P.L.; De La Rosa, L.B.; Budlayan, M.L.M.; Rodriguez, M.J.D.; Manigo, J.P.; Patricio, J.N.; Arco, S.D.; Austria, E.S.; Alguno, A.C.; Deocar, C.C.; et al. Simple one-pot in situ synthesis of gold and silver nanoparticles on bacterial cellulose membrane using polyethyleneimine. *J. Appl. Sci. Engin.* **2021**, *24*, 351–357.
94. Johnson, L.; Thielemans, W.; Walsh, D.A. Synthesis of carbon-supported Pt nanoparticle electrocatalysts using nanocrystalline cellulose as reducing agent. *Green Chem.* **2011**, *13*, 1686–1693. [[CrossRef](#)]
95. Faria-Tischer, P.C.S.; Costa, C.A.R.; Tozetti, I.; Dall’Antonia, L.H.; Vidotti, M. Structure and effects of gold nanoparticles in bacterial cellulose-polyaniline conductive membranes. *RSC Adv.* **2016**, *6*, 9571–9580. [[CrossRef](#)]
96. Wu, J.; Feng, Y.; Zhang, L.; Wu, W. Nanocellulose-based Surface-enhanced Raman spectroscopy sensor for highly sensitive detection of TNT. *Carbohydr. Polym.* **2020**, *248*, 116766. [[CrossRef](#)]
97. Majoinen, J.; Hassinen, J.; Haataja, J.S.; Rekola, H.T.; Kontturi, E.; Kostianen, M.A.; Ras, R.H.A.; Törmä, P.; Ikkala, O. Chiral Plasmonics Using Twisting along Cellulose Nanocrystals as a Template for Gold Nanoparticles. *Adv. Mater.* **2016**, *28*, 5262–5267. [[CrossRef](#)]
98. Hu, Z.; Meng, Q.; Liu, R.; Fu, S.; Lucia, L.A. Physical Study of the Primary and Secondary Photothermal Events in Gold/Cellulose Nanocrystals (AuNP/CNC) Nanocomposites Embedded in PVA Matrices. *ACS Sustain. Chem. Eng.* **2017**, *5*, 1601–1609. [[CrossRef](#)]
99. Wu, X.D.; Lu, C.H.; Zhou, Z.H.; Yuan, G.P.; Xiong, R.; Zhang, X.X. Green synthesis and formation mechanism of cellulose nanocrystal-supported gold nanoparticles with enhanced catalytic performance. *Environ. Sci. Nano* **2014**, *1*, 71–79. [[CrossRef](#)]
100. Schlesinger, M.; Giese, M.; Blusch, L.K.; Hamad, W.Y.; MacLachlan, M.J. Chiral nematic cellulose-gold nanoparticle composites from mesoporous photonic cellulose. *Chem. Commun.* **2015**, *51*, 530–533. [[CrossRef](#)]
101. Huang, J.L.; Gray, D.G.; Li, C.J. A(3)-Coupling catalyzed by robust Au nanoparticles covalently bonded to HS-functionalized cellulose nanocrystalline films. *Beilstein J. Org. Chem.* **2013**, *9*, 1388–1396. [[CrossRef](#)] [[PubMed](#)]
102. Chen, L.; Cao, W.; Quinlan, P.J.; Berry, R.M.; Tam, K.C. Sustainable Catalysts from Gold-Loaded Polyamidoamine Dendrimer-Cellulose Nanocrystals. *ACS Sustain. Chem. Eng.* **2015**, *3*, 978–985. [[CrossRef](#)]
103. Lam, E.; Hrapovic, S.; Majid, E.; Chong, J.H.; Luong, J.H.T. Catalysis using gold nanoparticles decorated on nanocrystalline cellulose. *Nanoscale* **2012**, *4*, 997–1002. [[CrossRef](#)] [[PubMed](#)]

104. Eisa, W.H.; Abdelgawad, A.M.; Rojas, O.J. Solid-State Synthesis of Metal Nanoparticles Supported on Cellulose Nanocrystals and Their Catalytic Activity. *ACS Sustain. Chem. Engin.* **2018**, *6*, 3974–3983. [[CrossRef](#)]
105. Xiong, Z.; Lin, M.; Lin, H.; Huang, M. Facile synthesis of cellulose nanofiber nanocomposite as a SERS substrate for detection of thiram in juice. *Carbohydr. Polym.* **2018**, *189*, 79–86. [[CrossRef](#)]
106. Semenikhin, N.S.; Kadasala, N.R.; Moon, R.J.; Perry, J.W.; Sandhage, K.H. Individually Dispersed Gold Nanoshell-Bearing Cellulose Nanocrystals with Tailorable Plasmon Resonance. *Langmuir* **2018**, *34*, 4427–4436. [[CrossRef](#)]
107. Dueñas-Mas, M.J.; Soriano, M.L.; Ruiz-Palmero, C.; Valcárcel, M. Modified nanocellulose as promising material for the extraction of gold nanoparticles. *Microchem. J.* **2018**, *138*, 379–383. [[CrossRef](#)]
108. Islam, M.T.; Sultana, K.A.; Noveron, J.C. Borohydride-free catalytic reduction of organic pollutants by platinum nanoparticles supported on cellulose fibers. *J. Mol. Liq.* **2019**, *296*, 111988. [[CrossRef](#)]
109. Yu, H.; Oh, S.; Han, Y.; Lee, S.; Jeong, H.S.; Hong, H.J. Modified cellulose nanofibril aerogel: Tunable catalyst support for treatment of 4-Nitrophenol from wastewater. *Chemosphere* **2021**, *285*, 131448. [[CrossRef](#)]
110. Benaissi, K.; Johnson, L.; Walsh, D.A.; Thielemans, W. Synthesis of platinum nanoparticles using cellulosic reducing agents. *Green Chem.* **2010**, *12*, 220–222. [[CrossRef](#)]
111. Lin, X.B.; Wu, M.; Wu, D.Y.; Kuga, S.; Endo, T.; Huang, Y. Platinum nanoparticles using wood nanomaterials: Eco-friendly synthesis, shape control and catalytic activity for p-nitrophenol reduction. *Green Chem.* **2011**, *13*, 283–287. [[CrossRef](#)]
112. Zhou, P.; Wang, H.; Yang, J.; Tang, J.; Sun, D.; Tang, W. Bacteria Cellulose Nanofibers Supported Palladium(0) Nanocomposite and Its Catalysis Evaluation in Heck Reaction. *Ind. Eng. Chem. Res.* **2012**, *51*, 5743–5748. [[CrossRef](#)]
113. Xiang, Z.; Chen, Y.; Liu, Q.; Lu, F. A highly recyclable dip-catalyst produced from palladium nanoparticle-embedded bacterial cellulose and plant fibers. *Green Chem.* **2018**, *20*, 1085–1094. [[CrossRef](#)]
114. Cirtiu, C.M.; Dunlop-Brière, A.F.; Moores, A. Cellulose nanocrystallites as an efficient support for nanoparticles of palladium: Application for catalytic hydrogenation and Heck coupling under mild conditions. *Green Chem.* **2011**, *13*, 288–291. [[CrossRef](#)]
115. Wu, X.; Lu, C.; Zhang, W.; Yuan, G.; Xiong, R.; Zhang, X. A novel reagentless approach for synthesizing cellulose nanocrystal-supported palladium nanoparticles with enhanced catalytic performance. *J. Mater. Chem. A* **2013**, *1*, 8645–8652. [[CrossRef](#)]
116. Sun, D.; Yang, J.; Li, J.; Yu, J.; Xu, X.; Yang, X. Novel Pd-Cu/bacterial cellulose nanofibers: Preparation and excellent performance in catalytic denitrification. *Appl. Surf. Sci.* **2010**, *256*, 2241–2244. [[CrossRef](#)]
117. Gopiraman, M.; Bang, H.; Yuan, G.; Yin, C.; Song, K.H.; Lee, J.S.; Chung, I.M.; Karvembu, R.; Kim, I.S. Noble metal/functionalized cellulose nanofiber composites for catalytic applications. *Carbohydr. Polym.* **2015**, *132*, 554–564. [[CrossRef](#)]
118. Hu, X.; Xu, X.; Fu, F.; Yang, B.; Zhang, J.; Zhang, Y.; Touhid, S.S.B.; Liu, L.; Dong, Y.; Liu, X.; et al. Synthesis of bimetallic silver-gold nanoparticle composites using a cellulose dope: Tunable nanostructure and its biological activity. *Carbohydr. Polym.* **2020**, *248*, 116777. [[CrossRef](#)]
119. Irfan, M.; Perero, S.; Miola, M.; Maina, G.; Ferri, A.; Ferraris, M.; Balagna, C. Antimicrobial functionalization of cotton fabric with silver nanoclusters/silica composite coating via RF co-sputtering technique. *Cellulose* **2017**, *24*, 2331–2345. [[CrossRef](#)]
120. Hu, H.; Wu, X.; Wang, H.; Wang, H.; Zhou, J. Photo-reduction of Ag nanoparticles by using cellulose-based micelles as soft templates: Catalytic and antimicrobial activities. *Carbohydr. Polym.* **2019**, *213*, 419–427. [[CrossRef](#)]
121. Ramaraju, B.; Imae, T.; Destaye, A.G. Ag nanoparticle-immobilized cellulose nanofibril films for environmental conservation. *Appl. Catal. A Gen.* **2015**, *492*, 184–189. [[CrossRef](#)]
122. Song, Y.; Jiang, Y.; Shi, L.; Cao, S.; Feng, X.; Miao, M.; Fang, J. Solution-processed assembly of ultrathin transparent conductive cellulose nanopaper embedding AgNWs. *Nanoscale* **2015**, *7*, 13694–13701. [[CrossRef](#)] [[PubMed](#)]
123. Dong, H.; Snyder, J.F.; Tran, D.T.; Leadore, J.L. Hydrogel, aerogel and film of cellulose nanofibrils functionalized with silver nanoparticles. *Carbohydr. Polym.* **2013**, *95*, 760–767. [[CrossRef](#)] [[PubMed](#)]
124. Hu, L.; Zheng, G.; Yao, J.; Liu, N.; Weil, B.; Eskilsson, M.; Karabulut, E.; Ruan, Z.; Fan, S.; Bloking, J.T.; et al. Transparent and conductive paper from nanocellulose fibers. *Energy Environ. Sci.* **2013**, *6*, 513–518. [[CrossRef](#)]
125. Yang, G.; Xie, J.; Hong, F.; Cao, Z.; Yang, X. Antimicrobial activity of silver nanoparticle impregnated bacterial cellulose membrane: Effect of fermentation carbon sources of bacterial cellulose. *Carbohydr. Polym.* **2012**, *87*, 839–845. [[CrossRef](#)] [[PubMed](#)]
126. Wang, M.S.; Jiang, F.; Hsieh, Y.L.; Nitin, N. Cellulose nanofibrils improve dispersibility and stability of silver nanoparticles and induce production of bacterial extracellular polysaccharides. *J. Mater. Chem. B* **2014**, *2*, 6226–6235. [[CrossRef](#)]
127. Koga, H.; Nogi, M.; Komoda, N.; Nge, T.T.; Sugahara, T.; Sukanuma, K. Uniformly connected conductive networks on cellulose nanofiber paper for transparent paper electronics. *NPG Asia Mater.* **2014**, *6*, e93. [[CrossRef](#)]
128. Parnsubsakul, A.; Ngoensawat, U.; Wutikhun, T.; Sukmanee, T.; Sapcharoenkun, C.; Pienpinijtham, P.; Ekgasit, S. Silver nanoparticle/bacterial nanocellulose paper composites for paste-and-read SERS detection of pesticides on fruit surfaces. *Carbohydr. Polym.* **2020**, *235*, 115956. [[CrossRef](#)]
129. Fu, L.H.; Liu, B.; Meng, L.Y.; Ma, M.G. Comparative study of cellulose/Ag nanocomposites using four cellulose types. *Mater. Lett.* **2016**, *171*, 277–280. [[CrossRef](#)]
130. Yang, G.; Xie, J.; Deng, Y.; Bian, Y.; Hong, F. Hydrothermal synthesis of bacterial cellulose/AgNPs composite: A “green” route for antibacterial application. *Carbohydr. Polym.* **2012**, *87*, 2482–2487. [[CrossRef](#)]
131. Maria, L.; Santos, A.L.; Oliveira, P.C.; Valle, A.S.; Barud, H.S.; Messaddeq, Y.; Ribeiro, S.J. Preparation and Antibacterial Activity of Silver Nanoparticles Impregnated in Bacterial Cellulose. *Polimeros* **2010**, *20*, 72–77. [[CrossRef](#)]

132. Barud, H.S.; Regiani, T.; Marques, R.F.; Lustri, W.R.; Messaddeq, Y.; Ribeiro, S.J. Antimicrobial Bacterial Cellulose-Silver Nanoparticles Composite Membranes. *J. Nanomater.* **2011**, *2011*, 721631. [[CrossRef](#)]
133. Chen, X.; Lin, H.; Xu, T.; Lai, K.; Han, X.; Lin, M. Cellulose nanofibers coated with silver nanoparticles as a flexible nanocomposite for measurement of flusilazole residues in Oolong tea by surface-enhanced Raman spectroscopy. *Food Chem.* **2020**, *315*, 126276. [[CrossRef](#)] [[PubMed](#)]
134. Huang, L.; Wu, C.; Xie, L.; Yuan, X.; Wei, X.; Huang, Q.; Chen, Y.; Lu, Y. Silver-Nanocellulose Composite Used as SERS Substrate for Detecting Carbendazim. *Nanomaterials* **2019**, *9*, 355. [[CrossRef](#)]
135. Johnson, L.; Thielemans, W.; Walsh, D.A. Nanocomposite oxygen reduction electrocatalysts formed using bioderived reducing agents. *J. Mater. Chem.* **2010**, *20*, 1737–1743. [[CrossRef](#)]
136. Wu, C.N.; Fuh, S.C.; Lin, S.P.; Lin, Y.Y.; Chen, H.Y.; Liu, J.M.; Cheng, K.C. TEMPO-Oxidized Bacterial Cellulose Pellicle with Silver Nanoparticles for Wound Dressing. *Biomacromolecules* **2018**, *19*, 544–554. [[CrossRef](#)]
137. Liu, H.; Wang, D.; Song, Z.; Shang, S. Preparation of silver nanoparticles on cellulose nanocrystals and the application in electrochemical detection of DNA hybridization. *Cellulose* **2011**, *18*, 67–74. [[CrossRef](#)]
138. Liu, H.; Song, J.; Shang, S.; Song, Z.; Wang, D. Cellulose Nanocrystal/Silver Nanoparticle Composites as Bifunctional Nanofillers within Waterborne Polyurethane. *ACS Appl. Mater. Interfaces* **2012**, *4*, 2413–2419. [[CrossRef](#)]
139. Xiong, R.; Lu, C.; Zhang, W.; Zhou, Z.; Zhang, X. Facile synthesis of tunable silver nanostructures for antibacterial application using cellulose nanocrystals. *Carbohydr. Polym.* **2013**, *95*, 214–219. [[CrossRef](#)]
140. Drogat, N.; Granet, R.; Sol, V.; Memmi, A.; Saad, N.; Klein Koerkamp, C.; Bressollier, P.; Krausz, P. Antimicrobial silver nanoparticles generated on cellulose nanocrystals. *J. Nanopart. Res.* **2011**, *13*, 1557–1562. [[CrossRef](#)]
141. Lokanathan, A.R.; Uddin, K.M.A.; Rojas, O.J.; Laine, J. Cellulose Nanocrystal-Mediated Synthesis of Silver Nanoparticles: Role of Sulfate Groups in Nucleation Phenomena. *Biomacromolecules* **2014**, *15*, 373–379. [[CrossRef](#)] [[PubMed](#)]
142. Tang, J.; Shi, Z.; Berry, R.M.; Tam, K.C. Mussel-Inspired Green Metallization of Silver Nanoparticles on Cellulose Nanocrystals and Their Enhanced Catalytic Reduction of 4-Nitrophenol in the Presence of beta-Cyclodextrin. *Ind. Eng. Chem. Res.* **2015**, *54*, 3299–3308. [[CrossRef](#)]
143. Shi, Z.; Tang, J.; Chen, L.; Yan, C.; Tanvir, S.; Anderson, W.A.; Berry, R.M.; Tam, K.C. Enhanced colloidal stability and antibacterial performance of silver nanoparticles/cellulose nanocrystal hybrids. *J. Mater. Chem. B* **2015**, *3*, 603–611. [[CrossRef](#)] [[PubMed](#)]
144. Hoeng, F.; Denneulin, A.; Neuman, C.; Bras, J. Charge density modification of carboxylated cellulose nanocrystals for stable silver nanoparticles suspension preparation. *J. Nanopart. Res.* **2015**, *17*, 244. [[CrossRef](#)]
145. Kaushik, M.; Li, A.Y.; Hudson, R.; Masnadi, M.; Li, C.J.; Moores, A. Reversing aggregation: Direct synthesis of nanocatalysts from bulk metal. Cellulose nanocrystals as active support to access efficient hydrogenation silver nanocatalysts. *Green Chem.* **2016**, *18*, 129–133. [[CrossRef](#)]
146. Bendi, R.; Imae, T. Renewable catalyst with Cu nanoparticles embedded into cellulose nano-fiber film. *RSC Adv.* **2013**, *3*, 16279–16282. [[CrossRef](#)]
147. Pérez-Alvarez, M.; Cadenas-Pliego, G.; Pérez-Camacho, O.; Comparán-Padilla, V.E.; Cabello-Alvarado, C.J.; Saucedo-Salazar, E. Green Synthesis of Copper Nanoparticles Using Cotton. *Polymers* **2021**, *13*, 1906. [[CrossRef](#)]
148. Toncheva, A.; Khelifa, F.; Paint, Y.; Voue, M.; Lambert, P.; Dubois, P.; Raquez, J.M. Fast IR-Actuated Shape-Memory Polymers Using in Situ Silver Nanoparticle-Grafted Cellulose Nanocrystals. *ACS Appl. Mater. Interfaces* **2018**, *10*, 29933–29942. [[CrossRef](#)]
149. Hebeish, A.; Farag, S.; Sharaf, S.; Shaheen, T.I. Development of cellulose nanowhisker- polyacrylamide copolymer as a highly functional precursor in the synthesis of nanometal particles for conductive textiles. *Cellulose* **2014**, *21*, 3055–3071. [[CrossRef](#)]
150. Goswami, M.; Das, A.M. Synthesis of cellulose impregnated copper nanoparticles as an efficient heterogeneous catalyst for CeN coupling reactions under mild conditions. *Carbohydr. Polym.* **2018**, *195*, 189–198. [[CrossRef](#)]
151. Dutta, A.; Chetia, M.; Ali, A.A.; Bordoloi, A.; Gehlot, P.S.; Kumar, A.; Sarma, D. Copper Nanoparticles Immobilized on Nanocellulose: A Novel and Efficient Heterogeneous Catalyst for Controlled and Selective Oxidation of Sulfides and Alcohols. *Catal. Lett.* **2019**, *149*, 141–150. [[CrossRef](#)]
152. Huang, D.; Hu, Z.; Peng, Z.; Zeng, G.; Chen, G.; Zhang, C.; Cheng, M.; Wan, J.; Wang, X.; Qin, X. Cadmium immobilization in river sediment using stabilized nanoscale zero-valent iron with enhanced transport by polysaccharide coating. *J. Environ. Manag.* **2018**, *210*, 191–200. [[CrossRef](#)] [[PubMed](#)]
153. Voisin, H.; Bergström, L.; Liu, P.; Mathew, A.P. Nanocellulose-Based Materials for Water Purification. *Nanomaterials* **2017**, *7*, 57. [[CrossRef](#)] [[PubMed](#)]
154. Borkow, G.; Zhou, S.S.; Page, T.; Gabbay, J. A Novel Anti-Influenza Copper Oxide Containing Respiratory Face Mask. *PLoS ONE* **2010**, *5*, e11295. [[CrossRef](#)]
155. Li, Y.; Li, L.; Cao, L.; Yang, C. Promoting dynamic adsorption of Pb²⁺ in a single pass flow using fibrous nano-TiO₂/cellulose membranes. *Chem. Eng. J.* **2016**, *283*, 1145–1153. [[CrossRef](#)]
156. Li, Y.; Cao, L.; Li, L.; Yang, C. In situ growing directional spindle TiO₂ nanocrystals on cellulose fibers for enhanced Pb²⁺ adsorption from water. *J. Hazard. Mater.* **2015**, *289*, 140–148. [[CrossRef](#)]
157. Zeng, J.; Liu, S.; Cai, J.; Zhang, L. TiO₂ Immobilized in Cellulose Matrix for Photocatalytic Degradation of Phenol under Weak UV Light Irradiation. *J. Phys. Chem. C* **2010**, *114*, 7806–7811. [[CrossRef](#)]

158. Kettunen, M.; Silvennoinen, R.J.; Houbenov, N.; Nykänen, A.; Ruokolainen, J.; Sainio, J.; Pore, V.; Kemell, M.; Ankerfors, M.; Lindström, T.; et al. Photoswitchable Superabsorbency Based on Nanocellulose Aerogels. *Adv. Funct. Mater.* **2011**, *21*, 510–517. [[CrossRef](#)]
159. Korhonen, J.T.; Kettunen, M.; Ras, R.H.A.; Ikkala, O. Hydrophobic Nanocellulose Aerogels as Floating, Sustainable, Reusable, and Recyclable Oil Absorbents. *ACS Appl. Mater. Interfaces* **2011**, *3*, 1813–1816. [[CrossRef](#)]
160. Donia, A.M.; Atia, A.A.; Abouzayed, F.I. Preparation and characterization of nano-magnetic cellulose with fast kinetic properties towards the adsorption of some metal ions. *Chem. Eng. J.* **2012**, *191*, 22–30. [[CrossRef](#)]
161. Zhu, H.; Jia, S.; Wan, T.; Jia, Y.; Yang, H.; Li, J.; Yan, L.; Zhong, C. Biosynthesis of spherical Fe₃O₄/bacterial cellulose nanocomposites as adsorbents for heavy metal ions. *Carbohydr. Polym.* **2011**, *86*, 1558–1564. [[CrossRef](#)]
162. Nata, I.F.; Sureshkumar, M.; Lee, C.K. One-pot preparation of amine-rich magnetite/bacterial cellulose nanocomposite and its application for arsenate removal. *RSC Adv.* **2011**, *1*, 625–631. [[CrossRef](#)]
163. Qin, Y.; Qin, Z.; Liu, Y.; Cheng, M.; Qian, P.; Wang, Q.; Zhu, M. Superparamagnetic iron oxide coated on the surface of cellulose nanospheres for the rapid removal of textile dye under mild condition. *Appl. Surf. Sci.* **2015**, *357*, 2103–2111. [[CrossRef](#)]
164. John, A.; Ko, H.U.; Kim, D.G.; Kim, J. Preparation of cellulose-ZnO hybrid films by a wet chemical method and their characterization. *Cellulose* **2011**, *18*, 675–680. [[CrossRef](#)]
165. Yu, H.Y.; Chen, G.Y.; Wang, Y.B.; Yao, J.M. A facile one-pot route for preparing cellulose nanocrystal/zinc oxide nanohybrids with high antibacterial and photocatalytic activity. *Cellulose* **2015**, *22*, 261–273. [[CrossRef](#)]
166. Zheng, W.L.; Hu, W.L.; Chen, S.Y.; Zheng, Y.; Zhou, B.H.; Wang, H.P. High Photocatalytic Properties of Zinc Oxide Nanoparticles with Amidoximated Bacterial Cellulose Nanofibers as Templates. *Chin. J. Polym. Sci.* **2014**, *32*, 169–176. [[CrossRef](#)]
167. Chen, S.; Zhou, B.; Hu, W.; Zhang, W.; Yin, N.; Wang, H. Polyol mediated synthesis of ZnO nanoparticles templated by bacterial cellulose. *Carbohydr. Polym.* **2013**, *92*, 1953–1959. [[CrossRef](#)]
168. Katepetch, C.; Rujiravanit, R.; Tamura, H. Formation of nanocrystalline ZnO particles into bacterial cellulose pellicle by ultrasonic-assisted in situ synthesis. *Cellulose* **2013**, *20*, 1275–1292. [[CrossRef](#)]
169. Ul-Islam, M.; Khattak, W.A.; Ullah, M.W.; Khan, S.; Park, J.K. Synthesis of regenerated bacterial cellulose-zinc oxide nanocomposite films for biomedical applications. *Cellulose* **2014**, *21*, 433–447. [[CrossRef](#)]
170. Yang, R.T.; Yu, H.Y.; Song, M.L.; Zhou, Y.W.; Yao, J.M. Flower-like zinc oxide nanorod clusters grown on spherical cellulose nanocrystals via simple chemical precipitation method. *Cellulose* **2016**, *23*, 1871–1884. [[CrossRef](#)]
171. Rull-Barrull, J.; d'Halluin, M.; Le Grogne, E.; Felpin, F.X. Harnessing the Dual Properties of Thiol-Grafted Cellulose Paper for Click Reactions: A Powerful Reducing Agent and Adsorbent for Cu. *Angew. Chem. Int. Ed.* **2016**, *55*, 13549–13552. [[CrossRef](#)] [[PubMed](#)]
172. Liu, S.; Yan, Q.; Tao, D.; Yu, T.; Liu, X. Highly flexible magnetic composite aerogels prepared by using cellulose nanofibril networks as templates. *Carbohydr. Polym.* **2012**, *89*, 551–557. [[CrossRef](#)] [[PubMed](#)]
173. Olsson, R.T.; Azizi Samir, M.A.S.; Salazar-Alvarez, G.; Belova, L.; Stroem, V.; Berglund, L.A.; Ikkala, O.; Nogue's, J.; Gedde, U.W. Making flexible magnetic aerogels and stiff magnetic nanopaper using cellulose nanofibrils as templates. *Nat. Nanotechnol.* **2010**, *5*, 584–588. [[CrossRef](#)] [[PubMed](#)]
174. Echeverry-Rendon, M.; Reece, L.M.; Pastrana, F.; Arias, S.L.; Shetty, A.R.; Pavón, J.J.; Allain, J.P. Bacterial Nanocellulose Magnetically Functionalized for Neuro-Endovascular Treatment. *Macromol. Biosci.* **2017**, *17*, 1600382. [[CrossRef](#)] [[PubMed](#)]
175. Nypelo, T.; Rodriguez-Abreu, C.; Rivas, J.; Dickey, M.D.; Rojas, O.J. Magneto-responsive hybrid materials based on cellulose nanocrystals. *Cellulose* **2014**, *21*, 2557–2566. [[CrossRef](#)]
176. Dong, P.; Cheng, X.; Huang, Z.; Chen, Y.; Zhang, Y.; Nie, X.; Zhang, X. In-situ and phase controllable synthesis of nanocrystalline TiO₂ on flexible cellulose fabrics via a simple hydrothermal method. *Mater. Res. Bull.* **2018**, *97*, 89–95. [[CrossRef](#)]
177. Chauhan, I.; Mohanty, P. In situ decoration of TiO₂ nanoparticles on the surface of cellulose fibers and study of their photocatalytic and antibacterial activities. *Cellulose* **2015**, *22*, 507–519. [[CrossRef](#)]
178. Noman, M.T.; Wienera, J.; Saskova, J.; Ashrafa, M.A.; Vikova, M.; Jamshaid, H.; Kejzlar, P. In-situ development of highly photocatalytic multifunctional nanocomposites by ultrasonic acoustic method. *Ultrason. Sonochem.* **2018**, *40*, 41–56. [[CrossRef](#)]
179. Chauhan, I.; Mohanty, P. Immobilization of titania nanoparticles on the surface of cellulose fibres by a facile single step hydrothermal method and study of their photocatalytic and antibacterial activities. *RSC Adv.* **2014**, *4*, 57885–57890. [[CrossRef](#)]
180. Zong, E.; Wang, C.; Yang, J.; Zhu, H.; Jiang, S.; Liu, X.; Song, P. Preparation of TiO₂/cellulose nanocomposites as antibacterial bio-adsorbents for effective phosphate removal from aqueous medium. *Int. J. Biol. Macromol.* **2021**, *182*, 434–444. [[CrossRef](#)]
181. Fallah, Z.; Isfahani, H.N.; Tajbakhsh, M.; Tashakkorian, H.; Amouei, A. TiO₂-grafted cellulose via click reaction: An efficient heavy metal ions bioadsorbent from aqueous solutions. *Cellulose* **2018**, *25*, 639–660. [[CrossRef](#)]
182. Oliveira, A.C.M.; dos Santos, M.S.; Brandao, L.M.S.; de Resende, I.T.F.; Leo, I.M.; Morillo, E.S.; Yerga, R.M.N.; Fierro, J.L.G.; Egues, S.M.S.; Figueiredo, R.T. The effect of cellulose loading on the photoactivity of cellulose-TiO₂ hybrids for hydrogen production under simulated sunlight. *Int. J. Hydrogen Energy* **2017**, *42*, 28747–28754. [[CrossRef](#)]
183. Schütz, C.; Sort, J.; Bacsik, Z.; Oliynyk, V.; Pellicer, E.; Fall, A.; Wågberg, L.; Berglund, L.; Bergström, L.; Salazar-Alvarez, G. Hard and Transparent Films Formed by Nanocellulose-TiO₂ Nanoparticle Hybrids. *PLoS ONE* **2012**, *7*, e45828. [[CrossRef](#)] [[PubMed](#)]
184. Missoum, K.; Sadocco, P.; Causio, J.; Belgacem, M.N.; Bras, J. Antibacterial activity and biodegradability assessment of chemically grafted nanofibrillated cellulose. *J. Mater. Sci. Eng. C* **2014**, *45*, 477–483. [[CrossRef](#)]

185. Wesarg, F.; Schlott, F.; Grabow, J.; Kurland, H.D.; Heßler, N.; Kralisch, D.; Müller, F.A. In Situ Synthesis of Photocatalytically Active Hybrids Consisting of Bacterial Nanocellulose and Anatase Nanoparticles. *Langmuir* **2012**, *28*, 13518–13525. [CrossRef]
186. Gao, R.; Chen, X.; Chen, C.; Shi, R.; Ouyang, F.; Yang, J.; Sun, D.; Liu, J. Synthesis of BC@mTiO₂ hybrid nanofibers for highly efficient enrichment and detection of phosphopeptides. *Cellulose* **2016**, *23*, 2475–2485. [CrossRef]
187. Sun, D.; Yang, J.; Wang, X. Bacterial cellulose/TiO₂ hybrid nanofibers prepared by the surface hydrolysis method with molecular precision. *Nanoscale* **2010**, *2*, 287–292. [CrossRef]
188. Gonzalez, Z.; Yus, J.; Bravo, Y.; Sanchez-Herencia, A.J.; Rodriguez, A.; Dewalque, J.; Manceri, L.; Henrist, C.; Ferrari, B. Heteroaggregation of lignocellulose fibers-based biotemplates and functionalized TiO₂ nanoparticles to tailor film microstructures. *Cellulose* **2020**, *27*, 7543–7559. [CrossRef]
189. Janpetch, N.; Vanichvattanadecha, C.; Rujiravanit, R. Photocatalytic disinfection of water by bacterial cellulose/N-F co-doped TiO₂ under fluorescent light. *Cellulose* **2015**, *22*, 3321–3335. [CrossRef]
190. Brandes, R.; Trindade, E.C.A.; Vanin, D.F.; Vargas, V.M.M.; Carminatti, C.A.; Al-Qureshi, H.A.; Recouvreux, D.O.S. Spherical Bacterial Cellulose/TiO₂ Nanocomposite with Potential Application in Contaminants Removal from Wastewater by Photocatalysis. *Fibers Polym.* **2018**, *19*, 1861–1868. [CrossRef]
191. Nabeela, K.; Thorat, M.N.; Backer, S.N.; Ramachandran, A.M.; Thomas, R.T.; Preethikumar, G.; Mohamed, A.P.; Asok, A.; Dastager, S.G.; Pillai, S. Hydrophilic 3D Interconnected Network of Bacterial Nanocellulose/Black Titania Photothermal Foams as an Efficient Interfacial Solar Evaporator. *ACS Appl. Bio Mater.* **2021**, *4*, 4373–4383. [CrossRef] [PubMed]
192. Shandilya, N.; Capron, I. Safer-by-design hybrid nanostructures: An alternative to conventional titanium dioxide UV filters in skin care products. *RSC Adv.* **2017**, *7*, 20430–20439. [CrossRef]
193. Evdokimova, O.L.; Svensson, F.G.; Agafonov, A.V.; Håkansson, S.; Seisenbaeva, G.A.; Kessler, V.G. Hybrid Drug Delivery Patches Based on Spherical Cellulose Nanocrystals and Colloid Titania—Synthesis and Antibacterial Properties. *Nanomaterials* **2018**, *8*, 228. [CrossRef] [PubMed]
194. Lu, M.; Li, L.; Xie, R.; Zhao, Z.; Mao, Z. Preparation of magnetic cotton fabric by surface micro-dissolution treatment. *Cellulose* **2017**, *24*, 1099–1106. [CrossRef]
195. Rotaru, R.; Savin, M.; Tudorachi, N.; Peptu, C.; Samoila, P.; Sacarescu, L.; Harabagiu, V. Ferromagnetic iron oxide–cellulose nanocomposites prepared by ultrasonication. *Polym. Chem.* **2018**, *9*, 860–868. [CrossRef]
196. Yusefi, M.; Lee-Kiun, M.S.; Shameli, K.; Teow, S.Y.; Ali, R.R.; Siew, K.K.; Chan, H.Y.; Wong, M.M.T.; Lim, W.L.; Kuča, K. 5-Fluorouracil loaded magnetic cellulose bionanocomposites for potential colorectal cancer treatment. *Carbohydr. Polym.* **2021**, *273*, 118523. [CrossRef]
197. Spiridonova, V.V.; Panova, I.G.; Makarova, L.A.; Afanasova, M.I.; Zezina, S.B.; Sybachina, A.V.; Yaroslavov, A.A. The one-step synthesis of polymer-based magnetic γ -Fe₂O₃/carboxymethyl cellulose nanocomposites. *Carbohydr. Polym.* **2017**, *177*, 269–274. [CrossRef]
198. Liu, S.; Zhou, J.; Zhang, L. In situ synthesis of plate-like Fe₂O₃ nanoparticles in porous cellulose films with obvious magnetic anisotropy. *Cellulose* **2011**, *18*, 663–673. [CrossRef]
199. Ni, W.; Zheng, Z.; Liu, H.; Wang, P.; Wang, L.; Wang, H.; Sun, X.; Yang, Q.; Tang, H.; Zhao, G. Synthesis of the carboxymethyl cellulose magnetic nanoparticles for efficient immobilization of prenyltransferase NovQ. *Carbohydr. Polym.* **2020**, *235*, 115955. [CrossRef]
200. Rashid, M.; Gafur, M.A.; Sharafat, M.K.; Minami, H.; Miah, M.A.J.; Ahmad, H. Biocompatible microcrystalline cellulose particles from cotton wool and magnetization via a simple in situ co-precipitation method. *Carbohydr. Polym.* **2017**, *170*, 72–79. [CrossRef]
201. Biliuta, G.; Sacarescu, L.; Socoliu, V.; Iacob, M.; Gheorghe, L.; Negru, D.; Coseri, S. Carboxylated Polysaccharides Decorated with Ultrasmall Magnetic Nanoparticles with Antibacterial and MRI Properties. *Macromol. Chem. Phys.* **2017**, *218*, 1700062. [CrossRef]
202. Zeng, M.; Laromaine, A.; Feng, W.; Levkin, P.A.; Roig, A. Origami magnetic cellulose: Controlled magnetic fraction and patterning of flexible bacterial cellulose. *J. Mater. Chem. C* **2014**, *2*, 6312–6318. [CrossRef]
203. Stoica-Guzun, A.; Stroescu, M.; Jinga, S.I.; Mihalache, N.; Botez, A.; Matei, C.; Berger, D.; Damian, C.M.; Ionita, V. Box-Behnken experimental design for chromium(VI) ions removal by bacterial cellulose-magnetite composites. *Int. J. Biol. Macromol.* **2016**, *91*, 1062–1072. [CrossRef]
204. An, X.; Cheng, D.; Dai, L.; Wang, B.; Ocampo, H.J.; Nasrallah, J.; Jia, X.; Zou, J.; Long, Y.; Ni, Y. Synthesis of nano-fibrillated cellulose/magnetite/titanium dioxide(NFC@Fe₃O₄@TNP) nanocomposites and their application in the photocatalytic hydrogen generation. *Appl. Catal. B* **2017**, *206*, 53–64. [CrossRef]
205. Guo, J.; Filpponen, I.; Johansson, L.S.; Mohammadi, P.; Latikka, M.; Linder, M.B.; Ras, R.H.A.; Rojas, O.J. Complexes of Magnetic Nanoparticles with Cellulose Nanocrystals as Regenerable, Highly Efficient, and Selective Platform for Protein Separation. *Biomacromolecules* **2017**, *18*, 898–905. [CrossRef]
206. Karimian, A.; Yousefi, B.; Sadeghi, F.; Feizi, F.; Najafzadehvarzi, H.; Parsian, H. Synthesis of biocompatible nanocrystalline cellulose against folate receptors as a novel carrier for targeted delivery of doxorubicin. *Chem.-Biol. Interact.* **2022**, *351*, 109731. [CrossRef]
207. Liu, K.; Nasrallah, J.; Chen, L.; Huang, L.; Ni, Y. Preparation of CNC-dispersed Fe₃O₄ nanoparticles and their application in conductive paper. *Carbohydr. Polym.* **2015**, *126*, 175–178. [CrossRef]
208. Xie, Y.; Pan, Y.; Cai, P. Cellulose-based antimicrobial films incorporated with ZnO nanopillars on surface as biodegradable and antimicrobial packaging. *Food Chem.* **2022**, *368*, 130784. [CrossRef]

209. Wang, Y.H.; Song, P.; Li, X.; Ru, C.; Ferrari, G.; Balasubramanian, P.; Amabili, M.; Sun, Y.; Liu, X. A Paper-Based Piezoelectric Accelerometer. *Micromachines* **2018**, *9*, 19. [[CrossRef](#)]
210. Ibrahim, N.A.; Nada, A.A.; Hassabo, A.G.; Eid, B.M.; Noor El-Deen, A.M.; Abou-Zeid, N.Y. Effect of different capping agents on physicochemical and antimicrobial properties of ZnO nanoparticles. *Chem. Pap.* **2017**, *71*, 1365–1375. [[CrossRef](#)]
211. Ibupoto, Z.; Khun, K.; Eriksson, M.; Al Salhi, M.; Atif, M.; Ansari, A.; Willander, M. Hydrothermal Growth of Vertically Aligned ZnO Nanorods Using a Biocomposite Seed Layer of ZnO Nanoparticles. *Materials* **2013**, *6*, 3584–3597. [[CrossRef](#)] [[PubMed](#)]
212. Li, Y.; Sun, H.; Zhang, Y.; Xu, M.; Shi, S.Q. The three-dimensional heterostructure synthesis of ZnO/cellulosic fibers and its application for rubber composites. *Compos. Sci. Technol.* **2019**, *177*, 10–17. [[CrossRef](#)]
213. Xiao, H.; Shan, Y.; Zhang, W.; Huang, L.; Chen, L.; Ni, Y.; Boury, B.; Wu, H. C-nanocoated ZnO by TEMPO-oxidized cellulose templating for improved photocatalytic performance. *Carbohydr. Polym.* **2020**, *235*, 115958. [[CrossRef](#)] [[PubMed](#)]
214. Costa, S.V.; Gonçalves, A.S.; Zaguete, M.A.; Mazon, T.; Nogueira, A.F. ZnO nanostructures directly grown on paper and bacterial cellulose substrates without any surface modification layer. *Chem. Commun.* **2013**, *49*, 8096–8098. [[CrossRef](#)]
215. Janpetch, N.; Saito, N.; Rujiravanit, R. Fabrication of bacterial cellulose-ZnO composite via solution plasma process for antibacterial applications. *Carbohydr. Polym.* **2016**, *148*, 335–344. [[CrossRef](#)]
216. Wang, P.; Zhao, J.; Xuan, R.; Wang, Y.; Zou, C.; Zhang, Z.; Wan, Y.; Xu, Y. Flexible and monolithic zinc oxide bionanocomposite foams by a bacterial cellulose mediated approach for antibacterial applications. *Dalton Trans.* **2014**, *43*, 6762–6768. [[CrossRef](#)]
217. Khalid, A.; Khan, R.; Ul-Islam, M.; Khan, T.; Wahid, F. Bacterial cellulose-zinc oxide nanocomposites as a novel dressing system for burn wounds. *Carbohydr. Polym.* **2017**, *164*, 214–221. [[CrossRef](#)]
218. Lizundia, E.; Urruchi, A.; Vilas, J.L.; León, L.M. Increased functional properties and thermal stability of flexible cellulose nanocrystal/ZnO films. *Carbohydr. Polym.* **2016**, *136*, 250–258. [[CrossRef](#)]
219. Azizi, S.; Ahmad, M.; Mahdavi, M.; Abdolmohammadi, S. Preparation, Characterization, and Antimicrobial Activities of ZnO Nanoparticles/Cellulose Nanocrystal Nanocomposites. *BioResources* **2013**, *8*, 1841–1851. [[CrossRef](#)]
220. Soltani, R.D.C.; Mashayekhi, M.; Naderi, M.; Boczkaj, G.; Jorfi, S.; Safari, M. Sonocatalytic degradation of tetracycline antibiotic using zinc oxide nanostructures loaded on nano-cellulose from waste straw as Nanosonocatalyst. *Ultrason. Sonochem.* **2019**, *55*, 117–124. [[CrossRef](#)]
221. Tavker, N.; Gaur, U.; Sharma, M. Cellulose supported bismuth vanadate nanocomposite for effective removal of organic pollutant. *J. Environ. Chem. Eng.* **2020**, *8*, 104027. [[CrossRef](#)]
222. Maqbool, Q.; Barucca, G.; Sabbatini, S.; Parlapiano, M.; Ruello, M.L.; Tittarelli, F. Transformation of industrial and organic waste into titanium doped activated carbon—cellulose nanocomposite for rapid removal of organic pollutants. *J. Hazard. Mater.* **2022**, *423*, 126958. [[CrossRef](#)] [[PubMed](#)]
223. Jiao, C.; Tao, J.; Xiong, J.; Wang, X.; Zhang, D.; Lin, H.; Chen, Y. In situ synthesis of MnO₂-loaded biocomposite based on microcrystalline cellulose for Pb²⁺ removal from wastewater. *Cellulose* **2017**, *24*, 2591–2604. [[CrossRef](#)]
224. Lu, Y.; Liu, H.; Gao, R.; Xiao, S.; Zhang, M.; Yin, Y.; Wang, S.; Li, J.; Yang, D. Coherent-Interface-Assembled Ag₂O Anchored Nanofibrillated Cellulose Porous Aerogels for Radioactive Iodine Capture. *ACS Appl. Mater. Interf.* **2014**, *24*, 29179–29185. [[CrossRef](#)] [[PubMed](#)]
225. Santos, M.V.; Barud, H.S.; Alencar, M.A.S.; Nalin, M.; Toma, S.H.; Araki, K.; Benedetti, A.V.; Maciel, I.O.; Fragneaud, B.; Legnani, C.; et al. Self-Supported Smart Bacterial Nanocellulose–Phosphotungstic Acid Nanocomposites for Photochromic Applications. *Front. Mater.* **2021**, *8*, 668835. [[CrossRef](#)]
226. Yin, J.; Gao, F.; Wu, Y.; Wang, J.; Lu, Q. Synthesis of Mn₃O₄ octahedrons and other manganese-based nanostructures through a simple and green route. *CrystEngComm* **2010**, *12*, 3401–3403. [[CrossRef](#)]
227. Dai, B.; Chao, C.; Lu, X.; Xia, Q.; Han, J.; Mao, F.; Yang, J.; Sun, D. Preparation of ZnO/CdS/BC Photocatalyst Hybrid Fiber and Research of Its Photocatalytic Properties. *J. Nanotechnol.* **2015**, *2015*, 614170. [[CrossRef](#)]
228. Zhang, G.; Liao, Q.; Zhang, Z.; Liang, Q.; Zhao, Y.; Zheng, X.; Zhang, Y. Novel Piezoelectric Paper-Based Flexible Nanogenerators Composed of BaTiO₃ Nanoparticles and Bacterial Cellulose. *Adv. Sci.* **2016**, *3*, 1500257. [[CrossRef](#)]
229. Choi, H.Y.; Jeong, Y.G. Microstructures and piezoelectric performance of eco-friendly composite films based on nanocellulose and barium titanate nanoparticle. *Compos. Part B* **2019**, *168*, 58–65. [[CrossRef](#)]
230. Yang, J.; Tang, W.; Liu, X.; Chao, C.; Liu, J.; Sun, D. Bacterial cellulose-assisted hydrothermal synthesis and catalytic performance of La₂CuO₄ nanofiber for methanol steam reforming. *Int. J. Hydrogen Energy* **2013**, *38*, 10813–10818. [[CrossRef](#)]
231. Menchaca-Nal, S.; Londono-Calderon, C.L.; Cerrutti, P.; Foresti, M.L.; Pampillo, L.; Bilovol, V.; Candal, R.; Martinez-Garcia, R. Facile synthesis of cobalt ferrite nanotubes using bacterial nanocellulose as template. *Carbohydr. Polym.* **2016**, *137*, 726–731. [[CrossRef](#)]
232. Gutierrez, J.; Fernandes, S.C.M.; Mondragon, I.; Tercjak, A. Conductive Photoswitchable Vanadium Oxide Nanopaper based on Bacterial Cellulose. *ChemSusChem* **2012**, *5*, 2323–2327. [[CrossRef](#)] [[PubMed](#)]
233. Almasi, H.; Jafarzadeh, P.; Mehryar, L. Fabrication of novel nanohybrids by impregnation of CuO nanoparticles into bacterial cellulose and chitosan nanofibers: Characterization, antimicrobial and release properties. *Carbohydr. Polym.* **2018**, *186*, 273–281. [[CrossRef](#)] [[PubMed](#)]
234. Almasi, H.; Mehryar, L.; Ghadertaj, A. Characterization of CuO-bacterial cellulose nanohybrids fabricated by in-situ and ex-situ impregnation methods. *Carbohydr. Polym.* **2019**, *222*, 114995. [[CrossRef](#)] [[PubMed](#)]

235. Zhou, Z.H.; Lu, C.H.; Wu, X.D.; Zhang, X.X. Cellulose nanocrystals as a novel support for CuO nanoparticles catalysts: Facile synthesis and their application to 4-nitrophenol reduction. *RSC Adv.* **2013**, *3*, 26066–26073. [[CrossRef](#)]
236. Lou, Z.; Cao, Z.; Xu, J.; Zhou, X.; Zhu, J.; Liu, X.; Baig, S.A.; Zhou, J.; Xu, X. Enhanced removal of As(III)/(V) from water by simultaneously supported and stabilized Fe-Mn binary oxide nanohybrids. *Chem. Eng. J.* **2017**, *322*, 710–721. [[CrossRef](#)]
237. Wang, W.; Zhang, B.; Jiang, S.; Bai, H.; Zhang, S. Use of CeO₂ Nanoparticles to Enhance UV-Shielding of Transparent Regenerated Cellulose Films. *Polymers* **2019**, *11*, 458. [[CrossRef](#)]
238. Korhonen, J.T.; Hiekkataipale, P.; Malm, J.; Karpinen, M.; Ikkala, O.; Ras, R.H.A. Inorganic Hollow Nanotube Aerogels by Atomic Layer Deposition onto Native Nanocellulose Templates. *ACS Nano* **2011**, *5*, 1967–1974. [[CrossRef](#)]
239. Shi, F.; Yu, T.; Hu, S.C.; Liu, J.X.; Yu, L.; Liu, S.H. Synthesis of highly porous SiO₂-(WO₃)_xTiO₂ composite aerogels using bacterial cellulose as template with solvothermal assisted crystallization. *Chem. Eng. J.* **2016**, *292*, 105–112. [[CrossRef](#)]
240. Qiu, J.; Li, M.; Ding, M.; Yao, J. Cellulose tailored semiconductors for advanced photocatalysis. *Renew. Sustain. Energy Rev.* **2022**, *154*, 111820. [[CrossRef](#)]
241. Hiltunen, A.; Or, T.; Lahtonen, K.; Ali-Löytty, H.; Tkachenko, N.; Valden, M.; Sarlin, E.; Cranston, E.D.; Moran-Mirabal, J.M.; Vapaavuori, J. Ultrathin-Walled 3D Inorganic Nanostructured Networks Templated from Cross-Linked Cellulose Nanocrystal Aerogels. *Adv. Mater. Interfaces* **2021**, *8*, 2001181. [[CrossRef](#)]
242. Sun, J.; Wenqiang Liu, W.; Wang, W.; Hu, Y.; Yang, X.; Chen, H.; Peng, Y.; Xu, M. CO₂ Sorption Enhancement of Extruded-Spheronized CaO-Based Pellets by Sacrificial Biomass Templating Technique. *Energy Fuels* **2016**, *30*, 9605–9612. [[CrossRef](#)]
243. Jabbour, L.; Bongiovanni, R.; Chaussy, D.; Gerbaldi, C.; Beneventi, D. Cellulose-based Li-ion batteries: A review. *Cellulose* **2013**, *20*, 1523–1545. [[CrossRef](#)]
244. Giese, M.; Blusch, L.K.; Khan, M.K.; MacLachlan, M.J. Functional Materials from Cellulose-Derived Liquid-Crystal Templates. *Angew. Chem. Int. Ed.* **2015**, *54*, 2888–2910. [[CrossRef](#)] [[PubMed](#)]
245. Yoon, Y.H.; Lee, S.Y.; Gwon, J.G.; Cho, H.J.; Wu, Q.; Kim, Y.H.; Lee, W.H. Photocatalytic performance of highly transparent and mesoporous molybdenum-doped titania films fabricated by templating cellulose nanocrystals. *Ceram. Int.* **2018**, *44*, 16647–16653. [[CrossRef](#)]
246. Shopsowitz, K.E.; Stahl, A.; Hamad, W.Y.; MacLachlan, M.J. Hard Templating of Nanocrystalline Titanium Dioxide with Chiral Nematic Ordering. *Angew. Chem. Int. Ed.* **2012**, *51*, 6886–6890. [[CrossRef](#)] [[PubMed](#)]
247. Huang, X.; Zhang, J.; Liu, Z.; Sang, T.; Song, B.; Zhu, H.; Wong, C. Facile preparation and microwave absorption properties of porous hollow BaFe₁₂O₁₉/CoFe₂O₄ composite microrods. *J. Alloys Compd.* **2015**, *648*, 1072–1075. [[CrossRef](#)]
248. Ivanova, A.; Fominykh, K.; Fattakhova-Rohlfing, D.; Zeller, P.; Döblinger, M.; Bein, T. Nanocellulose-Assisted Formation of Porous Hematite Nanostructures. *Inorg. Chem.* **2015**, *54*, 1129–1135. [[CrossRef](#)]
249. Guo, H.; Mao, R.; Yang, X.; Wang, S.; Chen, J. Hollow nanotubular SnO₂ with improved lithium storage. *J. Power Sources* **2012**, *219*, 280–284. [[CrossRef](#)]
250. Teng, Y.; Song, L.X.; Wang, L.B.; Xia, J. Face-Raised Octahedral Co₃O₄ Nanocrystals and Their Catalytic Activity in the Selective Oxidation of Alcohols. *J. Phys. Chem. C* **2014**, *118*, 4767–4773. [[CrossRef](#)]
251. Ma, M.G.; Qing, S.J.; Li, S.M.; Zhu, J.F.; Fu, L.H.; Sun, R.C. Microwave synthesis of cellulose/CuO nanocomposites in ionic liquid and its thermal transformation to CuO. *Carbohydr. Polym.* **2013**, *91*, 162–168. [[CrossRef](#)] [[PubMed](#)]
252. Hu, W.; Chen, S.; Zhou, B.; Wang, H. Facile synthesis of ZnO nanoparticles based on bacterial cellulose. *Mater. Sci. Eng. B* **2010**, *170*, 88–92. [[CrossRef](#)]
253. Kong, L.; Zhang, C.; Wang, J.; Long, D.; Qiao, W.; Ling, L. Ultrahigh intercalation pseudocapacitance of mesoporous orthorhombic niobium pentoxide from a novel cellulose nanocrystal template. *Mater. Chem. Phys.* **2015**, *149–150*, 495–504. [[CrossRef](#)]
254. Chu, G.; Feng, J.; Wang, Y.; Zhang, X.; Xu, Y.; Zhang, H. Chiral nematic mesoporous films of ZrO₂:Eu³⁺: New luminescent materials. *Dalton Trans.* **2014**, *43*, 15321–15327. [[CrossRef](#)]
255. Wang, F.; Cheong, J.Y.; Lee, J.; Ahn, J.; Duan, G.; Chen, H.; Zhang, Q.; Kim, I.D.; Jiang, S. Pyrolysis of Enzymolysis-Treated Wood: Hierarchically Assembled Porous Carbon Electrode for Advanced Energy Storage Devices. *Adv. Funct. Mater.* **2021**, *31*, 2101077. [[CrossRef](#)]
256. Li, L.; Xiao, R.; Tao, X.; Wu, Y.; Jiang, L.; Zhang, Z.; Qing, Y. Free-standing electrodes via coupling nanostructured Ni–NiO with hierarchical wood carbon for high-performance supercapacitors and Ni–Zn batteries. *J. Power Sources* **2021**, *491*, 229618. [[CrossRef](#)]
257. Chen, Y.; Yu, Y.; Zhang, X.; Guo, C.; Chen, C.; Shuangfei Wang, S.; Min, D. High performance supercapacitors assembled with hierarchical porous carbonized wood electrode prepared through self-activation. *Ind. Crops Prod.* **2022**, *181*, 114802. [[CrossRef](#)]
258. Subramaniam, T.; Krishnan, S.G.; Ansari, M.N.M.; Hamid, N.A.; Khalid, M. Recent progress on supercapacitive performance of agrowaste fibers: A review. *Crit. Rev. Solid State Mater. Sci.* **2022**, *1–43*. [[CrossRef](#)]
259. Dong, Y.; Jia, B.; Fu, F.; Zhang, H.; Zhang, L.; Zhou, J. Fabrication of Hollow Materials by Fast Pyrolysis of Cellulose Composite Fibers with Heterogeneous Structures. *Angew. Chem. Int. Ed.* **2016**, *55*, 13504–13508. [[CrossRef](#)]
260. Long, C.; Qi, D.; Wei, T.; Yan, J.; Jiang, L.; Fan, Z. Nitrogen-Doped Carbon Networks for High Energy Density Supercapacitors Derived from Polyaniline Coated Bacterial Cellulose. *Adv. Funct. Mater.* **2014**, *24*, 3953–3961. [[CrossRef](#)]
261. Xu, H.; Jin, M.; Geng, J.; Zhang, S.; Zhang, H. Bacterial cellulose-regulated synthesis of metallic Ni catalysts for high-efficiency electro-synthesis of hydrogen peroxide. *Sci. China Mater.* **2021**, *65*, 721–731. [[CrossRef](#)]

262. Hamad, H.; Bailón-García, E.; Morales-Torres, S.; Carrasco-Marín, F.; Pérez-Cadenas, A.F.; Maldonado-Hódar, F.J. A new platform for facile synthesis of hybrid TiO₂ nanostructures by various functionalizations of cellulose to be used in highly-efficient photocatalysis. *Mater. Lett.* **2020**, *274*, 128016. [[CrossRef](#)]
263. Habibi, S.; Jamshidi, M. Synthesis of TiO₂ nanoparticles coated on cellulose nanofibers with different morphologies: Effect of the template and sol-gel parameters. *Mater. Sci. Semicond. Proc.* **2020**, *109*, 104927. [[CrossRef](#)]
264. Ghani, M. Nanocrystalline cellulose as a biotemplate for preparation of porous titania thin film as a sorbent for thin film microextraction of ketorolac, meloxicam, diclofenac and mefenamic acid. *J. Chromatogr. B Anal. Technol. Biomed. Life Sci.* **2020**, *1142*, 122039. [[CrossRef](#)] [[PubMed](#)]
265. Zhang, L.R.H.; Wan, J.M.; Hu, Z.W.; Jiang, W.B. Preparation and Photocatalytic Activity of TiO₂-Wrapped Cotton Nanofiber Composite Catalysts. *BioResources* **2017**, *12*, 6062–6081. [[CrossRef](#)]
266. Wang, W.; Wang, J.; Shi, X.; Yu, Z.; Song, Z.; Dong, L.; Jiang, G.; Han, S. Synthesis of Mesoporous TiO₂ Induced by Nano-Cellulose and Its Photocatalytic Properties. *BioResources* **2016**, *11*, 3084–3093. [[CrossRef](#)]
267. Tajik, E.; Naeimi, A.; Amiri, A. Fabrication of iron oxide nanoparticles, and green catalytic application of an immobilized novel iron Schiff on wood cellulose. *Cellulose* **2018**, *25*, 915–923. [[CrossRef](#)]
268. Mikhaylov, V.I.; Krivoschapkina, E.F.; Belyy, V.A.; Krivoschapkin, P.V. Synthesis and characterization of sponge-like α -Fe microtubes. *Chem. Eng. Sci.* **2017**, *163*, 27–30. [[CrossRef](#)]
269. Mikhailov, V.I.; Krivoschapkina, E.F.; Ryabkov, Y.I.; Krivoschapkin, P.V. Influence of the Electrokinetic Properties of Cellulose on the Morphology of Iron(III) Oxide upon Template Synthesis. *Glass Phys. Chem.* **2016**, *42*, 582–589. [[CrossRef](#)]
270. Liu, S.; Tao, D.; Zhang, L. Cellulose scaffold: A green template for the controlling synthesis of magnetic inorganic nanoparticles. *Powder Technol.* **2012**, *217*, 502–509. [[CrossRef](#)]
271. Wan, Y.; Yang, Z.; Xiong, G.; Luo, H. A general strategy of decorating 3D carbon nanofiber aerogels derived from bacterial cellulose with nano-Fe₃O₄ for high performance flexible and binder-free lithium-ion battery anodes. *J. Mater. Chem. A* **2015**, *3*, 15386–15393. [[CrossRef](#)]
272. Wan, Y.; Yang, Z.; Xiong, G.; Guo, R.; Liu, Z.; Luo, H. Anchoring Fe₃O₄ nanoparticles on three-dimensional carbon nanofibers toward flexible high performance anodes for lithium-ion batteries. *J. Power Sources* **2015**, *294*, 414–419. [[CrossRef](#)]
273. Huang, Y.; Lin, Z.; Zheng, M.; Wang, T.; Yang, J.; Yuan, F.; Lu, X.; Liu, L.; Sun, D. Amorphous Fe₂O₃ nanoshells coated on carbonized bacterial cellulose nanofibers as a flexible anode for high-performance lithium ion batteries. *J. Power Sources* **2016**, *307*, 649–656. [[CrossRef](#)]
274. Yuan, Y.; Fu, A.; Wang, Y.; Guo, P.; Wu, G.; Li, H.; Zhao, X.S. Spray drying assisted assembly of ZnO nanocrystals using cellulose as sacrificial template and studies on their photoluminescent and photocatalytic properties. *Colloids Surf. A Physicochem. Eng. Asp.* **2017**, *522*, 173–182. [[CrossRef](#)]
275. Xiao, H.; Zhang, W.; Wei, Y.; Chen, L. Carbon/ZnO nanorods composites templated by TEMPO oxidized cellulose and photocatalytic activity for dye degradation. *Cellulose* **2018**, *25*, 1809–1819. [[CrossRef](#)]
276. Liu, S.; Yao, K.; Wang, B.; Ma, M.G. Microwave assisted hydrothermal synthesis of cellulose/ZnO composites and its thermal transformation to ZnO/carbon composites. *Iran. Polym. J.* **2017**, *26*, 681–691. [[CrossRef](#)]
277. Li, J.; Feng, X.; Jia, Y.; Yang, Y.; Cai, P.; Huang, J.; Li, J. Co-assembly of photosystem II in nanotubular indium–tin oxide multilayer films templated by cellulose substance for photocurrent generation. *J. Mater. Chem. A* **2017**, *5*, 19826. [[CrossRef](#)]
278. Liu, S.; Hu, H.; Zhou, J.; Zhang, L. Cellulose scaffolds modulated synthesis of Co₃O₄ nanocrystals: Preparation, characterization and properties. *Cellulose* **2011**, *18*, 1273–1283. [[CrossRef](#)]
279. Fu, L.H.; Li, S.M.; Bian, J.; Ma, M.G.; Long, X.L.; Zhang, X.M.; Liu, S.J. Compare study cellulose/Mn₃O₄ composites using four types of alkalis by sonochemistry method. *Carbohydr. Polym.* **2015**, *115*, 373–378. [[CrossRef](#)]
280. Ounnunkad, K.; Phanichphant, S. Cellulose-precursor synthesis of nanocrystalline Co_{0.5}Cu_{0.5}Fe₂O₄ spinel ferrites. *Mater. Res. Bull.* **2012**, *47*, 473–477. [[CrossRef](#)]
281. Henry, A.; Hesemann, P.; Alauzun, J.G.; Boury, B. Reductive mineralization of cellulose with vanadium, iron and tungsten chlorides and access to M_xO_y metal oxides and M_xO_y/C metal oxide/carbon composites. *Carbohydr. Polym.* **2017**, *174*, 697–705. [[CrossRef](#)] [[PubMed](#)]
282. Liu, S.; Yan, W.; Cao, X.; Zhou, Z.; Yang, R. Bacterial-cellulose-derived carbon nanofiber supported CoFe₂O₄ as efficient electrocatalyst for oxygen reduction and evolution reactions. *Int. J. Hydrogen Energy* **2016**, *41*, 5351–5360. [[CrossRef](#)]
283. Chen, L.F.; Huang, Z.H.; Liang, H.W.; Guan, Q.F.; Yu, S.H. Bacterial-Cellulose-Derived Carbon Nanofiber@MnO₂ and Nitrogen-Doped Carbon Nanofiber Electrode Materials: An Asymmetric Supercapacitor with High Energy and Power Density. *Adv. Mater.* **2013**, *25*, 4746–4752. [[CrossRef](#)] [[PubMed](#)]
284. Ahmad, H.; Haseen, U.; Umar, K.; Ansari, M.S.; Nasir, M.; Ibrahim, M. Bioinspired 2D carbon sheets decorated with MnFe₂O₄ nanoparticles for preconcentration of inorganic arsenic, and its determination by ICP-OES. *Microchim. Acta* **2019**, *186*, 649. [[CrossRef](#)]
285. Yang, E.H.; Moon, D.J. Synthesis of LaNiO₃ perovskite using an EDTA cellulose method and comparison with the conventional Pechini method: Application to steam CO₂ reforming of methane. *RSC Adv.* **2016**, *6*, 112885–112898. [[CrossRef](#)]
286. Wang, M.; Li, S.; Zhang, Y.; Huang, J. Hierarchical SnO₂/Carbon Nanofibrous Composite Derived from Cellulose Substance as Anode Material for Lithium-Ion Batteries. *Chem. Eur. J.* **2015**, *21*, 16195–16202. [[CrossRef](#)]

287. Wang, B.; Li, X.; Luo, B.; Yang, J.; Wang, X.; Song, Q.; Chen, S.; Zhi, L. Pyrolyzed Bacterial Cellulose: A Versatile Support for Lithium Ion Battery Anode Materials. *Small* **2013**, *9*, 2399–2404. [[CrossRef](#)]
288. Cazaña, F.; Galetti, A.; Meyer, C.; Sebastián, V.; Centeno, M.A.; Romeo, E.; Monzón, A. Synthesis of Pd-Al/biomorphic carbon catalysts using cellulose as carbon precursor. *Catal. Today* **2018**, *301*, 226–238. [[CrossRef](#)]
289. Wu, Q.; Liu, S.; Xie, C.; Yu, H.; Liu, Y.; Yu, S.; Huang, L. Ni-doped mesoporous carbon obtained from hydrothermal carbonization of cellulose and their catalytic hydrogenation activity study. *J. Mater. Sci.* **2018**, *53*, 7900–7910. [[CrossRef](#)]
290. Foo, Y.T.; Chan, J.E.M.; Ngoh, G.C.; Abdullah, A.Z.; Horrid, B.A.; Salamatinia, B. Synthesis and characterization of NiO and Ni nanoparticles using nanocrystalline cellulose (NCC) as a template. *Ceram. Int.* **2017**, *43*, 16331–16339. [[CrossRef](#)]
291. Tong, S.; Zheng, M.; Lu, Y.; Lin, Z.; Zhang, X.; He, P.; Zhou, H. Binder-free carbonized bacterial cellulose-supported ruthenium nanoparticles for Li–O₂ batteries. *Chem. Commun.* **2015**, *51*, 7302–7304. [[CrossRef](#)] [[PubMed](#)]
292. Wang, L.; Schutz, C.; Salazar-Alvarez, G.; Titirici, M.M. Carbon aerogels from bacterial nanocellulose as anodes for lithium ion batteries. *RSC Adv.* **2014**, *4*, 17549–17554. [[CrossRef](#)]
293. Zhang, F.; Tang, Y.; Yang, Y.; Zhang, X.; Lee, C.S. In-situ assembly of three-dimensional MoS₂ nanoleaves/carbon nanofiber composites derived from bacterial cellulose as flexible and binder-free anodes for enhanced lithium-ion batteries. *Electrochim. Acta* **2016**, *211*, 404–410. [[CrossRef](#)]
294. Lai, F.; Miao, Y.E.; Huang, Y.; Zhang, Y.; Liu, T. Nitrogen-Doped Carbon Nanofiber/Molybdenum Disulfide Nanocomposites Derived from Bacterial Cellulose for High-Efficiency Electrocatalytic Hydrogen Evolution Reaction. *ACS Appl. Mater. Interf.* **2016**, *8*, 3558–3566. [[CrossRef](#)] [[PubMed](#)]
295. Fan, H.; Liu, W.; Shen, W. Honeycomb-like composite structure for advanced solid state asymmetric supercapacitors. *Chem. Eng. J.* **2017**, *326*, 518–527. [[CrossRef](#)]
296. Gan, L.; Geng, A.; Song, C.; Xu, L.; Wang, L.; Fang, X.; Han, S.; Cui, J.; Mei, C. Simultaneous removal of rhodamine B and Cr(VI) from water using cellulose carbon nanofiber incorporated with bismuth oxybromide: The effect of cellulose pyrolysis temperature on photocatalytic performance. *Environ. Res.* **2020**, *185*, 109414. [[CrossRef](#)] [[PubMed](#)]
297. Foresti, M.L.; Vázquez, A.; Boury, B. Applications of bacterial cellulose as precursor of carbon and composites with metal oxide, metal sulfide and metal nanoparticles: A review of recent advances. *Carbohydr. Polym.* **2017**, *157*, 447–467. [[CrossRef](#)] [[PubMed](#)]
298. Liu, S.; Ke, D.; Zeng, J.; Zhou, J.; Peng, T.; Zhang, L. Construction of inorganic nanoparticles by micro-nanoporous structure of cellulose matrix. *Cellulose* **2011**, *18*, 945–956. [[CrossRef](#)]
299. Yang, L.; Mukhopadhyay, A.; Jiao, Y.; Yong, Q.; Chen, L.; Xing, Y.; Hamel, J.; Zhu, H. Ultralight, highly thermally insulating and fire resistant aerogel by encapsulating cellulose nanofibers with two-dimensional MoS₂. *Nanoscale* **2017**, *9*, 11452–11462. [[CrossRef](#)]
300. Padalkar, S.; Capadona, J.R.; Rowan, S.J.; Weder, C.; Moon, R.J.; Stanciu, L.A. Self-assembly and alignment of semiconductor nanoparticles on cellulose nanocrystals. *J. Mater. Sci.* **2011**, *46*, 5672–5679. [[CrossRef](#)]
301. Hokkanen, S.; Repo, E.; Johansson Westholm, L.; Lou, S.; Sainio, T.; Sillanpää, M. Adsorption of Ni²⁺, Cd²⁺, PO₄³⁻ and NO₃⁻ from aqueous solutions by nanostructured microfibrillated cellulose modified with carbonated hydroxyapatite. *Chem. Eng. J.* **2014**, *252*, 64–74. [[CrossRef](#)]
302. Zimmermann, K.A.; LeBlanc, J.M.; Sheets, K.T.; Fox, R.W.; Gatenholm, P. Biomimetic design of a bacterial cellulose/hydroxyapatite nanocomposite for bone healing applications. *Mater. Sci. Eng. C* **2011**, *31*, 43–49. [[CrossRef](#)]
303. Chen, Z.J.; Shi, H.H.; Zheng, L.; Zhang, H.; Cha, Y.Y.; Ruan, H.X.; Zhang, Y.; Zhang, X.C. A new cancellous bone material of silk fibroin/cellulose dual network composite aerogel reinforced by nano-hydroxyapatite filler. *Int. J. Biol. Mol.* **2021**, *182*, 286–297. [[CrossRef](#)] [[PubMed](#)]
304. Chen, Q.; Garcia, R.P.; Munoz, J.; Pérez de Larraya, U.; Garmendia, N.; Yao, Q.; Boccaccini, A.R. Cellulose Nanocrystals–Bioactive Glass Hybrid Coating as Bone Substitutes by Electrophoretic Co-deposition: In Situ Control of Mineralization of Bioactive Glass and Enhancement of Osteoblastic Performance. *ACS Appl. Mater. Interfaces* **2015**, *7*, 24715–24725. [[CrossRef](#)]
305. Kulpinski, P.; Namyslak, M.; Grzyb, T.; Lis, S. Luminescent cellulose fibers activated by Eu³⁺-doped nanoparticles. *Cellulose* **2012**, *19*, 1271–1278. [[CrossRef](#)]
306. Hobisch, M.A.; Müller, D.; Fischer, W.J.; Zankel, A.; Eckhart, R.; Bauer, W.; Zabler, S.; Spirk, S. Cobalt Ferrite Nanoparticles for Three-Dimensional Visualization of Micro- and Nanostructured Cellulose in Paper. *ACS Appl. Nano Mater.* **2019**, *2*, 3864–3869. [[CrossRef](#)]
307. Butwong, N.; Kunthadong, P.; Soisungnoen, P.; Chotichayapong, C.; Srijaranai, S.; Luong, J.H.T. Silver-doped CdS quantum dots incorporated into chitosan-coated cellulose as a colorimetric paper test stripe for mercury. *Microchim. Acta* **2018**, *185*, 126. [[CrossRef](#)]
308. Gomathi, P.T.; Sahatiya, P.; Badhulika, S. Large-Area, Flexible Broadband Photodetector Based on ZnS–MoS₂ Hybrid on Paper Substrate. *Adv. Funct. Mater.* **2017**, *27*, 1701611. [[CrossRef](#)]
309. Phiwchaia, I.; Thongtem, T.; Thongtem, S.; Pilapong, C. Deferoxamine-conjugated AgInS₂ nanoparticles as new nanodrug for synergistic therapy for hepatocellular carcinoma. *Int. J. Pharm.* **2017**, *524*, 30–40. [[CrossRef](#)]
310. Huang, X.; Hu, N.; Wang, X.; Zhang, Y.S.; Sun, R. Copper Sulfide Nanoparticle/Cellulose Composite Paper: Room-Temperature Green Fabrication for NIR Laser-Inducible Ablation of Pathogenic Microorganisms. *ACS Sustain. Chem. Eng.* **2017**, *5*, 2648–2655. [[CrossRef](#)]

311. Peng, S.; Fan, L.; Wei, C.; Liu, X.; Zhang, H.; Xu, W.; Xu, J. Flexible polypyrrole/copper sulfide/bacterial cellulose nanofibrous composite membranes as supercapacitor electrodes. *Carbohydr. Polym.* **2017**, *157*, 344–352. [[CrossRef](#)] [[PubMed](#)]
312. Yang, J.; Yu, J.; Fan, J.; Sun, D.; Tang, W.; Yang, X. Biotemplated preparation of CdS nanoparticles/bacterial cellulose hybrid nanofibers for photocatalysis application. *J. Hazard. Mater.* **2011**, *189*, 377–383. [[CrossRef](#)] [[PubMed](#)]
313. Tavker, N.; Sharma, M. Designing of waste fruit peels extracted cellulose supported molybdenum sulfide nanostructures for photocatalytic degradation of RhB dye and industrial effluent. *J. Environ. Manag.* **2020**, *255*, 109906. [[CrossRef](#)] [[PubMed](#)]
314. Zheng, W.; Chen, S.; Zhao, S.; Zheng, Y.; Wang, H. Zinc Sulfide Nanoparticles Template by Bacterial Cellulose and Their Optical Properties. *J. Appl. Polym. Sci.* **2014**, *131*, 40874. [[CrossRef](#)]
315. Wang, P.; Geng, Z.; Gao, J.; Xuan, R.; Liu, P.; Wang, Y.; Huang, K.; Wan, Y.; Xu, Y. Zn_xCd_{1-x}S /bacterial cellulose bionanocomposite foams with hierarchical architecture and enhanced visible-light photocatalytic hydrogen production activity. *J. Mater. Chem. A* **2015**, *3*, 1709–1716. [[CrossRef](#)]
316. Guo, X.; Cao, G.L.; Ding, F.; Li, X.; Zhen, S.; Xue, Y.F.; Yan, Y.M.; Liu, T.; Sun, K.N. A bulky and flexible electrocatalyst for efficient hydrogen evolution based on the growth of MoS₂ nanoparticles on carbon nanofiber foam. *J. Mater. Chem. A* **2015**, *3*, 5041–5046. [[CrossRef](#)]
317. Li, Z.; Ottmann, A.; Thauer, E.; Neef, C.; Sai, H.; Sun, Q.; Cendrowski, K.; Meyer, H.P.; Vaynzof, Y.; Mijowska, E.; et al. A facile synthesis method and electrochemical studies of a hierarchical structured MoS₂/C nanocomposite. *RSC Adv.* **2016**, *6*, 76084–76092. [[CrossRef](#)]
318. Luna-Martinez, J.F.; Hernandez-Uresti, D.B.; Reyes-Melo, M.E.; Guerrero-Salazar, C.A.; Gonzalez-Gonzalez, V.A.; Sepulveda-Guzman, S. Synthesis and optical characterization of ZnS-sodium carboxymethyl cellulose nanocomposite films. *Carbohydr. Polym.* **2011**, *84*, 566–570. [[CrossRef](#)]
319. Abdullah, H.; Hsu, C.N.; Shuwanto, H.; Gultom, N.S.; Kebede, W.L.; Wua, C.M.; Lai, C.C.; Murakami, R.I.; Hirota, M.; Nakagaito, A.N.; et al. Immobilization of cross-linked In-doped Mo(O,S)₂ on cellulose nanofiber for effective organic-compound degradation under visible light illumination. *Progr. Nat. Sci. Mater. Int.* **2021**, *31*, 404–413. [[CrossRef](#)]
320. Shao, D.; Ren, X.; Wen, J.; Hu, S.; Xiong, J.; Jiang, T.; Wang, X.; Wang, X. Immobilization of uranium by biomaterial stabilized FeS nanoparticles: Effects of stabilizer and enrichment mechanism. *J. Hazard. Mater.* **2016**, *302*, 1–9. [[CrossRef](#)]
321. Yu, W.; Lin, W.; Shao, X.; Hu, Z.; Li, R.; Yuan, D. High performance supercapacitor based on Ni₃S₂/carbon nanofibers and carbon nanofibers electrodes derived from bacterial cellulose. *J. Power Sources* **2014**, *272*, 137–143. [[CrossRef](#)]
322. Hokkanen, S.; Bhatnagar, A.; Repo, E.; Lou, S.; Sillanpää, M. Calcium hydroxyapatite microfibrillated cellulose composite as a potential adsorbent for the removal of Cr(VI) from aqueous solution. *Chem. Eng. J.* **2016**, *283*, 445–452. [[CrossRef](#)]
323. Sundberg, J.; Götherström, C.; Gatenholm, P. Biosynthesis and in vitro evaluation of macroporous mineralized bacterial nanocellulose scaffolds for bone tissue engineering. *Bio-Med. Mater. Eng.* **2015**, *25*, 39–52. [[CrossRef](#)] [[PubMed](#)]
324. Tabaght, F.E.; Azzouai, K.; Elidrissi, A.; Hamed, O.; Mejdoubi, E.; Jodeh, S.; Akartasse, N.; Lakrat, M.; Lamhamdi, A. New nanostructure based on hydroxyapatite modified cellulose for bone substitute, synthesis, and characterization. *Int. J. Polym. Mater. Polym. Biomater.* **2020**, *70*, 437–448. [[CrossRef](#)]
325. Salehia, G.; Behnamghader, A.; Hesaraki, S.; Mozafari, M. Synergistic effects of carbohydrate polymers on the performance of hybrid injectable bone pastes. *Eur. Polym. J.* **2019**, *119*, 523–530. [[CrossRef](#)]
326. Ohland, A.L.; Martins Salim, V.M.; Piacsek Borges, C. Nanocomposite membranes for osmotic processes: Incorporation of functionalized hydroxyapatite in porous substrate and in selective layer. *Desalination* **2019**, *463*, 23–31. [[CrossRef](#)]
327. Guo, W.; Wang, X.; Zhang, P.; Liu, J.; Song, L.; Hu, Y. Nano-fibrillated cellulose-hydroxyapatite based composite foams with excellent fire resistance. *Carbohydr. Polym.* **2018**, *195*, 71–78. [[CrossRef](#)]
328. Herdocia-Lluberres, C.S.; Laboy-López, S.; Morales, S.; Gonzalez-Robles, T.J.; González-Feliciano, J.A.; Nicolau, E. Evaluation of Synthesized Nanohydroxyapatite-Nanocellulose Composites as Biocompatible Scaffolds for Applications in Bone Tissue Engineering. *J. Nanomater.* **2015**, *2015*, 310935. [[CrossRef](#)]
329. Jin, Y.; Ni, Y.; Pudukudy, M.; Zhang, H.; Wang, H.; Jia, Q.; Shan, S. Synthesis of nanocrystalline cellulose/hydroxyapatite nanocomposites for the efficient removal of chlortetracycline hydrochloride in aqueous medium. *Mater. Chem. Phys.* **2022**, *275*, 125135. [[CrossRef](#)]
330. Ma, M.G.; Donga, Y.Y.; Fua, L.H.; Li, S.M.; Sun, R.C. Cellulose/CaCO₃ nanocomposites: Microwave ionic liquid synthesis, characterization, and biological activity. *Carbohydr. Polym.* **2013**, *92*, 1669–1676. [[CrossRef](#)]
331. Van Opdenbosch, D.; Maischa, P.; Fritsch-Popovski, G.; Paris, O.; Zollfrank, C. Transparent cellulose sheets as synthesis matrices for inorganic functional particles. *Carbohydr. Polym.* **2012**, *87*, 257–264. [[CrossRef](#)] [[PubMed](#)]
332. Wang, D.; Yu, H.; Guan, Y.; Zhu, M.; Liu, S.; Yao, J. A novel chemical reduction method to fabricate tunable selenium nanosphere and nanobelt based on cellulose nanocrystals. *Mater. Lett.* **2018**, *230*, 44–47. [[CrossRef](#)]
333. Jiao, L.; Li, Q.; Deng, J.; Okosi, N.; Xia, J.; Su, M. Nanocellulose templated growth of ultra-small bismuth nanoparticles for enhanced radiation therapy. *Nanoscale* **2018**, *10*, 6751–6757. [[CrossRef](#)] [[PubMed](#)]
334. Ma, L.; Liu, R.; Liu, L.; Wang, F.; Niu, H.; Huang, Y. Facile synthesis of Ni(OH)₂/graphene/bacterial cellulose paper for large areal mass, mechanically tough and flexible supercapacitor electrodes. *J. Power Sources* **2016**, *335*, 76–83. [[CrossRef](#)]
335. Vosmanská, V.; Kolářová, K.; Pišlová, M.; Švorčík, V. Reaction parameters of in situ silver chloride precipitation on cellulose fibres. *Mater. Sci. Eng. C* **2019**, *95*, 134–142. [[CrossRef](#)]

336. Dai, L.; Liu, R.; Hu, L.Q.; Si, C.L. Simple and green fabrication of AgCl/Ag-cellulose paper with antibacterial and photocatalytic activity. *Carbohydr. Polym.* **2017**, *174*, 450–455. [[CrossRef](#)]
337. Liu, R.; Ma, L.N.; Niu, G.D.; Li, X.L.; Li, E.Y.; Bai, Y.; Liu, Y.; Yuan, G.H. Flexible Ti-Doped FeOOH Quantum Dots/Graphene/Bacterial Cellulose Anode for High-Energy Asymmetric Supercapacitors. *Part. Part. Syst. Charact.* **2017**, *34*, 1700213. [[CrossRef](#)]
338. Du, X.; Zhang, Z.; Liu, W.; Deng, Y. Nanocellulose-based conductive materials and their emerging applications in energy devices—A review. *Nano Energy* **2017**, *35*, 299–320. [[CrossRef](#)]
339. Klemm, D.; Cranston, E.D.; Fischer, D.; Gama, M.; Kedzior, S.A.; Kralisch, D.; Kramer, F.; Kondo, T.; Lindström, T.; Nietzsche, S.; et al. Nanocellulose as a natural source for groundbreaking applications in materials science: Today's state. *Mater. Today* **2018**, *21*, 720–748. [[CrossRef](#)]
340. Oun, A.A.; Shankar, S.; Rhim, J.W. Multifunctional nanocellulose/metal and metal oxide nanoparticle hybrid nanomaterials. *Crit. Rev. Food Sci. Nutr.* **2020**, *60*, 435. [[CrossRef](#)]
341. Ge, S.; Zhang, L.; Zhang, Y.; Lan, F.; Yana, M.; Yu, J. Nanomaterials-modified cellulose paper as a platform for biosensing applications. *Nanoscale* **2017**, *9*, 4366–4382. [[CrossRef](#)] [[PubMed](#)]
342. Wu, L.; Ma, C.; Zheng, X.; Liu, H.; Yu, J. Paper-based electrochemiluminescence origami device for protein detection using assembled cascade DNA-carbon dots nanotags based on rolling circle amplification. *Biosens. Bioelectron.* **2015**, *68*, 413–420. [[CrossRef](#)] [[PubMed](#)]
343. Incel, A.; Akin, O.; Cagır, A.; Yıldız, Ü.H.; Demir, M.M. Smart phone assisted detection and quantification of cyanide in drinking water by paper based sensing platform. *Sens. Actuators B* **2017**, *252*, 886–893. [[CrossRef](#)]
344. Qi, H.; Shopsowitz, K.E.; Hamad, W.Y.; MacLachlan, M.J. Chiral Nematic Assemblies of Silver Nanoparticles in Mesoporous Silica Thin Films. *J. Am. Chem. Soc.* **2011**, *133*, 3728–3731. [[CrossRef](#)] [[PubMed](#)]
345. Bodelón, G.; Mourdikoudis, S.; Yate, L.; Pastoriza-Santos, I.; Pérez-Juste, J.; Liz-Marzán, L.M. Nickel Nanoparticle-Doped Paper as a Bioactive Scaffold for Targeted and Robust Immobilization of Functional Proteins. *ACS Nano* **2014**, *8*, 6221–6231. [[CrossRef](#)] [[PubMed](#)]
346. Bazant, P.; Kuritka, I.; Munster, L.; Kalina, L. Microwave solvothermal decoration of the cellulose surface by nanostructured hybrid Ag/ZnO particles: A joint XPS, XRD and SEM study. *Cellulose* **2015**, *22*, 1275–1293. [[CrossRef](#)]
347. Khatri, V.; Halász, K.; Trandafilović, L.V.; Dimitrijević-Branković, S.; Mohanty, P.; Djoković, V.; Csóka, L. ZnO-modified cellulose fiber sheets for antibody immobilization. *Carbohydr. Polym.* **2014**, *109*, 139–147. [[CrossRef](#)]
348. Liu, X.; Li, J.; Zhang, Y.; Huang, J. Bioinspired Hierarchical Nanotubular Titania Immobilized with Platinum Nanoparticles for Photocatalytic Hydrogen Production. *Chem. Eur. J.* **2015**, *21*, 7345–7349. [[CrossRef](#)]
349. Nagaraju, G.; Ko, Y.H.; Yu, J.S. Facile synthesis of ZnO/CuO nanostructures on cellulose paper and their p–n junction properties. *Mater. Lett.* **2014**, *116*, 64–67. [[CrossRef](#)]
350. Lv, P.; Xu, W.; Li, D.; Feng, Q.; Yao, Y.; Pang, Z.; Lucia, L.A.; Wei, Q. Metal-based bacterial cellulose of sandwich nanomaterials for anti-oxidation electromagnetic interference shielding. *Mater. Des.* **2016**, *112*, 374–382. [[CrossRef](#)]
351. Zhang, W.; Chen, S.; Hu, W.; Zhou, B.; Yang, Z.; Yin, N.; Wang, H. Facile fabrication of flexible magnetic nanohybrid membrane with amphiphobic surface based on bacterial cellulose. *Carbohydr. Polym.* **2011**, *86*, 1760–1767. [[CrossRef](#)]
352. Yang, X.; Shi, K.; Zhitomirsky, I.; Cranston, E.D. Cellulose Nanocrystal Aerogels as Universal 3D Lightweight Substrates for Supercapacitor Materials. *Adv. Mater.* **2015**, *27*, 6104–6109. [[CrossRef](#)] [[PubMed](#)]
353. Chen, L.; Berry, R.M.; Tam, K.C. Synthesis of β -Cyclodextrin-Modified Cellulose Nanocrystals (CNCs)@Fe₃O₄@SiO₂ Superparamagnetic Nanorods. *ACS Sustain. Chem. Eng.* **2014**, *2*, 951–958. [[CrossRef](#)]
354. Mahmoud, K.A.; Lam, E.; Hrapovic, S.; Luong, J.H.T. Preparation of Well-Dispersed Gold/Magnetite Nanoparticles Embedded on Cellulose Nanocrystals for Efficient Immobilization of Papain Enzyme. *ACS Appl. Mater. Interfaces* **2013**, *5*, 4978–4985. [[CrossRef](#)]
355. Gesesse, G.D.; Li, C.; Paineau, E.; Habibi, Y.; Remita, H.; Colbeau-Justin, C.; Ghazzal, M.N. Enhanced Photogenerated Charge Carriers and Photocatalytic Activity of Biotemplated Mesoporous TiO₂ Films with a Chiral Nematic Structure. *Chem. Mater.* **2019**, *31*, 4851–4863. [[CrossRef](#)]
356. Busbee, B.D.; Obare, S.O.; Murphy, C.J. An Improved Synthesis of High-Aspect-Ration Gold Nanorods. *Adv. Mater.* **2013**, *15*, 414–416. [[CrossRef](#)]
357. Ge, S.; Liu, W.; Ge, L.; Yan, M.; Yan, J.; Huang, J.; Yu, J. In situ assembly of porous Au-paper electrode and functionalization of magnetic silica nanoparticles with HRP via click chemistry for Microcystin-LR immunoassay. *Biosens. Bioelectron.* **2013**, *49*, 111–117. [[CrossRef](#)]
358. Sun, G.; Liu, H.; Zhang, Y.; Yu, J.; Yan, M.; Song, X.; He, W. Gold nanorods-paper electrode based enzyme-free electrochemical immunoassay for prostate specific antigen using porous zinc oxide spheres-silver nanoparticles nanocomposites as labels. *New J. Chem.* **2015**, *39*, 6062–6067. [[CrossRef](#)]
359. Yan, J.; Yan, M.; Ge, L.; Yu, J.; Ge, S.; Huang, J. A microfluidic origami electrochemiluminescence aptamer-device based on a porous Au-paper electrode and a phenyleneethynylene derivative. *Chem. Commun.* **2013**, *49*, 1383–1385. [[CrossRef](#)]
360. Alba-Patino, A.; Russell, S.M.; Borges, M.; Pazos-Perez, N.; Alvarez-Puebla, R.A.; de la Rica, R. Nanoparticle-based mobile biosensors for the rapid detection of sepsis biomarkers in whole blood. *Nanoscale Adv.* **2020**, *2*, 1253–1260. [[CrossRef](#)]
361. Sun, G.; Wang, P.; Zhu, P.; Ge, L.; Ge, S.; Yan, M.; Song, X.; Yu, J. A near-infrared light photoelectrochemical immunosensor based on a Au-paper electrode and naphthalocyanine sensitized ZnO nanorods. *J. Mater. Chem. B* **2014**, *2*, 4811–4817. [[CrossRef](#)] [[PubMed](#)]

362. Ge, S.; Wu, K.; Zhang, Y.; Yan, M.; Yu, J. Paper-based biosensor relying on flower-like reduced graphene guided enzymatically deposition of polyaniline for Pb²⁺ detection. *Biosens. Bioelectron.* **2016**, *80*, 215–221. [[CrossRef](#)] [[PubMed](#)]
363. Wu, K.; Zhang, Y.; Wang, Y.; Ge, S.; Yan, M.; Yu, J.; Song, X. Paper-Based Analytical Devices Relying on Visible-Light-Enhanced Glucose/Air Biofuel Cells. *ACS Appl. Mater. Interfaces* **2015**, *7*, 24330–24337. [[CrossRef](#)] [[PubMed](#)]
364. Li, L.; Kong, Q.; Zhang, Y.; Dong, C.; Ge, S.; Yu, J. A 3D electrochemical immunodevice based on a porous Pt-paper electrode and metal ion functionalized flower-like Au nanoparticles. *J. Mater. Chem. B* **2015**, *3*, 2764–2769. [[CrossRef](#)]
365. Li, L.; Zhang, Y.; Zhang, L.N.; Ge, S.G.; Liu, H.Y.; Ren, N.; Yan, M.; Yu, J.H. Paper-Based Device for Colorimetric and Photoelectrochemical Quantification of the Flux of H₂O₂ Releasing from MCF-7 Cancer Cells. *Anal. Chem.* **2016**, *88*, 5369–5377. [[CrossRef](#)]
366. Wang, Y.; Ge, L.; Ma, C.; Kong, Q.; Yan, M.; Ge, S.; Yu, J. Self-Powered and Sensitive DNA Detection in a Three-Dimensional Origami-Based Biofuel Cell Based on a Porous Pt-Paper Cathode. *Chem. Eur. J.* **2014**, *20*, 12453–12462. [[CrossRef](#)]
367. Liu, F.; Ge, S.; Yu, J.; Yan, M.; Song, X. Electrochemical device based on a Pt nanosphere-paper working electrode for in situ and real-time determination of the flux of H₂O₂ releasing from SK-BR-3 cancer cells. *Chem. Commun.* **2014**, *50*, 10315–10318. [[CrossRef](#)]
368. Li, W.; Li, L.; Ge, S.; Song, X.; Ge, L.; Yan, M.; Yu, J. A 3D origami multiple electrochemiluminescence immunodevice based on a porous silver-paper electrode and multi-labeled nanoporous gold-carbon spheres. *Chem. Commun.* **2013**, *49*, 7687–7689. [[CrossRef](#)]
369. Li, W.; Li, L.; Ge, S.; Song, X.; Ge, L.; Yan, M.; Yu, J. Multiplex electrochemical origami immunodevice based on cuboid silver-paper electrode and metal ions tagged nanoporous silver-chitosan. *Biosens. Bioelectron.* **2014**, *56*, 167–173. [[CrossRef](#)]
370. Wu, M.; Ma, B.; Pan, T.; Chen, S.; Sun, J. Silver-Nanoparticle-Colored Cotton Fabrics with Tunable Colors and Durable Antibacterial and Self-Healing Superhydrophobic Properties. *Adv. Funct. Mater.* **2016**, *26*, 569–576. [[CrossRef](#)]
371. Liang, L.L.; Lan, F.F.; Li, L.; Su, M.; Ge, S.G.; Yu, J.H.; Liu, H.Y.; Yan, M. Fluorescence “turn-on” determination of H₂O₂ using multilayer porous SiO₂/NGQDs and PdAu mimetics enzymatic/oxidative cleavage of single-stranded DNA. *Biosens. Bioelectron.* **2016**, *82*, 204–211. [[CrossRef](#)] [[PubMed](#)]
372. Liang, L.; Lan, F.; Li, L.; Ge, S.; Yu, J.; Ren, N.; Liu, H.; Yan, M. Paper analytical devices for dynamic evaluation of cell surface N-glycan expression via a bimodal biosensor based on multibranching hybridization chain reaction amplification. *Biosens. Bioelectron.* **2016**, *86*, 756–763. [[CrossRef](#)] [[PubMed](#)]
373. Ge, S.; Li, W.; Yan, M.; Song, X.; Yu, J. Photoelectrochemical detection of tumor markers based on a CdS quantum dot/ZnO nanorod/Au@Pt-paper electrode 3D origami immunodevice. *J. Mater. Chem. B* **2015**, *3*, 2426–2432. [[CrossRef](#)] [[PubMed](#)]
374. Li, L.; Ma, C.; Kong, Q.; Li, W.; Zhang, Y.; Ge, S.; Yan, M.; Yu, J. A 3D origami electrochemical immunodevice based on a Au@Pd alloy nanoparticle-paper electrode for the detection of carcinoembryonic antigen. *J. Mater. Chem. B* **2014**, *2*, 6669–6674. [[CrossRef](#)]
375. Lee, M.; Oh, K.; Choi, H.K.; Lee, S.G.; Youn, H.J.; Lee, H.L.; Jeong, D.H. Subnanomolar Sensitivity of Filter Paper-Based SERS Sensor for Pesticide Detection by Hydrophobicity Change of Paper Surface. *ACS Sens.* **2018**, *3*, 151–159. [[CrossRef](#)]
376. Saklya, N.; Marzouka, W.; Ouada, H.B.; Majdou, H. Enhancing performances of colorimetric response of carboxymethylcellulose-stabilized silver nanoparticles: A fully eco-friendly assay for Hg²⁺ detection. *Sens. Actuators B* **2017**, *253*, 918–927. [[CrossRef](#)]
377. Jatoi, A.W.; Kim, I.S.; Ni, Q.Q. Cellulose acetate nanofibers embedded with AgNPs anchored TiO₂ nanoparticles for long term excellent antibacterial applications. *Carbohydr. Polym.* **2019**, *207*, 640–649. [[CrossRef](#)]
378. Li, G.; Sun, Y.; Liu, H. Gold-Carboxymethyl Cellulose Nanocomposites Greenly Synthesized for Fluorescent Sensitive Detection of Hg(II). *J. Cluster Sci.* **2018**, *29*, 177–184. [[CrossRef](#)]
379. Li, L.; Zhang, Y.; Liu, F.; Su, M.; Liang, L.; Ge, S.; Yu, J. Real-time visual determination of the flux of hydrogen sulphide using a hollow-channel paper electrode. *Chem. Commun.* **2015**, *51*, 14030–14033. [[CrossRef](#)]
380. Wang, X.; Yang, C.; Zhu, S.; Yan, M.; Ge, S.; Yu, J. 3D origami electrochemical device for sensitive Pb²⁺ testing based on DNA functionalized iron-porphyrinic metal-organic framework. *Biosens. Bioelectron.* **2017**, *87*, 108–115. [[CrossRef](#)]
381. Sun, G.; Wang, P.; Ge, S.; Ge, L.; Yu, J.; Yan, M. Photoelectrochemical sensor for pentachlorophenol on microfluidic paper-based analytical device based on the molecular imprinting technique. *Biosens. Bioelectron.* **2014**, *56*, 97–103. [[CrossRef](#)] [[PubMed](#)]
382. Wang, W.; Li, H.Y.; Zhang, D.W.; Jiang, J.; Cui, Y.R.; Qiu, S.; Zhou, Y.L.; Zhang, X.X. Fabrication of Biezymatic Glucose Biosensor Based on Novel Gold Nanoparticles-Bacteria Cellulose Nanofibers Nanocomposite. *Electroanalysis* **2010**, *22*, 2543–2550. [[CrossRef](#)]
383. Lan, F.; Sun, G.; Liang, L.; Ge, S.; Yan, M.; Yu, J. Microfluidic paper-based analytical device for photoelectrochemical immunoassay with multiplex signal amplification using multibranching hybridization chain reaction and PdAu enzyme mimetics. *Biosens. Bioelectron.* **2016**, *79*, 416–422. [[CrossRef](#)] [[PubMed](#)]
384. Sun, G.; Yang, H.; Zhang, Y.; Yu, J.; Ge, S.; Yan, M.; Song, X. Branched zinc oxide nanorods arrays modified paper electrode for electrochemical immunosensing by combining biocatalytic precipitation reaction and competitive immunoassay mode. *Biosens. Bioelectron.* **2015**, *74*, 823–829. [[CrossRef](#)]
385. Sun, G.; Yang, H.; Ma, C.; Zhang, Y.; Yu, J.; He, W.; Song, X. Application of CuS-functionalized ZnO nanoflakes for a paper-based photoelectrochemical immunoassay using an insitu electron donor producing strategy. *New J. Chem.* **2015**, *39*, 7012–7018. [[CrossRef](#)]
386. Zhang, Y.; Ge, L.; Li, M.; Yan, M.; Ge, S.; Yu, J.; Song, X.; Cao, B. Flexible paper-based ZnO nanorod light-emitting diodes induced multiplexed photoelectrochemical immunoassay. *Chem. Commun.* **2014**, *50*, 1417–1419. [[CrossRef](#)]

387. Wang, Y.; Xu, J.; Ma, C.; Li, S.; Yu, J.; Ge, S.; Yan, M. A chemiluminescence excited photoelectrochemistry aptamer-device equipped with a tin dioxide quantum dot/reduced graphene oxide nanocomposite modified porous Au-paper electrode. *J. Mater. Chem. B* **2014**, *2*, 3462–3468. [[CrossRef](#)]
388. Li, L.; Xu, J.; Zheng, X.; Ma, C.; Song, X.; Ge, S.; Yu, J.; Yan, M. Growth of gold-manganese oxide nanostructures on a 3D origami device for glucose-oxidase label based electrochemical immunosensor. *Biosens. Bioelectron.* **2014**, *61*, 76–82. [[CrossRef](#)]
389. Ge, L.; Wang, P.; Ge, S.; Li, N.; Yu, J.; Yan, M.; Huang, J. Photoelectrochemical Lab-on-Paper Device Based on an Integrated Paper Supercapacitor and Internal Light Source. *Anal. Chem.* **2013**, *85*, 3961–3970. [[CrossRef](#)]
390. Sun, W.; Liu, J.; Wu, H.; Yue, X.; Wang, Z.; Rooney, D.; Feng, J.; Sun, K. Facile synthesis of copper-manganese spinel anodes with high capacity and cycling performance for lithium-ion batteries. *Mater. Lett.* **2016**, *182*, 147–150. [[CrossRef](#)]
391. Lin, F.; Cai, J.; Li, Y.; Yu, H.; Li, S. Constituting fully integrated colorimetric analysis system for Fe(III) on multifunctional nitrogen-doped MoO₃/cellulose paper. *Talanta* **2018**, *180*, 352–357. [[CrossRef](#)] [[PubMed](#)]
392. Peng, S.; Xu, Q.; Fan, L.; Wei, C.; Bao, H.; Xu, W.; Xu, J. Flexible polypyrrole/cobalt sulfide /bacterial cellulose composite membranes for supercapacitor application. *Synth. Met.* **2016**, *222*, 285–292. [[CrossRef](#)]
393. Mukherjee, S.; Ramireddy, H.; Baidya, A.; Amala, A.K.; Sudhakar, C.; Mondal, B.; Philip, L.; Pradeep, T. Nanocellulose-Reinforced Organo-Inorganic Nanocomposite for Synergistic and Affordable Defluoridation of Water and an Evaluation of Its Sustainability Metrics. *ACS Sustain. Chem. Eng.* **2020**, *8*, 139–147. [[CrossRef](#)]
394. Azizi, S.; Ahmad, M.B.; Hussein, M.Z.; Ibrahim, N.A. Synthesis, Antibacterial and Thermal Studies of Cellulose Nanocrystal Stabilized ZnO-Ag Heterostructure Nanoparticles. *Molecules* **2013**, *18*, 6269–6280. [[CrossRef](#)] [[PubMed](#)]
395. Wang, K.; Huang, J. Natural cellulose derived nanofibrous Ag-nanoparticle/SnO₂/carbon ternary composite as an anodic material for lithium-ion batteries. *J. Phys. Chem. Solids* **2019**, *126*, 155–163. [[CrossRef](#)]
396. Kargar, P.G.; Bagherzade, G.; Eshghi, H. Novel biocompatible core/shell Fe₃O₄@NFC@Co(II) as a new catalyst in a multicomponent reaction: An efficient and sustainable methodology and novel reusable material for one-pot synthesis of 4H-pyran and pyranopyrazole in aqueous media. *RSC Adv.* **2020**, *10*, 37086. [[CrossRef](#)]
397. Nair, S.S.; Chen, J.; Slabon, A.; Mathew, A.P. Converting cellulose nanocrystals into photocatalysts by functionalisation with titanium dioxide nanorods and gold nanocrystals. *RSC Adv.* **2020**, *10*, 37374. [[CrossRef](#)]
398. Chen, Y.; Luo, H.; Guo, H.; Liu, K.; Mei, C.; Li, Y.; Duan, G.; He, S.; Han, J.; Zheng, J.; et al. Anisotropic cellulose nanofibril composite sponges for electromagnetic interference shielding with low reflection loss. *Carbohydr. Polym.* **2022**, *276*, 118799. [[CrossRef](#)]